For Reference

NOT TO BE TAKEN FROM THIS ROOM

For Reference

NOT TO BE TAKEN FROM THIS ROOM

Ex libris
universitatis
albertaensis




*The University of Alberta*
*Printing Department*
*Edmonton, Alberta*

Digitized by the Internet Archive
in 2019 with funding from
University of Alberta Libraries

https://archive.org/details/Clowes1969

THE UNIVERSITY OF ALBERTA

# SEISMIC REFLECTION INVESTIGATIONS OF CRUSTAL STRUCTURE IN SOUTHERN ALBERTA

by

RONALD MARTIN CLOWES

A THESIS

SUBMITTED TO THE FACULTY OF GRADUATE STUDIES

IN PARTIAL FULFILMENT OF THE REQUIREMENTS FOR THE DEGREE

OF DOCTOR OF PHILOSOPHY

DEPARTMENT OF PHYSICS

EDMONTON, ALBERTA

FALL, 1969

THE UNIVERSITY OF ALBERTA

FACULTY OF GRADUATE STUDIES

The undersigned certify that they have read, and recommend to the Faculty of Graduate Studies for acceptance, a thesis entitled SEISMIC REFLECTION INVESTIGATIONS OF CRUSTAL STRUCTURE IN SOUTHERN ALBERTA, submitted by Ronald Martin Clowes in partial fulfilment of the requirements for the degree of Doctor of Philosophy.

## ABSTRACT

The recording of deep crustal reflections at near-vertical incidence along a 90-kilometer continuous profile in southern Alberta has demonstrated the applicability of the seismic reflection technique for research of the lower crustal section. The field procedure included the use of multiple holes and arrays of detectors designed to discriminate against the shot-generated long period surface waves. Velocity or fan-pass filtering is shown to be a very effective means of enhancing individual reflection events.

A method of incorporating the effects of attenuation into synthetic seismograms has been developed. Comparison of the autopower spectra of selected time intervals on field records with similar spectra computed from theoretical seismograms is an effective means of inverting the seismic wave data into models representing the properties of the lower crust. Such studies yield information on the variation of the specific attenuation factor, Q, with depth and the nature of the transition zones which reflect seismic energy. Thin sills of alternating high and low velocity material appear to satisfy all the observational data. The layers are generally less than 200 meters thick.

From an interpretation of the seismograms, a cross section of the crust in southern Alberta is derived. Large structural variations with relief of more than 10 kilometers over horizontal distances of 50 kilometers are found. On the basis of the reflection data and a detailed refraction survey, good evidence is given for major steeply dipping faults in the middle and lower crust. The interpretation indicates that the M discontinuity has similar variations. Combined gravity, magnetic,

refraction and reflection data provide strong evidence for a buried Precambrian rift. From the gravity and magnetic trends, the feature has been traced for several hundred kilometers across southern Alberta and under the Rocky Mountains into British Columbia.

ACKNOWLEDGEMENTS

It is with great pleasure and sincerity that I am able to acknowledge Dr. E. R. Kanasewich for his encouragement and guidance throughout the course of this research.

The gravity stations occupied by the Geophysics Division in 1966-67 and the ground magnetometer survey were run by Mr. Charles McCloughan. His thorough job enabled the compilation of reliable maps. Mr. McCloughan also spent many long hours converting the analog tapes to digital form.

Messrs. Mike Burke and Dave Malinsky of the Geophysics Laboratory did a fine job of organizing, installing and maintaining the field equipment. The efforts of the many persons who assisted with the acquisition of the field data are gratefully acknowledged.

Tenneco Oil and Minerals, Limited and Amerada Petroleum Corporation provided exploration reflection seismograms from the area of this study.

The Gravity Division, Dominion Observatory of Canada, supplied their compilation of Bouguer gravity values comprised of their own base stations plus data supplied by oil companies.

Without the assistance of the Seismology Division, Dominion Observatory of Canada, the refraction survey described in this thesis would never have materialized. They provided the personnel at the shot point as well as two recording crews who did an exceptionally good job.

Financial support for all phases of the research was provided by grants from the Defence Research Board of Canada and the National Research Council.

Throughout the course of his doctoral studies, the writer was the recipient of a Graduate Research Fellowship from the International Nickel

Company of Canada, Limited. Their generous support is greatly appreciated.

Mrs. Kay Baert did an extremely fine job of typing the manuscript. Her willingness to work long hours under the pressure of a deadline is gratefully recognized.

And finally, I would like to acknowledge the patience and understanding displayed by my wife, Gail, especially throughout the last few arduous months.

TABLE OF CONTENTS


| | | Page |
|---|---|---|
| ABSTRACT | | ii |
| ACKNOWLEDGEMENTS | | iv |
| LIST OF ILLUSTRATIONS | | viii |
| CHAPTER I | INTRODUCTION | |
| | 1.1 Why the reflection method? | 1 |
| | 1.2 History of the reflection method | 4 |
| | 1.3 The project | 17 |
| | 1.4 The technique | 21 |
| | 1.5 The field observations | 24 |
| CHAPTER 2 | DIGITAL PROCESSING | |
| | 2.1 Digitization and initial processing | 30 |
| | 2.2 Autopower spectra | 37 |
| | 2.3 The zero-phase band-pass filter | 40 |
| | 2.4 The velocity filter | 45 |
| CHAPTER 3 | CRUSTAL ATTENUATION AND THE NATURE OF THE REFLECTING HORIZONS | |
| | 3.1 The synthetic seismogram with spatial attenuation | 55 |
| | 3.2 Q of the crust | 64 |
| | 3.3 Properties of the crustal reflectors | 75 |

| | | Page |
|---|---|---|
| CHAPTER 4 | INTERPRETATION OF THE DATA | |
| | 4.1 The analog reflection seismograms | 87 |
| | 4.2 The digitally processed seismograms | 92 |
| | 4.3 The refraction seismograms | 99 |
| | 4.4 The gravity and magnetic observations | 101 |
| | 4.5 A buried Precambrian rift | 110 |
| CHAPTER 5 | CONCLUSION | 114 |
| BIBLIOGRAPHY | | 118 |
| APPENDIX | FORTRAN SOURCE LISTINGS OF COMPUTER PROGRAMS | |
| | The velocity filter program | 126 |
| | The synthetic seismogram program | 135 |

# LIST OF ILLUSTRATIONS


| *Figure* | | *Page* |
|---|---|---|
| 1.1 | Location map for the seismic profiles. | 19 |
| 1.2 | Normalized amplitude response curves for a tapered array of 16 geophones, 5 holes with differing charge size, and the geophone-hole combination. | 22 |
| 1.3 | Reproductions of deep reflection seismograms recorded along the Lomond and Blackfoot profiles. | 26 |
| 1.4 | Reproductions of two seismograms recorded in the refraction survey. | 28 |
| 2.1 | Block diagram of analog-to-digital conversion system. | 31 |
| 2.2 | Frequency response of the filters used in the digitization process. | 32 |
| 2.3 | Averaged autopower spectra for selected time intervals of four different seismograms. | 39 |
| 2.4 | Plot of digitized seismic reflection records before and after applying a 7 to 13 Hz. Butterworth digital band-pass filter. | 42 |
| 2.5 | An example of different filters and filtering techniques applied to one seismogram. | 44 |
| 2.6 | Ideal f-k transfer function of a velocity filter. | 47 |
| 2.7 | Application of the velocity filter to synthetic data. | 49 |
| 2.8 | Application of the velocity filter to real data. | 51 |
| 2.9 | An example of signal enhancement by digital data processing techniques. | 53 |
| 3.1 | Autopower spectra for selected time intervals on four field seismograms. | 67 |
| 3.2 | Histogram of the rates of attenuation of frequency as measured from 52 seismograms. | 69 |
| 3.3 | Various quantities computed by the synthetic seismogram program. | 71 |
| 3.4 | Effects of different distributions of Q on the rates of attenuation of frequency for reflections centered about the R and M horizons modelled as first-order discontinuities. | 73 |

| *Figure* | | *Page* |
|---|---|---|
| 3.5 | Autopower spectra for three-second time intervals centered about the R and M reflections on synthetic seismograms. | 78 |
| 3.6 | Details of the models for which the autopower spectra of Figure 3.5 are computed. | 79 |
| 3.7 | Comparison of the autopower spectra for two-second intervals centered about the R and M reflections on field seismograms with spectra computed from reflections on synthetic seismograms. | 83 |
| 4.1 | Residual total magnetic intensity, Bouguer gravity and surface topography along the seismic profiles. The reflection seismic cross section. | 89 |
| 4.2 | Velocity filtered reflection record section along a 90-kilometer profile. | 94 |
| 4.3 | Velocity filtered seismograms from Figure 4.2C showing evidence for the central fault in Figure 4.1. | 98 |
| 4.4 | Traveltime curves for $P_g$ and $P_n$ from profiles A and B (Figure 1.1). | 100 |
| 4.5 | Residual $P_g$ and $P_n$ traveltime curves for Profile C (Figure 1.1). | 102 |
| 4.6 | Gravity station locations for the map of Figure 4.7. Outline of the assumed boundaries of the ancient rift valley. | 104 |
| 4.7 | Bouguer gravity anomaly map for southern Alberta and southeastern British Columbia. | 105 |
| 4.8 | Residual total magnetic field intensity map for southern Alberta and southeastern British Columbia. | 107 |
| 4.9 | Generalized crustal section across southern Alberta. | 108 |

# CHAPTER 1

## INTRODUCTION

### 1.1 Why the reflection method?

The crust, or outermost shell of the earth, constitutes only about 1.5 percent of the total volume and one percent of the total mass of the earth. However, this relatively thin portion of the planet is of much greater importance to our understanding of the earth's dynamics and historical evolution than such figures might suggest. Beneath the earth's crust, whose base is generally defined by the Mohorovičić seismic discontinuity, lies the upper mantle. The crust completely encloses this part of the earth and all regions below it—the lower mantle, the outer and inner cores. Thus the direct observation of these deeper domains is prevented, except for samples which are derived from the mantle by volcanic activity. Consequently we must rely on indirect observations. But since these measurements are necessarily made on or near the surface of the earth, the effects of the crustal section are included in the observations. Before unravelling the structure of the deep earth, it becomes necessary to know to what extent the shallow earth has affected any observations. In many cases this requires detailed knowledge concerning crustal structure.

As evidenced by the numerous mountain chains, ocean ridges and deep-sea trenches, the crust itself is continually undergoing mammoth deformations. Some aspects of this activity, notably earthquakes, have proven catastrophic. By studying the structure of the earth's crust, can we help to understand the underlying causes for such phenomena? For example, will we be able to give warnings of future earthquakes? The answer is hopefully "yes". But this requires a knowledge of not just the general characteristics, but the detailed anatomy of the crust, as well

as the upper mantle.

Of more economic importance, we might ask what role the tectonic evolution of the crust has played in the formation and distribution of ore and mineral deposits. Are there any correlations between deep-seated geological phenomena and the occurrence of known mineral reserves? Once again it is only details of crustal structure, as deduced by all possible geophysical methods, which can help to answer the question.

The importance of the aforementioned and other considerations have not been overlooked by the scientific community. Such cooperative ventures as the International Geophysical Years, Project VELA UNIFORM and the Upper Mantle Project, have provided tremendous impetus to geophysical investigations of the earth's crust and upper mantle. Much has been accomplished; much more remains to be done.

The geophysical studies of crustal structure have normally involved one or more of the following methods of investigation: refracted body waves and surface waves from earthquakes and from controlled explosions, gravity and magnetic analyses, electromagnetic studies both of natural and of induced fields, and geochemical observations. Of these methods, refraction seismology using controlled explosions has proven most successful in delineating gross crustal structure. However, the wavelengths of the refracted waves limit the precision of the method for detailing the fine structure. As well, velocity decreases cannot be directly observed, but must be inferred by other means. Thus none of the foregoing methods has the analytic power necessary for high resolution studies of the deep crust.

The seismic reflection technique is singularly suitable for such studies. Observed wavelengths of the reflected waves are several times

shorter than their refracted counterparts, thus increasing the resolution of the method. Common exploration seismology techniques such as continuous depth profiling and expanding spreads for velocity information provide means by which our detailed knowledge of the deeper crust can be significantly increased. Spectral analyses of waves reflected from deep horizons can provide information regarding the nature of the reflective process. In turn this may increase our understanding of the physical processes which can occur in the lower crust. By combining the results of various analyses with those from theoretical studies it should prove possible to place limits on elastic properties of this outer shell. Consequently, the seismic reflection method can provide a powerful tool for extending our knowledge of crustal structure.

Some of the expectations for the reflection technique can be attributed to advances in scientific technology over the past decade. Magnetic tape recorders, both analog and digital, provide systems with wideband recording and a dynamic range far exceeding that of the photographically recording apparatus. The data may then be played back through various types of filters to enhance the desired signals relative to the unwanted noise. Digital computers have greatly facilitated the handling of large quantities of data and enable the implementation of sophisticated data processing techniques. Together these facilities make the effective separation of reflected energy on the seismogram a more distinct possibility.

But the reflection method is not without its limitations. Considerable effort must be expended in eliminating noise and surface waves which may obscure the reflected energy arriving at near-vertical incidence. It is also necessary to cover an area in detail if miscorrelations of

reflecting horizons are to be avoided. This causes the method to be very expensive and time consuming. However by intensively studying a few small areas, then combining the results with broad-scale gravity, magnetic and refraction surveys, it should prove possible to extrapolate the results over a widespread area. This approach has been followed in the present research.

## 1.2 History of the reflection method

The use of near-vertical incidence reflected energy as a means of investigating total crustal structure is a quite recent innovation. As far as the writer knows, until 1968 the University of Alberta was the only North American institution systematically applying deep reflected waves as a means of crustal investigation. The situation is quite different in Europe where for a number of years German and Russian geophysicists have been using the method to advantage. In contrast to this fact, for more than 35 years seismic reflection prospecting has been successfully used in North America to discover many major petroleum reserves located in the upper sedimentary strata. Probably the first application of the reflection method of seismic prospecting took place in Oklahoma on June 4, 1921 (Schriever, 1952). A number of scientists—Dr. J. C. Karcher, Dr. W. P. Haseman, Dr. I. Perrine and Mr. W. C. Kite—from the University of Oklahoma undertook this preliminary experiment to test whether the fundamental idea had any validity. Financial problems slowed the introduction of the method to the general industry, but within a decade it had achieved recognition as a viable technique for the discovery of oil and gas deposits. No one involved with this initial work could have foreseen the success which was to follow in the next few decades. Reflection seismology is by far the most effective and widely

used of all petroleum prospecting methods (Tucker, 1968).

While development of the reflection technique for seismic prospecting has continued, the extension of the method for studying crustal structure has been slow. The first published report of reflections from the lower crust was that of Junger (1951). By extending the recording time in routine seismic prospecting to ten seconds, reflections in the time range of 7.0 to 8.5 seconds were recorded in Big Horn County, Montana. On the basis of repeatable results and identical reflections for one shot from perpendicular spreads, Junger effectively argues that the energy is arriving from some interface in the deep basement. By assuming a velocity distribution, the depth to this horizon is placed in the range from 18 to 21 kilometers. Many other isolated instances of the recording of deep crustal reflections have since been reported. Those published before 1961 are well documented by Steinhart and Meyer (1961). In a similar review, James and Steinhart (1966) have chronicled the results of reflection crustal studies from 1960 to 1965 in many different countries.

Geophysicists in the Soviet Union and in Germany have had considerable success with seismic programs which include the recording of subcritical reflected waves. Before considering their work, a few more recent cases of reported deep reflections in Europe will be mentioned. Båth and Tryggvason (1962) reported on the first seismic investigations of crustal structure in Fennoscandia. Their experiment was designed to record near-vertical incidence reflections from discontinuities in the crust or upper mantle. The sources of energy were large quarry blasts (360 to 8000 kilograms of explosives) and the receivers were individual vertical geophones whose output was recorded on refraction apparatus.

Considering the experience of our own work and that of other investigators, it is not surprising that with their method the results were inconclusive. Chamo (1962) reported on a feasibility study to determine whether the reflection technique could be used to investigate deep crustal structure. The results were positive for depths up to 15 to 20 kilometers and it was suggested that further work on the procedure in the Turkmen S.S.R. be carried out.

In Greece, Papazachos et al. (1966) have reported on crustal structure in southeastern Europe, and particularly about Athens. Part of their experiment included recording of near-earthquakes ($\Delta$ = 0 to 80 kilometers) on a three-component short-period seismograph station. By a careful analysis of the resulting seismograms, many events which were attributed to reflections from within the crust were noted and the squares of the travel times were plotted against the squares of the distances. Their resulting curves indicate a three-layered crust, an interpretation which agrees with their conclusions from the analysis of refracted and direct waves. No indication is given as to how many events may have been picked that wouldn't fit the plots. In a similar study, White (1969) reported on some unusual seismic phases recorded in South Australia. From a small network of seismograph stations set up to monitor local earthquakes, a phase reflected from the Mohorovičić discontinuity was regularly recorded and identifiable out to a distance of $\Delta = 2^{\circ}$. In addition some converted phases of the S to P type reflected from the M discontinuity were found. It is important to note from such studies that with good instrumentation, reasonable evidence is provided for the recording of sub-critical reflected arrivals from within the crust when the source is a shallow, low-magnitude earthquake.

The first investigations in the U.S.S.R. concerning the recording of deep reflected waves were carried out by G. A. Gamburtsev and others as early as 1939 (Beloussov et al., 1962). However the utilization of such waves does not appear to have been realized until the 1950's and the development of deep seismic sounding (DSS) methods. In 1956 detailed investigations were begun. These made use of the continuous profiling method with a large number of shot points and closely spaced seismometer groupings, thus enabling simultaneous study of the sedimentary strata and the deep crust. Such deep seismic sounding does not rely on any one seismic method for interpretation. Wave types generally used are the refracted plus sub- and super-critically reflected compressional waves, but some efforts are made to employ converted, transverse and surface waves as well. Attention is paid to both amplitude (dynamic) and velocity (kinematic) properties of the arrivals in order to achieve the best application of the recorded data. A survey of most aspects of the entire DSS program is presented in a book recently translated from the Russian (Zverev, 1967). In this monograph, various papers indicate Soviet methodology up to about 1962. Instrumentation is described, data is presented, analysis methods are shown and the resulting interpretations are given. This collection probably provides the most comprehensive accumulation of papers concerning the Soviet Union crustal study program presently available in English.

In an earlier paper, Kosminskaya and Riznichenko (1964) provided a summary of the results from seismic studies in various parts of Russia. Their review, while not giving the details that were possible in the book, does include information on observational methods, on the use of refracted and reflected waves and on the crustal cross sections obtained.

They also discuss the nature of crustal stratification in a section similar to a paper by Kosminskaya (1964). A very brief summary of the activities in the DSS field by all East-European countries is given in a report prepared by Kosminskaya (1965). As is usual in the Soviet method of crustal investigations, the use of reflected waves is dealt with as only one part of a comprehensive crustal study program.

An exception to this generalization is an article by Beloussov et al. (1962) which deals specifically with the recording of deep reflected waves. The experiment concerned a crustal structure study using a system of observations that ensured a continuous correlation of sub-critically reflected energy. It is worthwhile to mention that their method required a grouping of sources and receivers with dimensions similar to those the present research found necessary. The results of their investigations indicated a number of reflecting horizons within the lower crust and even in the upper mantle. But their detailed summary of the reflections shows that individual phases could not be continuously correlated over more than about ten kilometers, although the 'grouping' with depth of reflecting horizons was concentrated within a few kilometers. Some indication of fractures in the deep crust was given by this paper.

In the first article of the monograph previously mentioned, Fursov and Yaroshevskaya (1967) include a section on the recording of sub-critically reflected waves using magnetic tape recorders. They exhibit a number of records with reflected energy in the time range of 12 to 16 seconds. These indicate that certain amplifier characteristics are preferable and replaying the tapes with mixing is advantageous for the enhancement of reflected signals. Khalevin et al. (1966) also

point out that mixing improved the signals from deep reflectors. They show no examples of seismograms but give a crustal cross section for the Middle Urals based on DSS data. This cross section depicts the crust as being horizontally layered, but non-continuously, and of block structure with a number of reflecting horizons. Zones of faulting within the lower crust and on the Mohorovičić discontinuity are indicated. Considerable structural relief is suggested, the maximum depth variation of the Moho lying between 33 and 47 kilometers over the extent of the 450 kilometer profile.

While geophysicists in the Soviet Union have been developing their DSS program, including the study of deep reflected waves, German geophysicists have been the most active in using such waves for crustal investigation. In cooperative studies among geophysicists from oil companies, governmental agencies and university groups, thousands of reflection seismograms with coherent energy arriving at long travel times have been recorded in Germany. One of the first reports from such efforts was that of Dohr (1957) in which more than 250 deep reflections recorded in the course of routine seismic prospecting were observed. Because the deep reflections could not be phase correlated over more than a few kilometers, Dohr suggested that a statistical analysis could still yield a reasonable interpretation. Such a method involved the construction of histograms in which the number of observed deep reflections within a short time interval (0.1 or 0.2 seconds) from seismograms in a specific region were plotted against arrival time. Subsequent to this work, nearly all German interpretations of events reflected from the lower crust have followed the same procedure. A question might be raised as to whether such a statistical approach was absolutely essential in these cases and

that possibly some reflections could have been continuously correlated over considerable horizontal distances.

An exception to Dohr's approach is given in a paper by Krey et al. (1961). In an investigation using seismic reflection measurements to determine whether tectonics of the sub-basement could be correlated with known regions of ore veins, three profiles were recorded in the Siegerland district. Reflections from the immediate sub-basement were generally weak and uncorrelatable, but much to their surprise, reasonably strong reflections occurring at traveltimes of 5 to 9 seconds could often be well correlated. These led to the discovery of extensive horizons and of large-sized structural features, including faults, in the lower crust (approximate depths of 10 to 25 kilometers). Since none of the German review papers mention the methodology of recording, other than it being an extension of routine seismic investigations, it is worthwhile to mention the experimental techniques revealed by Krey et al. As receiver arrays, twelve geophones grouped in a star-shaped pattern were selected. The source generally consisted of about 150 kilograms of explosive per shot, distributed among at least six boreholes of about 15 meters depth. The experiment was unsuccessful in showing a relationship between the vein features and tectonics in the basement. However the authors state that the deep structure and zones of fracturing could be correlated with the regions of occurrence of the ore veins.

In a general review of crustal structure in Western Germany, the German Research Group for Explosion Seismology (1964) included a brief section on deep reflection investigations. A good list of references is given and one 15-kilometer profile is presented. Although the correlation of one phase over more than a few kilometers was not possible, the profile

shows the accumulation of reflections at certain levels. Such levels are then related to different crustal layers interpreted from refraction seismology. In a recent paper Dohr and Fuchs (1967) give a comprehensive review of deep crustal reflections in Germany. By displaying examples of seismograms, they indicate that it is preferable and advantageous to employ groups of about twelve seismometers with higher natural frequencies than refraction instruments in order to successfully record and identify deep reflections. Dohr and Fuchs present good arguments and evidence for the existence of the deep reflections in light of criticism, which is enumerated, against the reality of such events. Arguments are also made in favor of their statistical approach to the interpretation and some questions are raised as to the physical significance of their results. In the course of interpretation, it is assumed that multiple reflections have no significance at the long traveltimes of their observations. In contrast to such an assumption, our investigations have shown that reverberations within the sedimentary layers can produce multiple reflections which have significant amplitude within one second of the onset of a primary event (Clowes et al., 1968).

The question of the physical properties of the deep crustal reflectors and their relation to the observed reflections is considered in two subsequent papers by Fuchs (1968, 1969). In the more recent paper, he concludes from the German data that levels of accumulated reflections cannot represent first order discontinuities nor can they represent transition zones of monotonically increasing velocity with depth. By use of synthetic seismogram studies and other arguments, it is shown that laminated transition zones with a series of velocity reversals and increases most nearly give results concordant with the observations.

In order to supplement and confirm the findings from near-vertical incidence profiling, the German Research Group for Explosion Seismology (1966) decided to record a wide-angle profile (sub- and super-critical reflections from 0 to 150 kilometers) about a common subsurface point. This reference describes the field procedures and exhibits some record sections with reflections from the Moho. In some respects this work is similar to the initial deep reflection program at the University of Alberta. An areal pattern of shot holes was used, with a total dynamite charge ranging from 45 to 200 kilograms. Receiver arrays using four vertically recording geophones, with group spacings of about 100 meters, were generally laid in a line. In order to distinguish between P and SV waves, the output from one vertical- and one horizontal-component geophone at the same location was recorded. Meissner (1966) presented a preliminary interpretation of the resultant profile. Four different horizons, corresponding to the basement, the Conrad[1] discontinuity, a sub-Conrad reflector and the M discontinuity have been analysed on a $T^2 - X^2$ plot. The strongest amplitudes were for reflections from the Moho. From a consideration of irregular traveltime arrivals which did not exactly fit the expected hyperbolic curve, Meissner concludes that velocity gradients over about two kilometers, as opposed to sharp discontinuities, explain the discrepancies best. In a later paper, Meissner (1967*a*) considers these problems in a more complete study. He points out the advantages of greater amplitudes for wide-angle measurements than for near-vertical ones, especially as deeper interfaces are being investigated. This is especially true in the region of the

---

[1]In Europe, the Conrad discontinuity is generally regarded as the top of an intermediate layer below which the crust is more basic.

critical distance where the writer refers to the large amplitudes expected for "diving waves" (waves for which the turning point of the ray is within the gradient zone). Rather strong proof is given for the existence of these diving waves. The conclusions from this study indicate that the transition zone at the depth of the M discontinuity is comprised of a series of lamellas with material of stepwise different velocity and each less than about 150 meters thick. Meissner points out that temperatures at this depth are in the region of the melting points of most components of sialic and even of some gabbroic material. Thus he postulates that the transition from sialic to basic and ultrabasic matter is stepwise, interrupted by rhythmically arranged series of partial melts with lower velocities. For a more comprehensive study of the interpretation of the wide-angle measurements, Meissner (1967*b*, in German) should probably be consulted.

Since the review by Steinhart and Meyer (1961), further instances of the recording of waves reflected from within the crust have been reported in North America. Although James and Steinhart (1966) have updated the review, some results are worth repeating and a few others should be mentioned. Narans et al. (1961) carried out an experiment in Utah to determine the possibility of obtaining normal incidence reflections from the lower crust. The quality of the seismograms was not very good so a statistical approach, similar to that used in Germany, was applied. However they were considering only ten records in contrast to the thousands examined by the German geophysicists. From the histogram, four to six possible reflections could be noted and two of these were at times which in depth would correlate well with known refracting horizons. In a paper discussing crustal structure in New Mexico as determined from the GNOME

underground nuclear explosion, Stewart and Pakiser (1962) suggest that some arrivals can be attributed to sub- and super-critical reflections from within the crust and from the M discontinuity. This identification is based on reflection traveltimes calculated from the crustal model. By extending the recording time in routine seismic petroleum prospecting, Robertson (1963) found a continuous reflecting horizon in the sub-basement. He argues quite effectively that the arrivals are true normal incidence reflections and estimates that the depth of the horizon varies from 7.5 to 14 kilometers over the 29-kilometer length of the profile. Roller (1965) reported on the results of a reversed seismic refraction profile in which reflections beyond the critical angle were recorded from an intermediate and the M discontinuity. In an interesting study, Sanford and Long (1965) have found crustal reflections on about 25 percent of hundreds of high-magnification seismograms produced from microearthquakes near Socorro, New Mexico. The best interpretation of two sharp arrivals which are found 2.5 and 5.0 seconds after the direct S wave makes them the reflected phases $S_xP$[1] and $S_xS$[1] from a discontinuity in the crust at a depth of 18 kilometers.

Dix (1965) conceived a detailed experiment for recording near-vertical incidence reflections in a region of the Mojave Desert having a very thin sedimentary section. Experimentally the procedure used three to five holes per shot with a total charge of 100 to 300 kilograms. Fourteen-cycle geophones were set out in pairs at each recording station and normal reflection prospecting instrumentation was used. To ensure

---

[1]The nomenclature for these phases refers to transverse waves converted to longitudinal waves upon reflection at a depth of x kilometers ($S_xP$) or transverse waves reflected at a depth of x kilometers ($S_xS$).

the arrivals were true reflections, some cross-spread recordings were made. Many good quality reflections were observed but some difficulties of interpretation are mentioned. One strong series of pulses corresponds to a depth of 25 kilometers, the depth to the Moho in that region. Perret (1967) reported the recording of vertical incidence deep reflections on four special high sensitivity vertical accelerometers in a borehole offset just 166 meters from the Salmon underground nuclear explosion. The data were recorded on magnetic tape and digitized. By time shifting and compositing, the individual reflections are shown quite clearly. In addition to the basement contact, interfaces were determined at depths of 13, 17.1, 33 and 34.6 kilometers. On the basis of a crustal study in the area, the last depth is associated with the M discontinuity and Perret suggests that the existence of the two closely spaced deep reflections implies a transition zone at the crust-mantle boundary.

The work reviewed in the last two paragraphs has provided good evidence for the existence of crustal reflections from a variety of sources: relatively small chemical explosions, nuclear explosions and near-earthquakes. The fact that reflections are recorded from such different source types and in widely separated areas strengthens the contention that horizons of some form within the crust are able to reflect sufficient coherent energy.

However until quite recently, the University of Alberta was the only North American group systematically using the seismic reflection technique for the investigation of crustal structure (Clowes et al., 1968; Kanasewich and Clowes, 1968; Kanasewich et al., 1969; Clowes and Kanasewich, 1969). But in the summer of 1968, Professor R.A. Phinney of Princeton University began a program which would use reflected waves to determine crustal structure. For this initial work one crew from the University

of Alberta joined them in a cooperative experiment. Reflections from deep within the crust were successfully recorded near Riverton, Wyoming. Realizing the success of the technique in continental areas, the group at Princeton undertook a similar project at sea. The experiment was successful and demonstrated that their method could be used to investigate structure at least to depths of the Moho. Important to the success of the project was the utilization of a receiver array with low noise level, recording of data on FM magnetic tape and the ability for subsequent digitization which allowed the application of signal enhancement techniques, particularly beam forming (velocity) filters. Perkins (1969) and Phinney and Perkins (1969) have reported on this preliminary study. It is worthwhile mentioning that the Seismology Division of the United Kingdom Atomic Energy Authority is preparing an experimental program to record reflection arrivals from the oceanic crust (Thirlaway, personal communication). As well, the Bureau of Mineral Resources in Canberra, Australia, presently has a group actively and successfully working on deep crustal reflections (Cleary, personal communication).

The detailed seismic studies by geophysicists in the Soviet Union, the thousands of seismograms examined and interpreted by researchers in Germany, the success of the program at the University of Alberta and all the other preceding documentations suggest that reflections from within the earth's crust can be obtained and used to determine crustal structure. Even the earlier critics of such work (Steinhart and Meyer, 1961) are accepting this contention, but with some reservations (James and Steinhart, 1966). However, some researchers remain unconvinced that reliable subcritical reflections are recorded from the M discontinuity (Knopoff, 1969). Other geophysicists are suggesting that the method of reflection

seismology, utilizing both normal incidence and wide-angle reflections, should be applied to a much greater extent in the future in order to obtain a more detailed picture of the anatomy of the crust (Francis, 1969).

## 1.3 The project

In 1964, the Geophysics Division of the Department of Physics started an experimental program to investigate the possibility of obtaining reflected seismic energy from boundaries within the lower crust and from the Mohorovičić discontinuity. The area chosen for the experiment was an east-west line in southern Alberta where the general crustal layering was known from the results of reversed refraction profiles (Cumming et al., 1962, and Maureau, 1964). For this initial work a modification of the expanding reflection profiling technique about a common depth point (Musgrave, 1962) was employed, with the hope of obtaining average vertical velocities to any reflecting interfaces. The results of this preliminary attempt were very gratifying and were reported by Kanasewich and Cumming (1965).

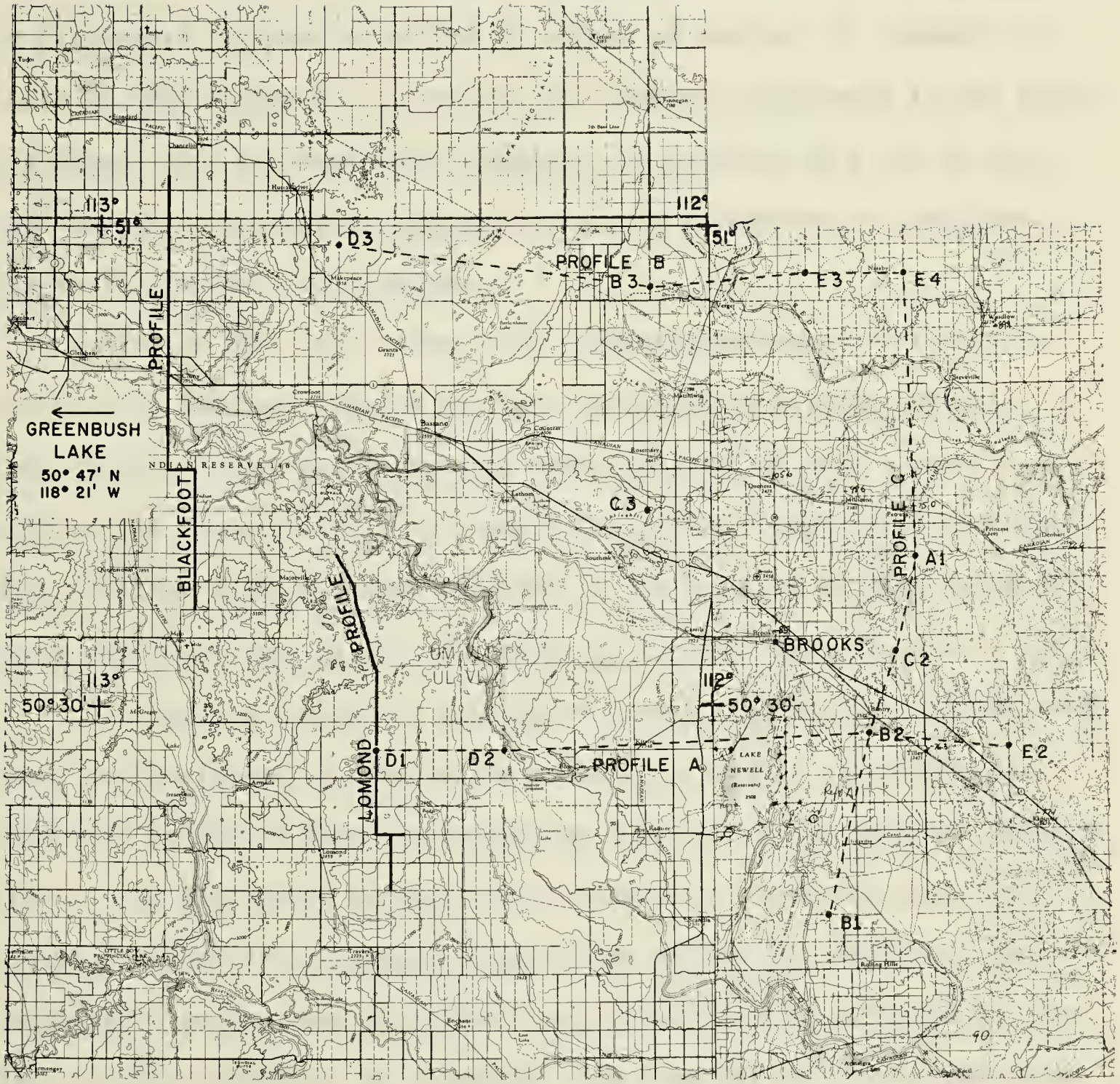
During the following summer, efforts were directed toward extending the expanding spread profile and toward obtaining crustal reflections in regions separated by as much as 120 kilometers. While many problems were encountered, this work could also be termed successful. At the same time the compilation of a Bouguer gravity anomaly map for southern Alberta was begun. Subsequent to this field program, some theoretical seismogram studies of transition layers were initialized. As well, the seismic data from 1964 had been digitized thus enabling the application of signal enhancement techniques by digital processing. For this preliminary study, compositing of traces from a common reflection

point was the principal technique followed. The foregoing paragraphs are a very brief summary of the content of the present writer's M.Sc. thesis (Clowes, 1966).

Because of the success of this initial experiment and because some evidence, from both seismic and gravity anomalies, had been obtained for a fault in the lower crust, we decided to make an intensive study of this region in the summer of 1966. The method by which this was accomplished was continuous seismic reflection profiling, whereby 'continuous' is meant continuous sub-surface coverage of any regions which might reflect incident energy. The resulting profile covered approximately 40 kilometers, beginning at the NE corner of Section 34, Township 15, Range 19 W4M; proceeding north but angling slightly west to follow roads and trails in the area; finally terminating at the NE corner of Section 31, Township 19, Range 19 W4M. To this line was appended the name "Lomond profile" and it is so indicated in Figure 1.1. About three weeks of field work were necessary to obtain the data along the Lomond profile. During the same summer, further gravity station locations were occupied and the data from these were added to the previous survey and the general compilation of gravity values kindly supplied by the Gravity Division, Dominion Observatory of Canada. In addition a start was made on covering much of southern Alberta with a network of ground magnetometer stations to supplement the gravity and seismic data.

The reflections obtained from the Lomond profile were of good quality and showed considerable structural relief in the lower crust and probably on the Mohorovičić discontinuity. Thus the following summer it was decided to extend the continuous reflection profile northward toward a large Bouguer gravity anomaly which suggested further possible structure.

Figure 1.1 *Location map for the seismic profiles. The heavy dark lines are the two continuous reflection profiles. The dots represent locations of the recording stations for the refraction survey. Dashed lines show the profiles considered for the interpretation of the refraction data.*


GREENBUSH LAKE
50° 47' N
118° 21' W
BLACKFOOT
PROFILE
LOMOND
PROFILE
PROFILE B
PROFILE A
PROFILE C
D3
B3
E3
E4
C3
A1
BROOKS
C2
B2
E2
D1
D2
B1
LAKE NEWELL
113°
51°
112°
50° 30'
INDIAN RESERVE 146
CANADIAN PACIFIC
CRAWLING VALLEY
HUNTING HILLS
LITTLE BOW PROVINCIAL PARK
Rolling Hills

To avoid a difficult crossing of the Bow River it was necessary to offset this second line, named the "Blackfoot profile", 18 kilometers to the west. Specifically the profile started at the NE corner of Section 9, Township 19, Range 21 W4M, ran north for 14.5 kilometers where it made a 3.2 kilometer jog to the west and then proceeded north for an additional 32 kilometers terminating at the NE corner of Section 17, Township 24, Range 21 W4M (Figure 1.1). Because of increased efficiency in the field procedure, only two weeks were necessary to complete this set of data. Together the two profiles represent about 90 kilometers of continuous sub-surface reflection coverage.

Also in 1967, the survey with ground magnetometer stations was extended in southern Alberta and into southeastern British Columbia, thus enabling large-scale magnetic trends to show up more clearly. As well it was found possible to augment the gravity compilation with data from stations which had been occupied in southeastern British Columbia on an earlier survey by the University of Alberta (Garland et al., 1961).

To further extend the methods of geophysical analysis of the area under consideration, a cooperative seismic refraction experiment was made with personnel from the Seismology Division of the Dominion Observatory. Four 4500-pound charges were detonated in Greenbush Lake, British Columbia, about 450 kilometers west of the reflection profiles. Some recording stations were positioned on a broadside arc, parallel to, but east of these profiles, at locations such that the critically refracted energy would be incident from the crustal layering directly below the profiles. Other stations were positioned in the same region but in-line so that apparent velocity values for the refracted waves could be obtained. The locations of the recording instruments which provided useable data

and the designations of the profiles are also shown in Figure 1.1.

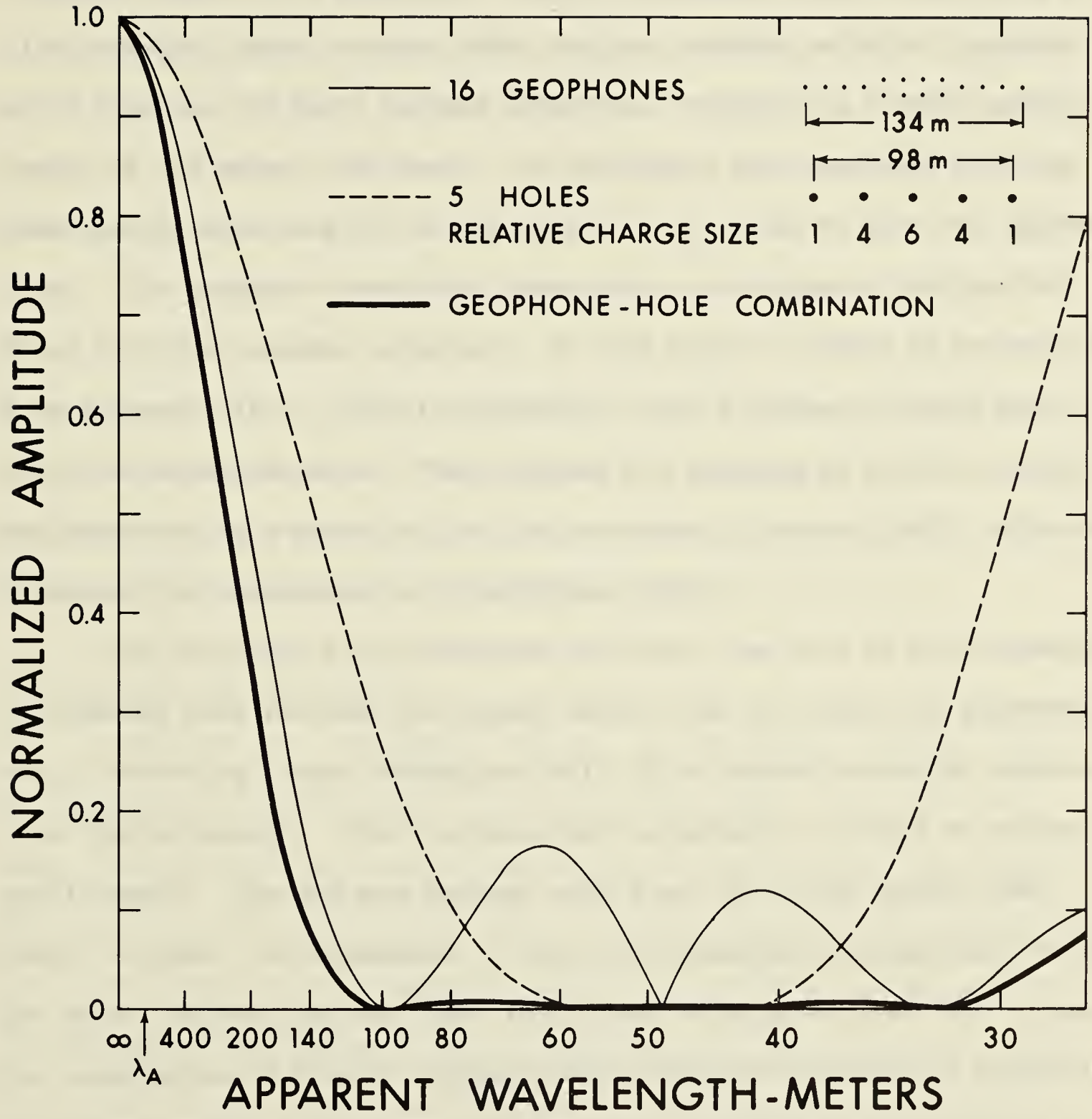
By combining the results of these various methods of geophysical investigation, it proved possible to confirm interpretations made by any one method and at the same time extrapolate detailed structure obtained from the reflection data over a more widespread area.

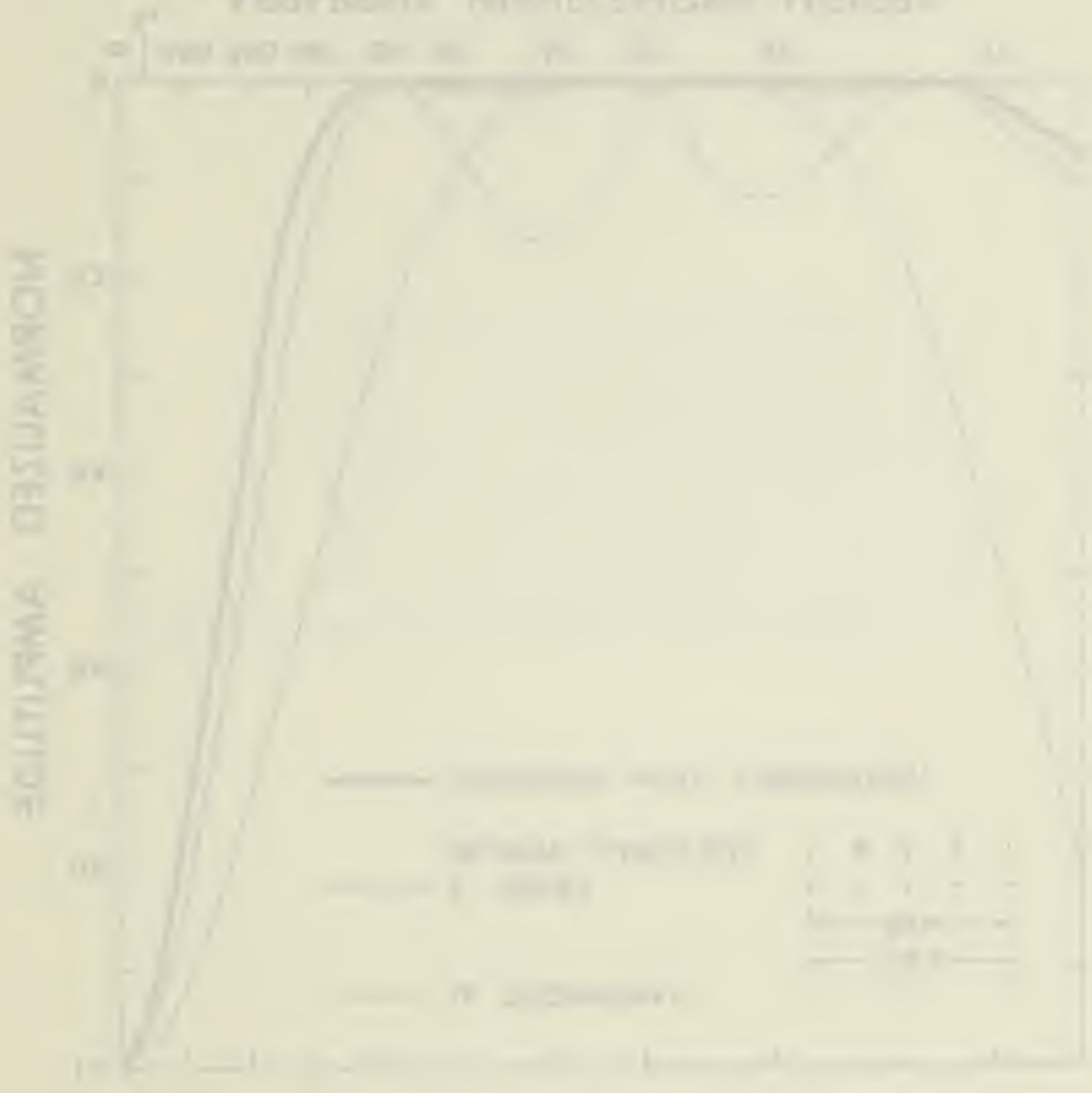
## 1.4 The technique

Clowes (1966) described in detail the instrumentation and methods utilized in the deep crustal reflection program. However, certain modifications made for the subsequent field projects in 1966 and 1967 should be mentioned and the important facets of the method can withstand repetition.

The generally good quality of the field data can be attributed principally to the use of specially designed arrays of sources and receivers. Before implementing the field program, theoretical amplitude responses of various combinations of hole and geophone arrays were computed using a method adapted from antenna theory (Savit et al., 1958). Figure 1.2 illustrates the linear system of seismometer and hole patterns which were generally used, together with their normalized amplitude responses. The combination effectively discriminates against incoming waves with apparent wavelengths small relative to those of the desired signals. The "relative charge size" indicated on the figure was determined by a binomial distribution which approximates the desirable spectral characteristics of a Gaussian function. Typically the amount of explosives planted in the five holes was 2.3, 9.1, 13, 9.1 and 2.3 kilograms (5, 20, 30, 20 and 5 pounds), respectively. In regions where the energy coupling of the explosion with the ground was very good, these quantities were sometimes reduced by one half.

Figure 1.2 *Normalized amplitude response curves for a tapered array of 16 geophones, 5 holes with differing charge sizes, and the geophone-hole combination. The arrow at* $\lambda_A$ *indicates the shortest apparent wavelength of the desired signals as determined from seismograms.*


1.0
0.8
0.6
0.4
0.2
0
AMPLITUDE
NORMALIZED
16 GEOPHONES
134 m
98 m
5 HOLES
RELATIVE CHARGE SIZE 1 4 6 4 1
GEOPHONE - HOLE COMBINATION
∞
λA
400 200 140 100 80 60 50 40 30
APPARENT WAVELENGTH - METERS



The type of receiver array which could be used was restricted by the number of geophones per take-out, since field efficiency had to be considered, and by the fact that only pre-made strings, each consisting of four geophones, could be rented. These considerations resulted in a 'tapered' array of 16 geophones. Twelve seismometers were laid along a line symmetric about the main cable station location and with a spacing of 12.2 meters (40 feet) between detectors, resulting in a total spread length of 134 meters (440 feet). An additional four geophones with the same spacing were laid out at the center of the group to give the tapered array. The geophones comprising these arrays consisted of Electro-Tech EVS-4 7-1/2 Hz. seismic detectors. At this point it should be reiterated that Beloussov et al. (1962) successfully used a system of arrays much like that described here. They regarded the grouping of seismic sources and receivers as a necessity for the isolation of sub-critically reflected waves and the suppression of interference waves.

For the project of continuous profiling, two sets of truck-mounted instruments each recorded the ground motion from six arrays of geophones, the 12 resulting traces forming one half of the normal petroleum exploration 'split-spread'. Thus two shots were necessary to record an entire split-spread. The distance between arrays was set at 292 meters (960 feet), so that 1.61 kilometers (1 mile) of subsurface coverage was recorded per shot. In some earlier work, twice this distance was used but it made the correlation of steeply dipping phases across one record too difficult. The data from the arrays were simultaneously recorded on photographic film and on Precision Instruments 6-channel FM tape transports, with a seventh channel for timing purposes. These data were later digitized in the laboratory using our own analog-to-digital conversion facilities. In

addition to the array data, three Hall-Sears HS-10 2 Hz. geophones were used to record vertical and horizontal components of earth motion on the photographic film. In general filters on the amplifiers were set so that energy above 24 Hz. was attenuated at a rate of 24 db per octave. The Texas Instruments recording system used does not include a low-cut filter so the low frequency attenuation was essentially that of the 7-1/2 Hz. geophones. No automatic gain control is incorporated into the instrumentation so that data between 0 and 4 to 6 seconds generally exceeded the dynamic range of the amplifiers.

The experimental method just described proved quite successful for recording reflected waves from the lower crust. In retrospect it was found that at least one set of instruments which recorded the reflections over a wider range of frequencies, perhaps by a factor of three or four, and also included some type of calibrated automatic gain control would have been extremely valuable for the subsequent interpretation.

## 1.5 The field observations

More than 100 seismograms from the two continuous profiles have been recorded photographically and on FM analog tape. The quality of these field observations varied from very good to very bad, but generally they were of acceptable quality (i.e., reflected energy could normally be seen on the photographic monitors). Changing shot-hole conditions with the resultant differences in energy coupling (each set of boreholes had to be used at least twice) and variation in the near-surface unconsolidated layers on which the geophones were planted probably contributed significantly to the variation in quality of the reflections. One further major contribution to this variation was likely due to the shape of structures being investigated—concave or convex reflectors would cause

focussing or spreading, respectively, of any reflected energy. Thus the intensity of recorded wavelets could vary quite rapidly along even a relatively short distance. The quality of some of the seismograms was severely reduced by high amplitude 60 Hz. signals whenever it was necessary to lay a string of geophones near a commercial power line.

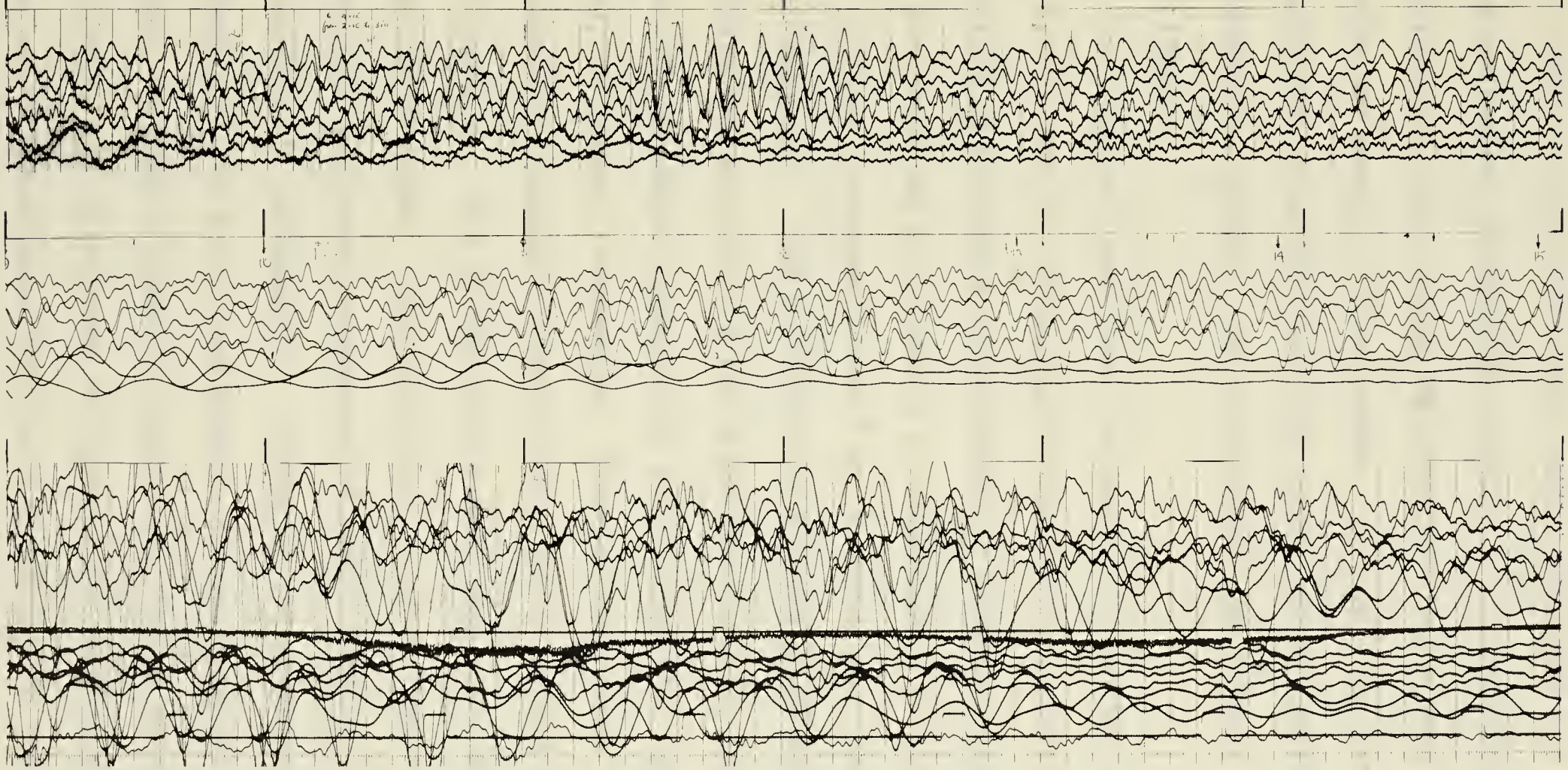
In Figure 1.3, reproductions of some of the originally recorded seismograms are illustrated. This diagram attempts to indicate the variation in quality of the recordings. The upper three sets of traces are from different regions on the Lomond profile and show examples of good, average and poor quality seismograms, respectively. The lower record is an example of a good quality recording from the Blackfoot profile. For each set of traces illustrated, the upper six channels are the output from the geophone arrays and the following three channels represent ground motion obtained from single 2 Hz. seismometers recording vertical, radial and transverse motions, respectively. A duplicate of these nine traces with a fourfold reduction of gain was simultaneously transcribed on the lower half of each record, but these are not shown in the figure except on the poor quality seismogram. Since the instrumentation does not allow automatic gain control, such channels can be used for interpretation if the attenuation factors were set too low and excessive amplitudes were recorded on the high gain traces. Only the array data with normal attenuation were recorded on magnetic tape.

As evidenced by the illustration, it was usually possible to identify some reflections on the photographic seismograms and thus make a preliminary interpretation. Although normal moveout is insignificant at the traveltimes shown, in many cases the reflected events are exhibiting considerable stepout, in both directions on the same recording.

Figure 1.3 *Reproductions of deep reflection seismograms recorded along the Lomond and Blackfoot profiles.*

TIME (SECONDS)

9 10 11 12 13 14 15



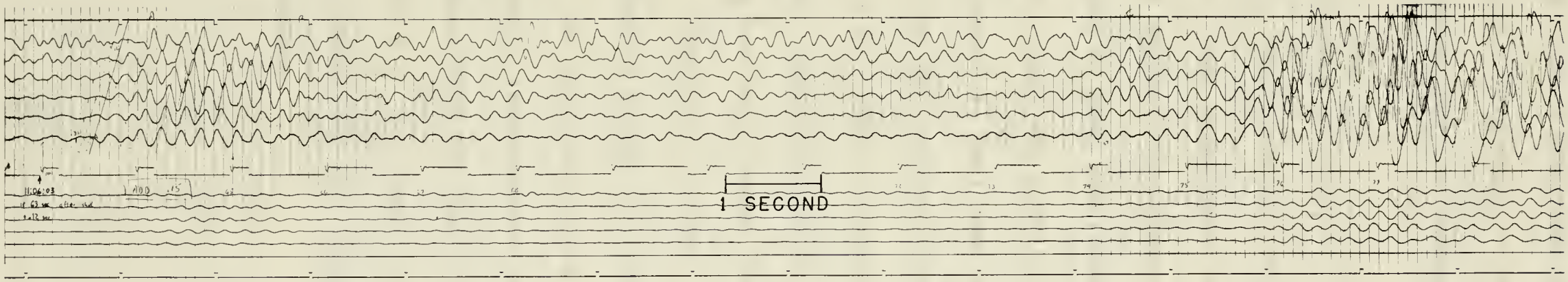
7 8 9 10 11 12 13

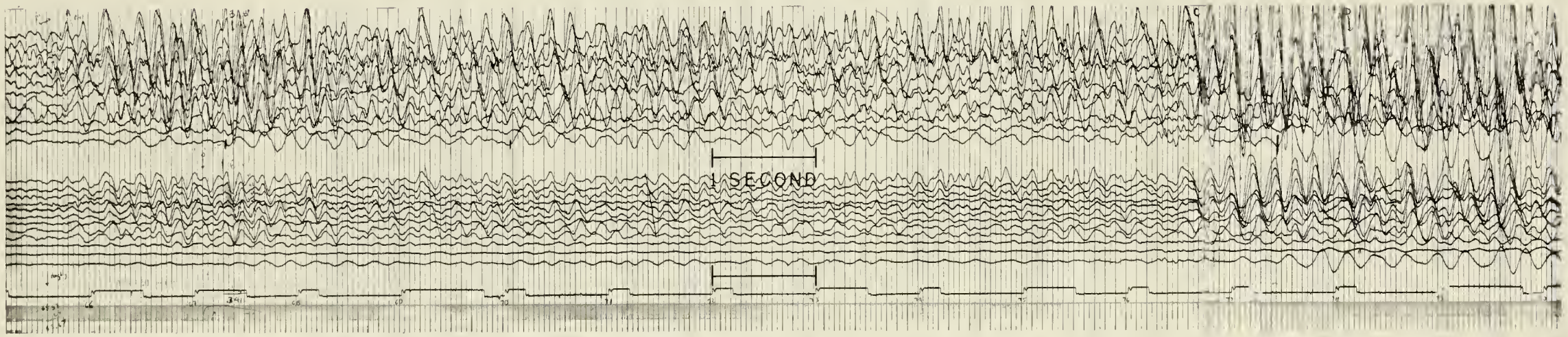
TIME (SECONDS)

This must be indicative of dipping structures in the deep crust. The poor quality data set shows one of the main reasons for the difficulty in obtaining reflection information suitable for interpretation—despite the source-receiver array, large amplitude and long period ground motion obscure the reflected energy in these cases. It should be pointed out that after the seismogram in question had been digitized and suitable signal enhancement techniques applied, some reflections were evident on the resultant set of traces.

As previously mentioned the special refraction profile was a combined effort with the Seismology Division of the Dominion Observatory. In addition to providing the personnel at the shot point, two of their crews each recorded six channels of seismic data on either Hall Sears HS-10 or Texas Instruments S-36 2 Hz. seismometers, these being separated by 0.5 kilometers. Two University of Alberta crews equipped with the same instrumentation as for the reflection studies, except for the use of single S-36 geophones separated by 0.29 kilometers, each recorded twelve channels of seismic information. Three of these were the vertical, radial and transverse components obtained from HS-10 seismic detectors located at one position. Six of the other traces were also recorded on the FM analog tape transport. One additional U. of A. crew registered the vertical and horizontal components of ground velocity as produced by two Willmore Mark II seismometers. Twelve of the seventeen seismic records were considered to be of good quality for interpretation. Two examples of these, one from a Dominion Observatory (upper) and one from a U. of A. crew (lower) are illustrated in Figure 1.4. On this diagram the initial arrival of the head waves from the M discontinuity followed by a later arrival but of much greater amplitude can be seen. The second arrival

Figure 1.4 *Reproductions of two seismograms recorded in the refraction survey.*


1 SECOND


1 SECOND

is interpreted to be a head wave from an interface within the Precambrian basement complex. This small refraction project provided significant corroborative evidence for the interpretation made from the reflection seismograms.

The following chapters will show that valuable and useful information concerning deep crustal structure is being obtained from the program of geophysical study undertaken in southern Alberta. In Chapter 2, the application of digital data processing techniques to the reflection seismograms is shown to have considerable importance for delineating individual reflected wave trains and providing an improved correlation of reflected events. In Chapter 3, amplitude spectra of the observed deep reflections are compared with the spectra from synthetic seismograms in order to give some indication of elastic properties in the crustal section. Coincident with this study, some information relating to the physical properties of the reflecting horizons (sharp discontinuities versus transition zones) is provided. Throughout the text, the feasibility of using near-vertical incidence reflected energy to identify horizons in the lower crust is demonstrated. In contrast to the assumptions of small dips and planar interfaces usually incorporated into crustal study analyses, Chapter 4 provides evidence from the deep reflection seismograms of large-sized structural relief in the deep crust and on the M discontinuity, structures which rival in magnitude the largest topographical features observed at the earth's surface.

# CHAPTER 2

# DIGITAL PROCESSING

## 2.1 Digitization and initial processing

All the seismograms recorded on FM analog magnetic tape were subsequently digitized by the technical staff of the geophysics laboratory. A block diagram of the system is illustrated in Figure 2.1. The digital tape transports indicated on the illustration were Kennedy incremental tape recorders having seven tracks and a packing density of 200 characters per inch. In order to provide the required bandwidth for the seismic conversion, the original analog tape drive speed of 30 inches per second was reduced prior to digitization to a drive speed of 3-3/4 inches per second, a factor of eight. On this reduced time scale, 90 conversions per second were made. But since six channels were being sequentially digitized (that is, N points for each channel were being produced as in a matrix $X_{ij}$ where i varies from 1 to 6, as j goes from 1 to N), this meant that each individual channel was being sampled at a rate of 15 conversions per second. When the factor of eight is considered, a true conversion rate of 120 conversions per second for each channel is realized. The filters used prior to digitization were specially designed to prevent aliasing of power from frequencies greater than half the conversion frequency, that is the Nyquist frequency for the digitized data. Figure 2.2 shows the amplitude response of the filter plotted as a function of frequency as recorded in the field.

The digital tapes so produced in the laboratory were not FORTRAN readable on the IBM 360/67 computing system which is available at the university. Consequently a machine language program was used to transfer the data onto new digital tapes and in a format such that the information

Figure 2.1 *Block diagram of analog-to-digital conversion system. Blocks of data are read alternately in each of the two digital transports in order to provide the Inter-Record Gap required for the* IBM 360/67 *computing system.* E.O.F.: *end of frame;* E.O.C.: *end of conversion.*

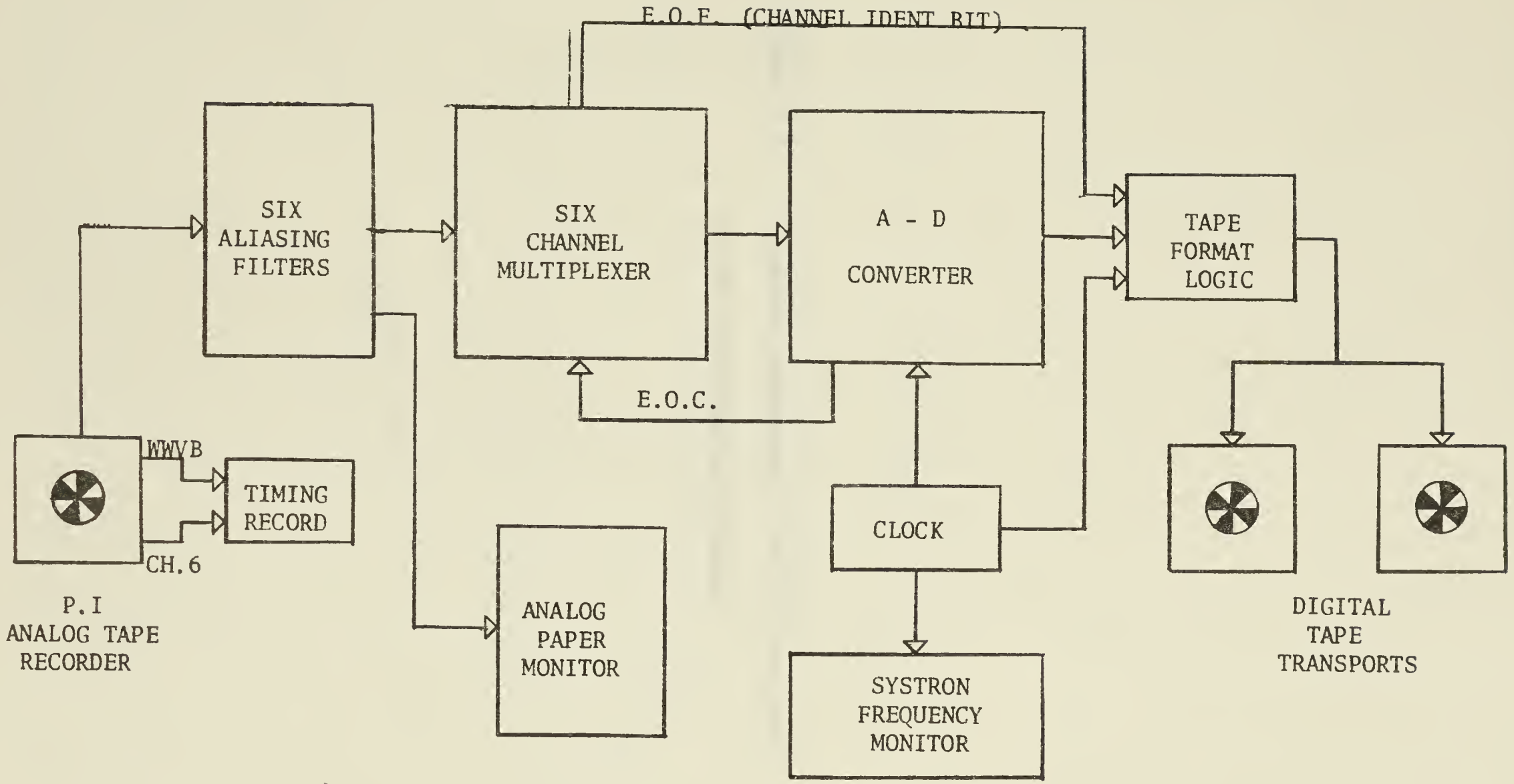
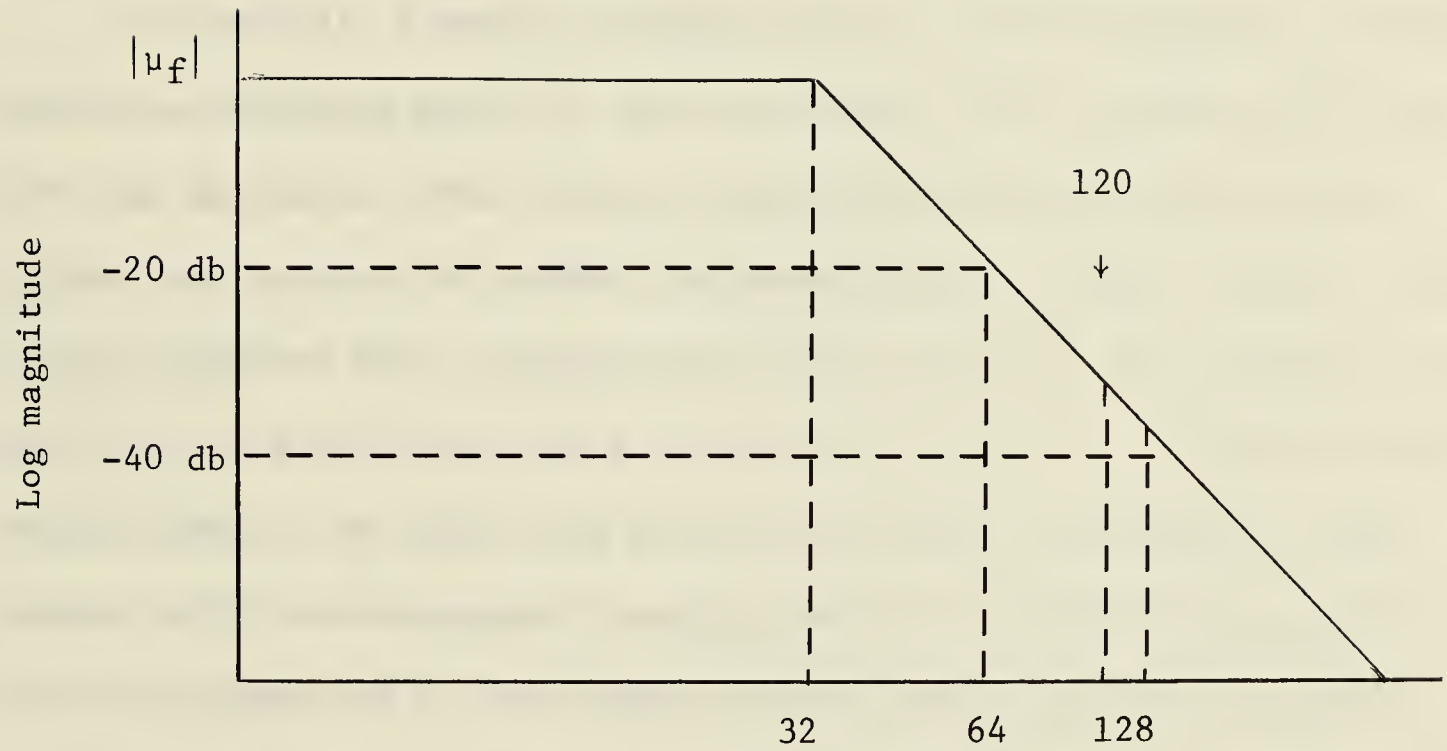

E.O.F. (CHANNEL IDENT BIT)
SIX ALIASING FILTERS
SIX CHANNEL MULTIPLEXER
A - D CONVERTER
TAPE FORMAT LOGIC
E.O.C.
WWVB
TIMING RECORD
CH. 6
P.I ANALOG TAPE RECORDER
ANALOG PAPER MONITOR
CLOCK
SYSTRON FREQUENCY MONITOR
DIGITAL TAPE TRANSPORTS

Figure 2.2 *Frequency response of the filters used in the digitization process.*


$|\mu_f|$
120
-20 db
-40 db
Log magnitude
32
64
128
Frequency (Hz.)

would be FORTRAN readable. For this procedure, the two tapes containing the digitized data from six channels of one record had to be mounted simultaneously on two tape drives, the program then transferring the data onto one new digital tape. All necessary checks to ensure that the seismic information was being transferred as originally written were included in the program. As a further check, parts of some records were plotted and compared to the original photographic records. In this manner all the digitized seismograms from one field season were compiled on one FORTRAN readable tape. A duplicate copy of each tape was kept as a safeguard against possible destruction of the original.

In general, a total of either thirty or fifty seconds of two-way traveltime starting prior to the shot instant and continuing from that time was digitized. The timing record produced in the digitization process was supposed to enable the determination of shot instant relative to the digitized data. However more often than not, the resultant traces were of poor quality and could not be relied upon. It became necessary to plot some of the data from each record which was on digital tape, compare with the photographic analog records on which timing accuracy was ±2 milliseconds and in this manner relate which point corresponded to zero time. This procedure proved quite reliable and it is estimated that the determination of shot instant is generally accurate to within one digital increment or ±8.3 milliseconds and certainly not more than twice this amount.

One further problem was illuminated by this method of timing. The process of digitization took place over periods of four to six weeks in two different years. It was found that the actual sampling rate, nominally set at 120 conversions per second, varied significantly

from record to record depending on when the actual digitization was done. The rate varied from about 117 to 120 conversions per second. Since some of the analysis techniques which were to be applied on the data required a constant conversion rate and for the sake of convenience in data handling, this problem was corrected as discussed in a later paragraph. It was a tedious process. In order to eliminate such problems in the future, the writer suggests that the shot instant be recorded directly on one channel of the FM tape transport. At the same time, two unique and identifiable signals (one could be shot instant), carefully timed so that they are exactly separated by a preset value, could be generated on the same channel, thus allowing for a quick check of the digital conversion rate.

Since the separation of the source and receiver arrays usually varied from 0 to 3.2 kilometers, reflected energy did not arrive at vertical incidence, even for plane layers at the base of the crust. For such a case the actual variance is from zero to less than three degrees. The difference in time of arrival between station locations due to non-vertical incidence is called normal moveout (NMO). Thus the initial processing step involved the removal of NMO, effectively reducing the time on each trace to that for vertically travelling waves. While doing this it was considered advantageous to select a specified time range of interest, usually 2 to 22 or 3 to 23 seconds of two-way traveltime. At the same time, it was deemed expedient to reduce the arithmetic mean for each channel to zero:

$$X_{ij}^{new} = X_{ij}^{old} - \frac{1}{N} \sum_{j=1}^{N} X_{ij}^{old}, \quad i = 1, 6.$$

Removal of the NMO was actually achieved in two separate steps.

First a computer program written in APL (A Programming Language, used on remote terminals connected to the central processing system) was utilized to generate the time differences between vertical ray paths and oblique incidence ray paths for all times in the range of interest and for the entire range of geophone-hole offsets. For the program two crustal models, one for each half of the total profile, were considered. Velocity and depth information for the sedimentary layers were readily available from logs of wells in the area. Below the Paleozoic sediments, the results from reversed refraction profiles and the preliminary interpretation of the reflection data provided the necessary information. This of course was a case of requiring a preliminary interpretation before subsequent analyses could provide one based on more favorable evidence. However, such a procedure simplified the computations and considering the low sensitivity of NMO at long traveltimes to differences in crustal structure, even for source-geophone distances of a few kilometers, the method was deemed sufficiently accurate. Results generated by this APL program were plotted as a form of normal moveout chart.

Values appropriate for each channel of a given seismogram were read from the chart and fed into a FORTRAN language computer program which performed the required time shifting of data points. Thus a new tape containing all the desired records from one field season and consisting of data for the selected time range with d.c. bias and NMO removed was generated. In another suggestion for future work, it is felt that this two-step procedure could be combined into one program, thus eliminating manual plotting of the NMO chart, reducing the number of data input cards required and facilitating the introduction of other crustal models. Alternatively, if sufficient data are available, corrections for NMO can

be applied in a manner analagous to such determinations in the seismic prospecting field (see Brown, 1969).

Previously, mention was made of the necessity for correcting a variation in the sampling interval from one seismic record to another. Thus the data with NMO removed had to be reprocessed. Because of the small differences between the actual digitizing rate and the specified standard rate of 120 conversions per second and to make the calculations simple and efficient, a linear interpolation between adjacent data points at the appropriate time was employed in the redigitization program. In the same FORTRAN program, channels showing instrumental difficulties were zeroed, those with reversed polarity were corrected and amplitudes of the individual channels on all records were normalized within a specified range. For this normalization, one trace considered to have a good average amplitude over a period of time was selected as standard and all other traces were modified to give a similar average amplitude within the constraints specified in the program. The multiplication factor for each trace was noted. Such a process is not ideal, but with the variation in quality and amplitudes of the original recordings, it proved quite effective as a general standardization technique.

Finally a complete set of data, redigitized to 120 conversions per second with NMO removed and other modifications made, was obtained on digital tape. For the 20 seconds of recording time selected for each seismogram, this amounted to more than 1.5 million words of seismic information. A comparison of some of the processed seismograms, reproduced in analog form with appended time scales by means of a CALCOMP plotter, was made with the original photographic analog records. For traces near the shot, where NMO would be a minimum, it was found that

the timing of identical peaks and troughs was the same to less than 20 milliseconds, the timing accuracy on the CALCOMP plotted data being about ten milliseconds. This complete initial processing procedure was tedious and time-consuming, but absolutely necessary for the application of signal enhancement techniques and the efficient handling of the large amount of data.

## 2.2 Autopower spectra

For the purpose of investigating the frequency content of the reflection seismograms, a FORTRAN language program for the computation of autopower spectra was written. The actual calculations were based on a fast Fourier transform (F.F.T.) algorithm (Gentleman and Sande, 1966) for which the basic subroutine programs were given to the magnetotelluric analysis group of the Geophysics Division by G. Sande and provided by them to the writer.

Basically the program worked in the following manner. After specifying the time interval of one seismic trace for which the spectrum was desired, the first and last ten percent of the data points were tapered with a cosine bell so that no energy from sharp steps, which generate power at all frequencies, would be introduced into the spectrum. The F.F.T. algorithm was applied to produce first the Fourier coefficients. These were used to obtain the autocovariance of the tapered data which was then modified by a Parzen lag window. The principle of applying a lag window to the autocovariance is to provide a statistically reliable power spectrum estimate, that is one for which the variance of the spectral estimate is reduced. One characteristic of the Parzen window is that it is positive definite so negative power estimates should never be obtained. In addition, only a fraction of all the autocovariance values

are required for the calculations, thus increasing the efficiency of the computer program while not increasing its core storage requirements. After applying the window, the F.F.T. subroutines are again used to compute the power spectrum estimate. The geophone and amplifier responses are removed using the manufacturer's specifications for the geophones and measured data for the amplifiers. Values were taken at the appropriate frequencies, normalized, squared and multiplied with the power spectrum estimate to yield the spectral density of the surface particle motion. A facility is included in the program to compute the autopower spectrum of any time interval on individual traces or provide a spectrum averaged over several channels of one record. The resultant data are plotted on the CALCOMP plotter.

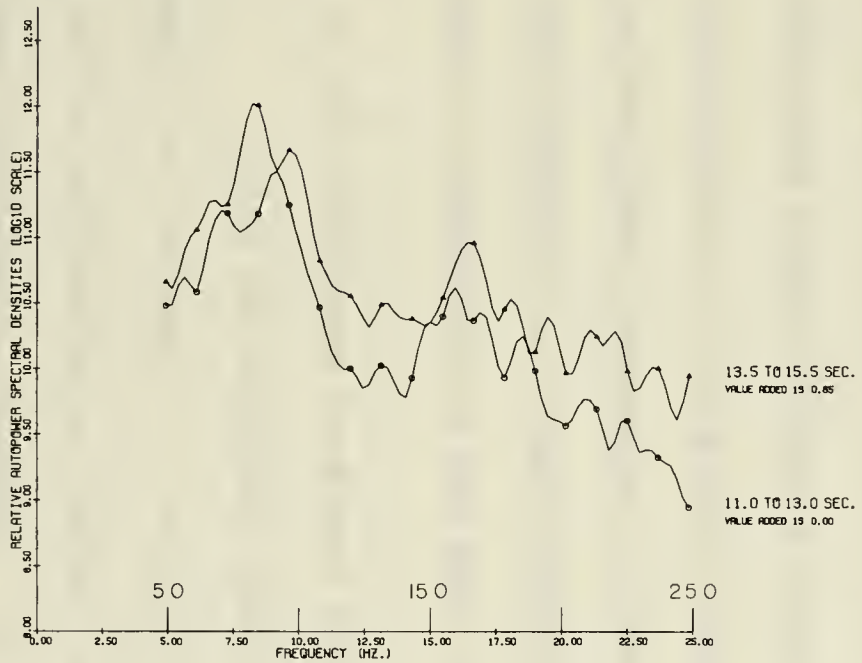
Figure 2.3 illustrates the averaged relative autopower spectrum of four different seismograms, these being chosen as representative of the general spectral characteristics observed from an analysis of all available records. The two spectra on each plot are from different traveltime intervals, as indicated to the right of the curves, and correspond to increments which contain good reflections from the R discontinuity (lower curve), an intermediate crustal reflector, and from the M discontinuity (upper curve). In order to facilitate presentation, the latter has been shifted by adding a constant to each estimate, this value also being noted on the right. The ordinate is a logarithmic scale, but since the autopower amplitudes vary from plot to plot and the computer program automatically scales these to fit the diagram dimensions, this scale can change from one diagram to the next.

Record 07, 1966 (upper right) shows a feature which was observed on a number of the power spectrum plots—two large peaks, one usually centered from 9 to 11 Hz., the other from 16 to 19 Hz. This same

Figure 2.3 *Averaged autopower spectra for selected time intervals of four different seismograms. Spectral modifications due to seismometer and amplifier characteristics have been removed.*

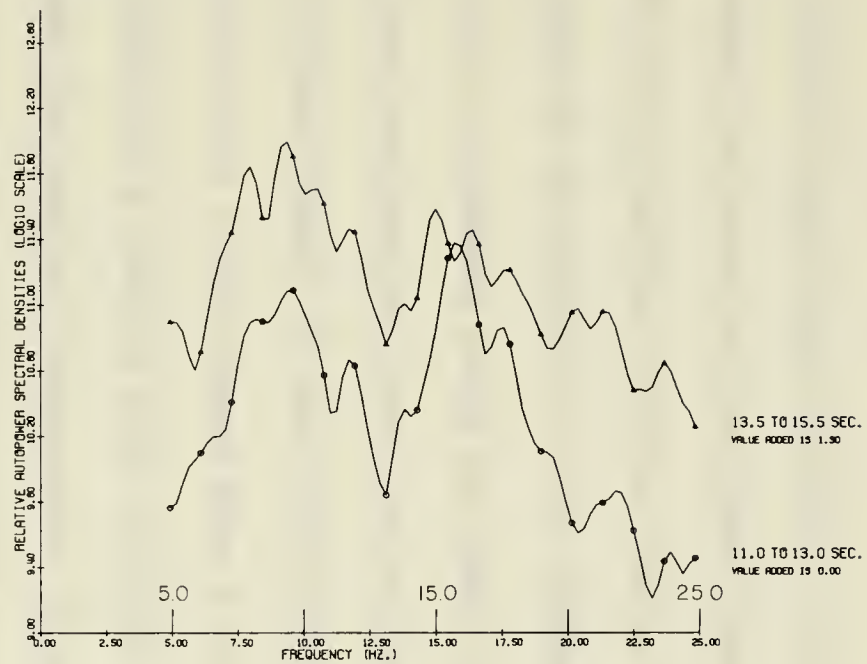
RECORD 05 1966

AVERAGED SPECTRUM FROM 6 TRACES



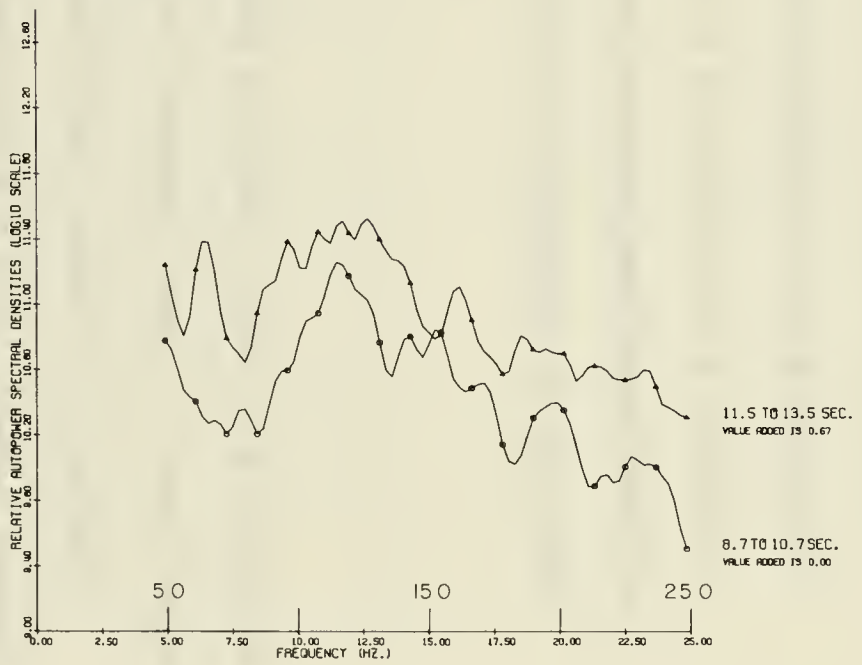

RECORD 07 1966

AVERAGED SPECTRUM FROM 6 TRACES



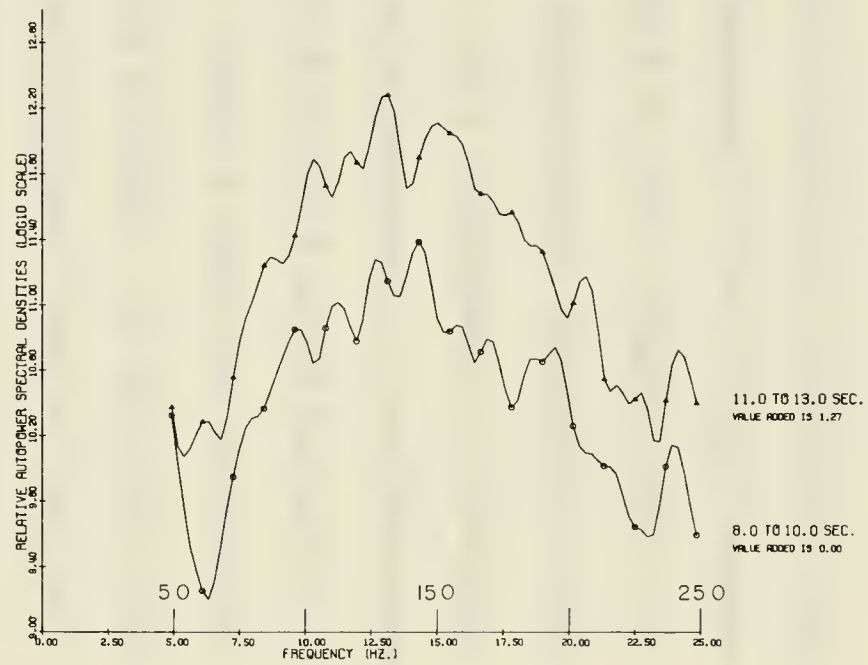

RECORD 55 1967

AVERAGED SPECTRUM FROM 6 TRACES




RECORD 25 1967

AVERAGED SPECTRUM FROM 6 TRACES



tendency is shown in the plot for Record 05, 1966 (upper left) but the second peak is much subdued relative to the first. As well, these curves exhibit the lower limit of frequency range (7 to 10 Hz.) for which spectral peaks were observed. In contrast, Record 25, 1967 (lower right) shows the range of the higher limit of frequency (12 to 17 Hz.) observed for the principal spectral peak. On Record 55, 1967 (lower left), the peaks do not appear so well defined but their central frequency is about 12 Hz., a common value for many records. As a consequence of examining these and similar plots for all available seismograms, it was found that the main energy of the reflected arrivals from the R and M discontinuities lay in the range from 8 to 15 Hz. Quite a number of recordings exhibited a doublet peak in their spectral estimate. It was also noted that the central frequencies of spectra at different times on the same seismogram were often shifted relative to one another, the later reflection usually having a lower central frequency (see Record 05). Another aspect of the general character of the plots was a tendency for the higher frequencies to have a lower average amplitude than the lower frequencies. These observations are of importance to the study which is considered in the next chapter.

## 2.3 The zero-phase band-pass filter

Since the autopower spectra showed that most often the reflected energy was confined to a relatively narrow frequency band, it was thought that the application of digital band-pass filters would be a suitable signal enhancement technique. In the course of his M.Sc. thesis research at the University of Alberta, Alpaslan (1968) developed a FORTRAN computer program for a zero-phase-shift recursive Butterworth band-pass filter. In his thesis, a good summary of the theory is given and

references are provided. The Butterworth filter is an optimum filter when signal and noise occur in separate bands of the frequency domain and does not exhibit the undesirable Gibb's effect, a high frequency oscillation superimposed on the amplitude spectrum of the filter. By utilizing recursion relations for the computation of filter coefficients and the application of these to the data, the computer program is made efficient and accurate. A desirable characteristic of such filters when applied to real data is that they be zero phase. Otherwise, a differential lag would exist between different frequency components thus introducing distortion into the filtered data. In the program used, the zero-phase aspect was introduced in a simple but effective manner. The output is obtained directly from a product of the z transform of the input vector and a digital filter operator, then it is time reversed. The time reversed data are filtered in the same manner as the original input, and finally this output is time reversed to produce the desired filtered trace with no distortion. Mathematically it can be shown that such a process does indeed realize a zero-phase response, the only significant difference being that the amplitude response of the filter is squared relative to that of a single pass filter.

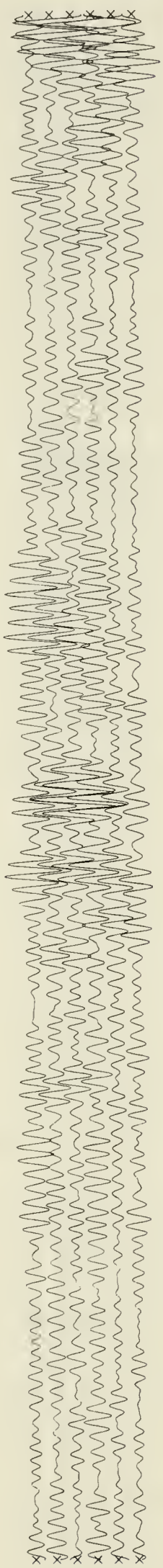
An eighth-order band-pass filter of the type just described was applied to a number of digitized seismograms. Figure 2.4 shows the original recorded data (after the initial processing described in Section 2.1) for four records and the same seismograms filtered with a 7 to 13 Hz. Butterworth filter. Considerable improvement is rendered by the process, but an important disadvantage was noted. Because of the relatively narrow frequency specifications of this filter or similar ones, the output seismogram appeared quite oscillatory and the character of the

Figure 2.4 *Plot of digitized seismic reflection records before and after applying a 7 to 13 Hz. Butterworth digital band-pass filter. The illustration is on two separate pages.*

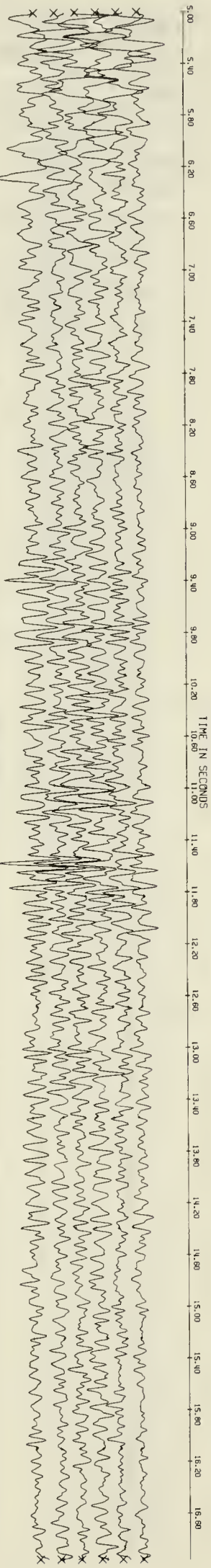
First page: *seismograms from the Lomond profile.*

Second page: *seismograms from the Blackfoot profile.*

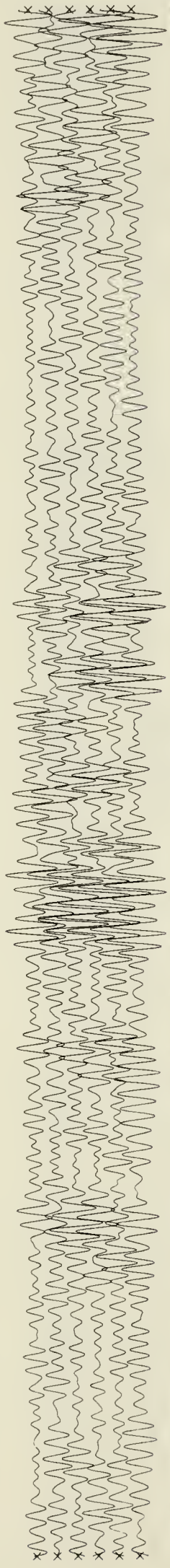
BUTTERWORTH FILTER
7.0 HZ. TO 13.0 HZ.
RECORD 08 1966



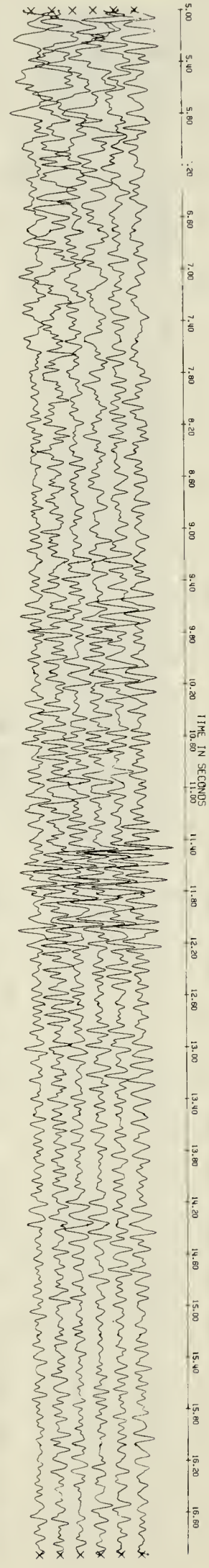
RECORD 08 1966



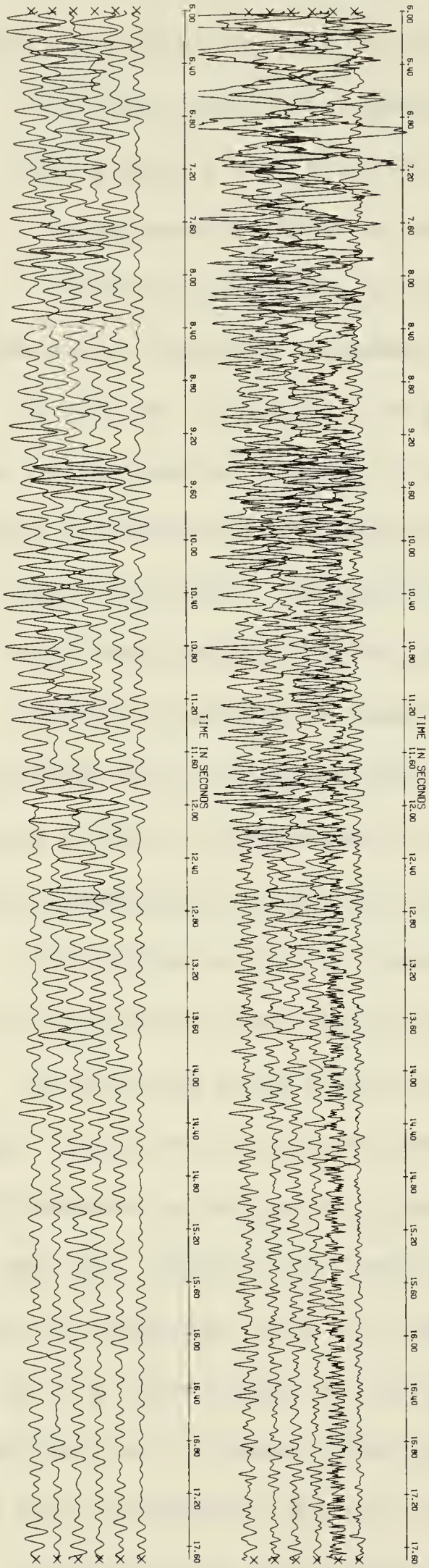

BUTTERWORTH FILTER
7.0 HZ. TO 13.0 HZ.
RECORD 07 1966



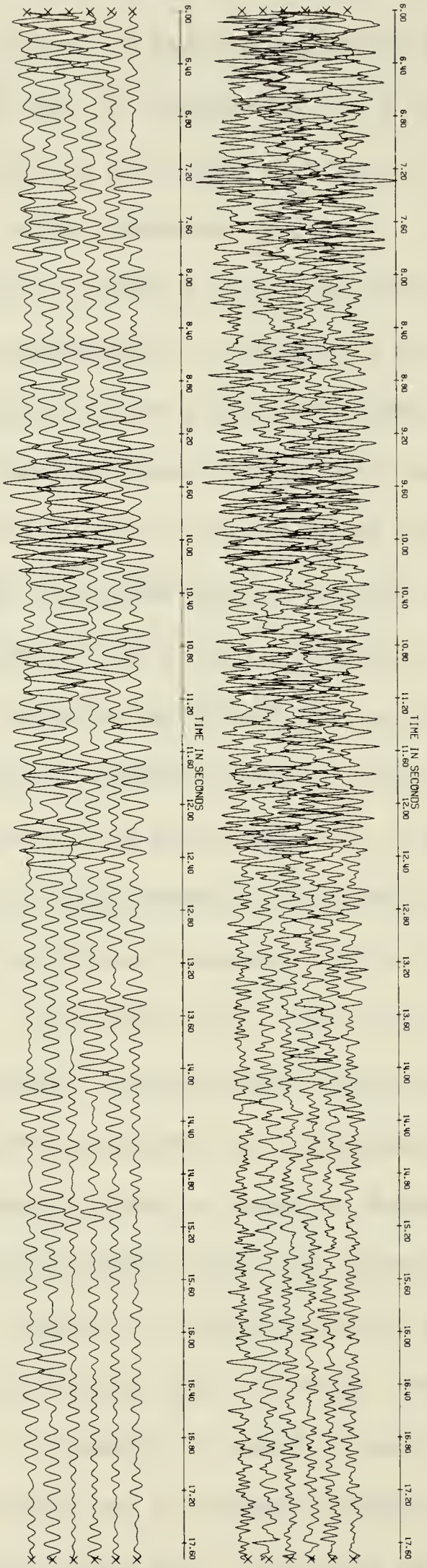
RECORD 07 1966



BUTTERWORTH FILTER
7.0 HZ. TO 13.0 HZ.
RECORD 16 1967



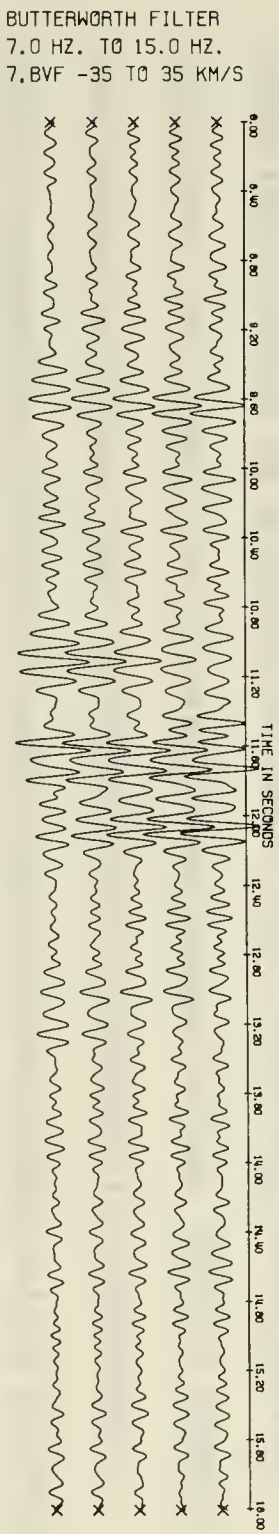

BUTTERWORTH FILTER
7.0 HZ. TO 13.0 HZ.
RECORD 15 1967

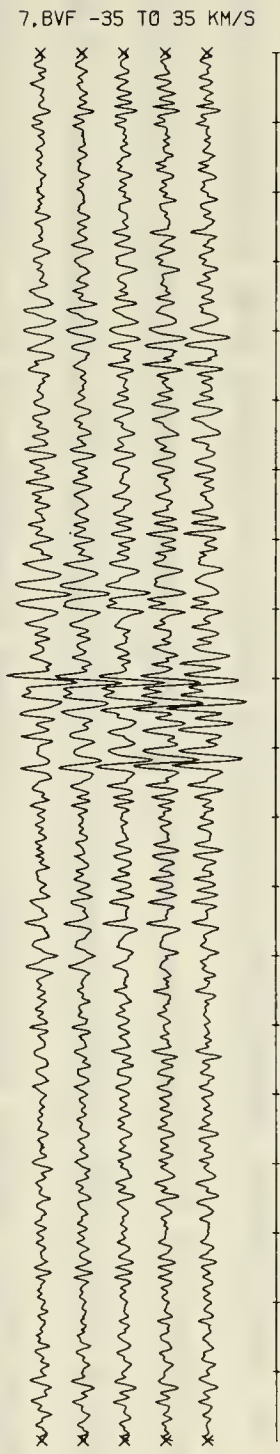


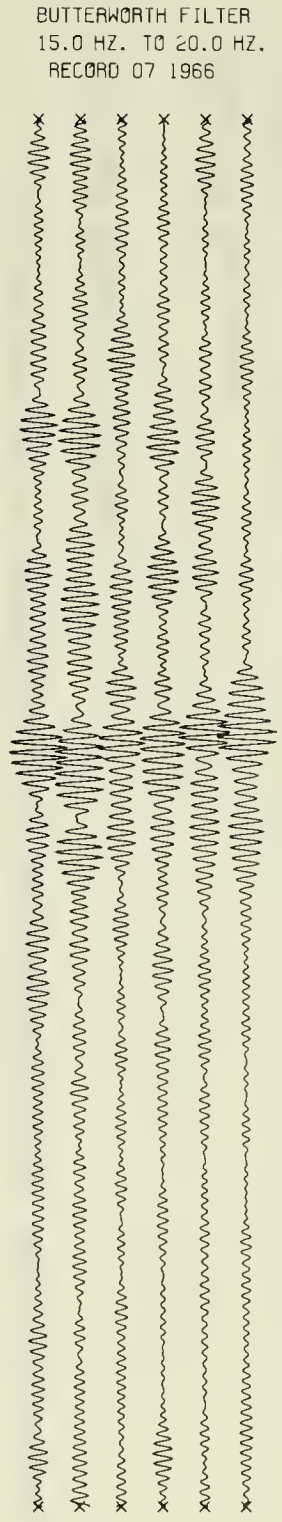
records was destroyed, thus making phase correlations more difficult.

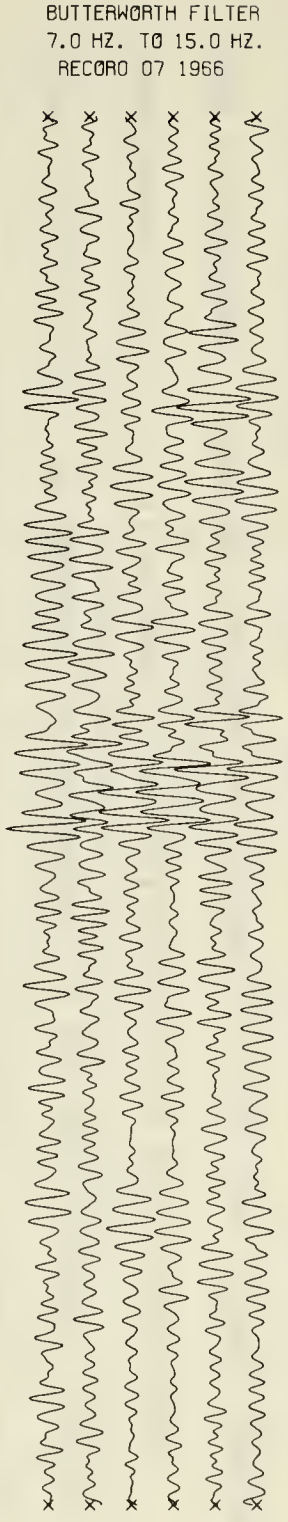
A further example of the application of the zero-phase filter to recorded data is given in Figure 2.5. The upper record is the unfiltered seismogram. Below it, the result of applying an eighth-order 7 to 15 Hz. band-pass filter is shown. A certain amount of noise reduction is evident especially for some coherent energy about 14.4 seconds, the time corresponding in depth to the M discontinuity as derived by reversed refraction profiles. The autopower amplitude spectrum of Record 07, 1966, the record under consideration, showed two strong peaks centered at about 10 and 17 Hz. (see Figure 2.3). To obtain some indication as to where the higher frequency energy was present on the seismogram, the original record was processed with a filter having cut-off frequencies of 15 and 20 Hz. The third set of traces illustrates the results which are indicative of other records to which similar filters were applied. Evidently the high amplitude sequence at about 11.6 seconds contains most of the energy in the higher frequency range, although some other envelopes of considerable amplitude can be observed. Since the times about which the envelopes centre are coincident with the observed reflection times, this higher frequency must be intimately related to the reflected signal and should not be isolated or attenuated. As will be noted later in Chapter 3, considerable information relating to the nature of the discontinuities at depth is present in the spectral density estimates. Therefore secondary peaks such as those illustrated in Figure 2.3 should be preserved for later analysis, not filtered out. In the light of our experience, it can be stated that narrow band-pass filtering should be avoided as it destroys not only the character of the reflected impulse, but valuable information contained therein.

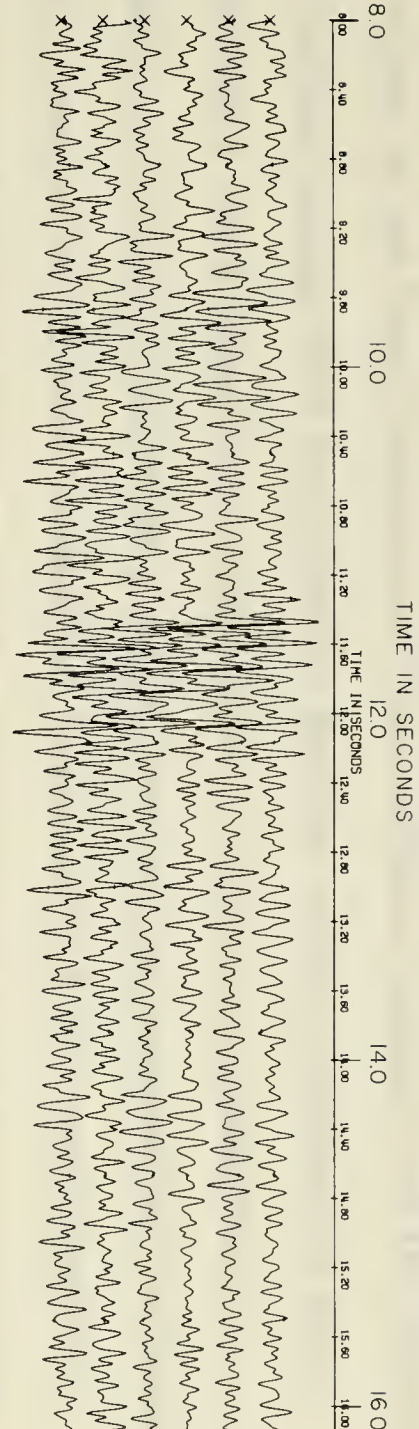
Figure 2.5 *An example of different filters and filtering techniques applied to one seismogram. Upper: unfiltered record; second: 7 to 15 Hz. band-pass filter; third: 15 to 20 Hz. band-pass filter; fourth: velocity filter (see Section 2.4) with a pass band of -35.2 to +35.2 km/sec; lower: the velocity filtered output passed through a 7 to 15 Hz. band-pass filter.*


BUTTERWORTH FILTER
7.0 HZ. TO 15.0 HZ.
7.BVF -35 TO 35 KM/S
TIME IN SECONDS


7.BVF -35 TO 35 KM/S
TIME (SECONDS)


BUTTERWORTH FILTER
15.0 HZ. TO 20.0 HZ.
RECORD 07 1966
TIME IN SECONDS


BUTTERWORTH FILTER
7.0 HZ. TO 15.0 HZ.
RECORD 07 1966
TIME IN SECONDS


RECORD 07 1966
8.0
10.0
12.0
14.0
16.0
TIME IN SECONDS

Fuchs (1969) points out two aspects of the German deep reflection observations which should be mentioned in connection with these results. He refers to the "band character of the reflected signal" and the shifting of the main energy from one phase to another so that correlation over more than a few kilometers is impossible. Since the seismograms in Germany are recorded via normal seismic reflection prospecting instrumentation, perhaps the filters so applied cause some of the band character. It was noted earlier that even the application of a low frequency band-pass filter from 7 to 15 Hz. gave an oscillatory appearance to the resultant seismogram. From the results of processing with the higher frequency zero-phase filter, it is evident that correlation of one phase might prove difficult but in general the envelope of the oscillations can be clearly seen. Thus some part of the observed results in Germany may be caused by the recording apparatus rather than by the nature of the reflecting horizons.

## 2.4 The velocity filter

In the process of analysing the photographically recorded seismograms, it was noted that reflection arrivals with varying apparent velocities, negative and positive, could be seen at different traveltimes on one record. Quite often these dipping events were obscured by other noise or by interference with one another. It seemed obvious that some form of filter which would discriminate against all reflected energy with apparent velocities outside of a specified range, thus enhancing those inside, could prove very useful in distinguishing among various dipping events. Such selective filters have been designed and applied in exploration seismic prospecting within the past decade and have been called by various names: velocity, fan-pass, pie-slice or beam-forming filters (for example

see Fail and Grau, 1963; Embree et al., 1963; Wiggins, 1966; Treitel et al., 1967, or Sengbush and Foster, 1968).

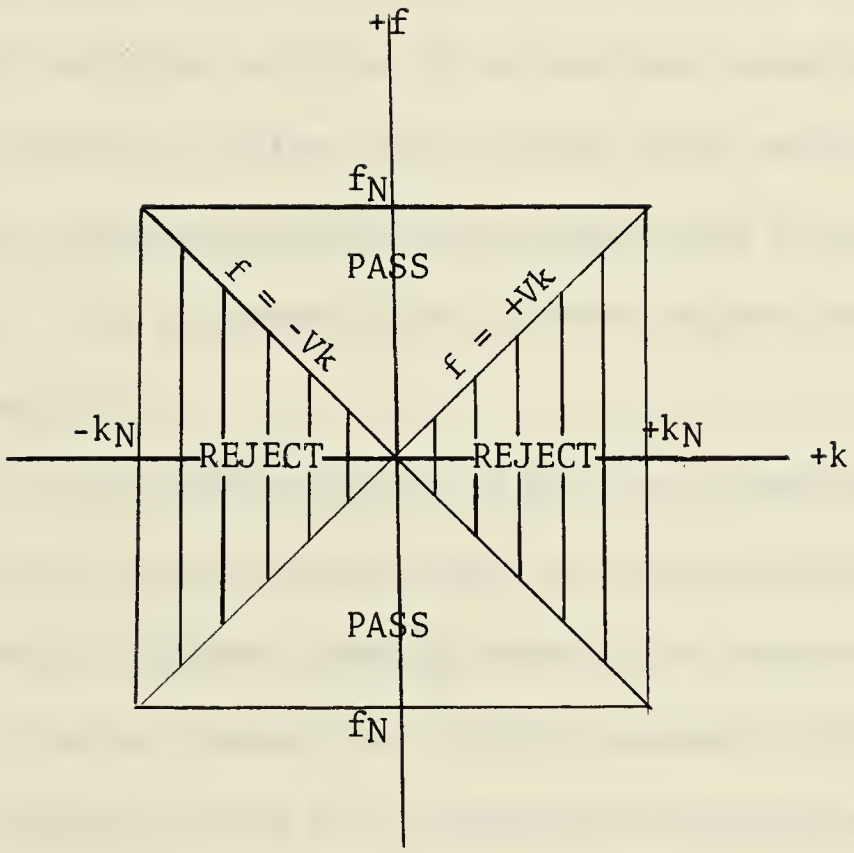
The basic idea behind such filters can be explained quite simply. By designing a two-dimensional time-space operator in the f-k (frequency-wave number or frequency-spatial frequency) domain, it is desired to pass all events on a multichannel seismogram whose apparent velocities fall within the range -V to +V. The ideal transfer function for such a filter is

$$Y(f,k) = \begin{cases} +1, & -\frac{|f|}{V} \leq k \leq +\frac{|f|}{V} \\ 0, & \text{otherwise,} \end{cases} \qquad (2.1)$$

where k is the spatial frequency related to the wave number K by $K = 2\pi k$. Figure 2.6 illustrates the ideal filter characteristic of equation (2.1).

Evaluation of the two-dimensional Fourier transform of the transfer function in equation (2.1) will produce a filter operator in the time-space domain. This operator represents a two-dimensional array of weighting coefficients which must be convolved with the data points representing traces of a seismogram in order to generate the velocity filtered output data. However, Treitel et al. (1967) have derived an algorithm which effectively reduces the computational labor from the original formulation of the problem. They then make use of a recursive filter (Shanks, 1967) to further reduce the amount of calculations required. Because of the efficiency of this method, the author has programmed the appropriate equations in order to apply this form of filtering to the deep reflection data. The basic procedure can be briefly described in the following manner. At a given record time, the digitized data points representing a specified number of equally spaced input traces are appropriately weighted, time shifted and summed. This weighted sum

Figure 2.6 *Ideal f-k plane transfer function of a velocity filter.* $f_N$ *and* $k_N$ *are the temporal Nyquist and the spatial Nyquist frequencies, respectively.*

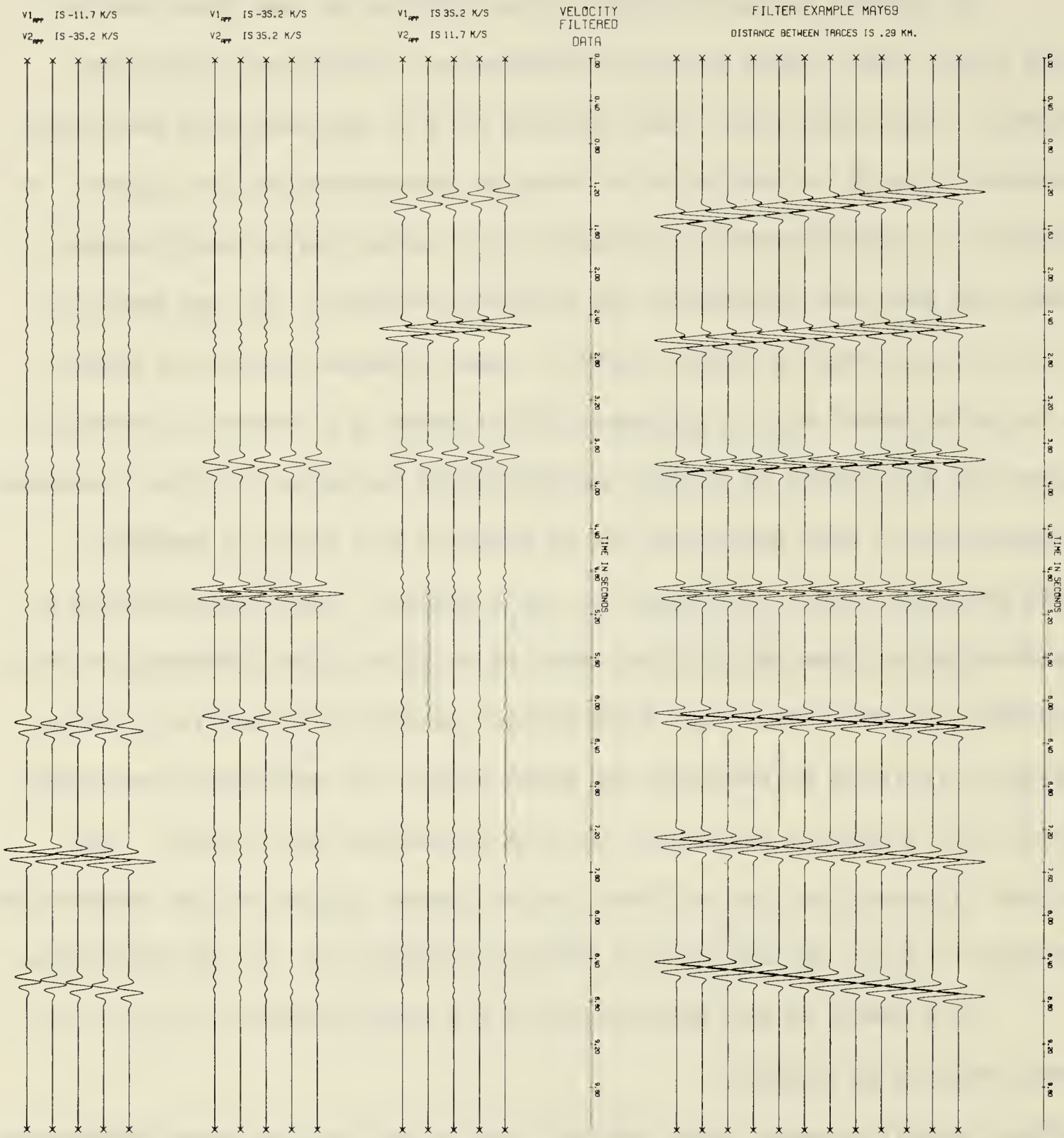

+f
$f_N$
PASS
f = -Vk
f = +Vk
$-k_N$
REJECT
REJECT
$+k_N$
+k
PASS
$f_N$

of time-shifted traces is then convolved with the fan filter. By successively incrementing along the vectors of data points and repeating the process, one velocity filtered output trace is produced. A complete development of the theory is given by Treitel et al. (loc. cit.). The Appendix contains a listing of the computer program to implement such a velocity filtering process, with adaptability for application of three different filter characteristics to each set of input data and for CALCOMP plotting of all results.

Previously it has been mentioned that six seismic channels from each of two truck-mounted instruments were recorded for each shot, these twelve traces then yielding one mile of sub-surface coverage. While the program allowed a velocity filter with a range (even number) of traces, it was decided that the application of an eight-trace fan-pass filter would be adequate. This generated five filtered output traces for every twelve input channels.

An example of the effectiveness of this two-dimensional operator in passing events with apparent velocities in the specified range is given in Figure 2.7. Seven different dipping events with apparent velocities ranging from +11.7 km/sec through an infinite apparent velocity and down to -11.7 km/sec (stepouts of +3 to -3 sampling intervals per trace) are synthesized in the input channels which form the upper part of the figure. The three lower sets of five traces each are the result of processing the input data with the three different pass bands indicated on the diagram. It is evident from this illustration that similar dipping events with apparent velocities inside the specified range are passed with no modification and events whose apparent velocities fall on the cutoff velocities have their amplitudes attenuated by a factor of one half. All reflections whose apparent velocities lie outside the range of the fan-pass

Figure 2.7 *Application of the velocity filter to synthetic data.* Upper: *twelve synthesized traces with coherent events having a range of apparent velocities from +11.7 through 0 to -11.7 km/sec.* Lower: *the results of three different pass bands (+35.2 to +11.7 km/sec, -35.2 to +35.2 km/sec, and -11.7 to -35.2 km/sec, respectively) applied to the synthetic data. An eight-trace filter was used.*


V1 IS -11.7 K/S
V2 IS -35.2 K/S
V1 IS -35.2 K/S
V2 IS 35.2 K/S
V1 IS 35.2 K/S
V2 IS 11.7 K/S
VELOCITY FILTERED DATA
FILTER EXAMPLE MAY69
DISTANCE BETWEEN TRACES IS .29 KM.
TIME IN SECONDS

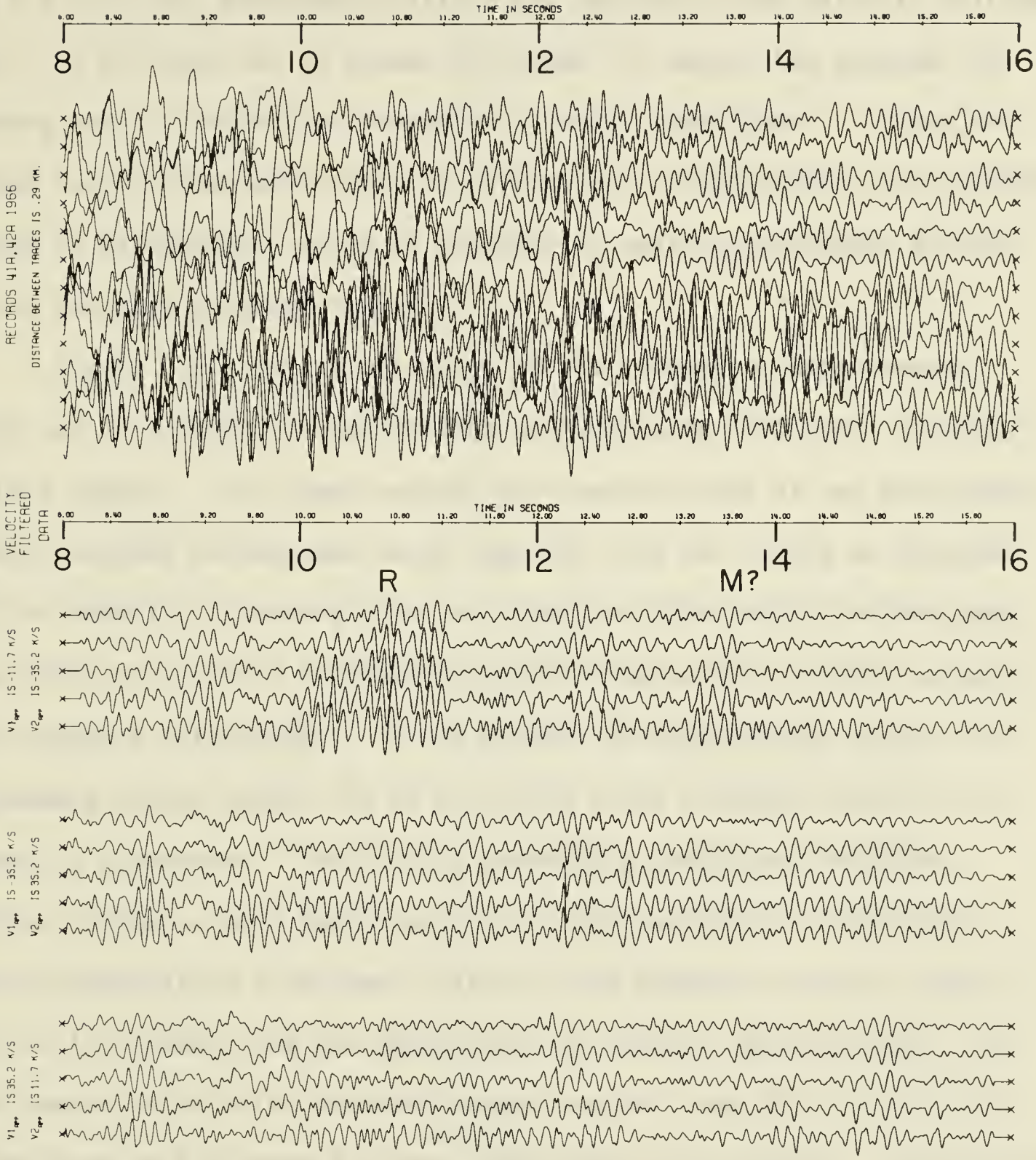
filter are severely attenuated. It should be mentioned that the resolution of the velocity filtering method is limited by the sampling increment in the time domain and by the distance between adjacent station locations in the space domain. For the present research, the resolution limits were found to be acceptable, but if more precise determination of dips of specific events were desired, one or both of the above parameters would have to be reduced.

An example of the application of the same filters (+11.7 to -11.7 km/sec) to a set of real data is given in Figure 2.8. In the upper part of the illustration, the original twelve traces (after initial processing) which have a spatial separation of 0.29 kilometers are plotted. The velocity filtered seismograms are drawn below, all amplitudes remaining constant for each plot. The good quality reflections labelled R and M were extracted from the original data by a filter whose apparent velocity pass band was from -11.7 km/sec to -35.2 km/sec. Two other possible reflections with less amplitude can be found at 9.2 and 12.4 seconds. These are not nearly so clearly delineated by the other filters. However a reflected event with a different dip at about 8.6 seconds is shown on the lower two sets of output traces. Other coherent phases of lesser amplitude are seen throughout the filtered sections. Yet one must be cautious in interpreting such output since random noise could produce a coherent line-up of energy which would be accentuated by the filter. In general, continuity over a few adjacent sets of filtered data was necessary before such events would be interpreted as possible reflections.

An example of the fan-pass filter applied to some good quality data was included in the fourth set of traces displayed in Figure 2.5. For this case the pass band of apparent velocities was from -11.7 to

Figure 2.8 *Application of the velocity filter to real data.*

First: *the unfiltered input traces;* second: *pass band from -11.7 to -35.2 km/sec;* third: *pass band from -35.2 to +35.2 km/sec;* fourth: *pass band from +35.2 to +11.7 km/sec.*


TIME IN SECONDS
8
10
12
14
16
RECORDS 41A, 42A 1966
DISTANCE BETWEEN TRACES IS .29 KM.
VELOCITY FILTERED DATA
R
M?
V1 apr IS -11.7 K/S
V2 apr IS -35.2 K/S
V1 apr IS -35.2 K/S
V2 apr IS 35.2 K/S
V1 apr IS 35.2 K/S
V2 apr IS 11.7 K/S

-35.2 kilometers per second. It was initially thought that band-pass filtering of such output would provide a very good seismogram. To this end a 7 to 15 Hz. Butterworth filter was applied to the velocity filtered data. As the last set of traces on Figure 2.5 shows, the problem concerning loss of reflection character is still significant. It was concluded that little improvement of reflection identification, and possibly a loss of information, would be rendered by applying band-pass filters to the fan-pass filtered output.

Figure 2.9 is an illustration of the tremendous improvements which can be attained by application of processing techniques described in this chapter. The upper records are reproductions of two photographically recorded seismograms which together form one record as required for the velocity filtering process. They are poor quality seismograms from which no reliable information could be derived, even when compared with adjacent seismograms. In the process of digitization of the corresponding analog tapes, the 60 Hz. noise which overrides some of the traces is attenuated. The initial processing procedures described earlier include a gain factor applied to the amplitude of the traces. After processing by a fan-pass filter in the apparent velocity range of 35.2 to 11.7 km/sec and the application of further amplitude gain, the five traces of velocity filtered output for the same data as the upper seismograms is illustrated in the lower part of the figure. The improvement is self-evident. Reflection events with significant amplitude are seen throughout the plot and most of these could be correlated with similar phases on adjacent traces. Needless to say, the improvement of all records by the application of signal enhancement techniques, and particularly velocity filtering, was not so spectacular as that of the

Figure 2.9 *An example of signal enhancement by digital data processing techniques. Upper: reproductions of two field seismograms obtained from one shot. Lower: the resultant seismogram after digitization, amplitude gain and application of a velocity filter with a pass band of +35.2 to +11.7 km/sec.*

TIME (SECONDS)

9 10 11 12 13 14

RECORD 11, 1966

RECORD 12, 1966

11.12 VF 35.12 KM/S

.90 8.10 8.30 8.50 8.70 8.90 9.10 9.30 9.50 9.70 9.90 10.10 10.30 10.50 10.70 10.90 11.10 11.30 11.50 11.70 11.80 12.10 12.30 12.50 12.70 12.80 13.10 13.30 13.50 13.70 13.80 14.10

TIME (SECONDS)

9 10 11 12 13 14

present example. However, such an illustration emphasizes the considerable importance of data processing methods for improvement of the quality of deep reflection seismograms.

# CHAPTER 3

# CRUSTAL ATTENUATION AND THE NATURE OF THE REFLECTING HORIZONS

## 3.1 The synthetic seismogram with spatial attenuation

An important parameter of the solid earth, and one to which much attention has recently been given, is the attenuation of seismic energy. If this fundamental property were absent, the energy of past earthquakes would still be reverberating throughout the earth today. Nevertheless, in some studies it is found that agreement between theoretical results and observational data is sufficient to a first-order approximation without including an attenuation factor in the theory. With the recent availability of broad-band systems capable of recording a large dynamic range, it is possible to obtain data by which such a factor may be studied. As a measure of the anelasticity of a medium, Knopoff (1956) first introduced Q, the specific attenuation factor or dimensionless quality factor, into the field of seismology. The quantity, Q, represents a reduction to a dimensionless form of the more usual measures of attenuation. All of these definitions are related to an expression in electrical circuit theory which gives the relative efficiency of energy storage at resonance (Ryder, 1959):

$$Q = \frac{2\pi E}{\Delta E}$$

where $\Delta E$ is the energy dissipated per cycle and E is the maximum energy stored per cycle. To relate more closely to seismology, $\Delta E$ can be considered as the amount of energy dissipated per cycle of a harmonic excitation in a certain volume and E is the maximum elastic energy in the system in the same volume (Knopoff, 1964). The various means of

defining Q are related to the type of observation being used—for example, standing waves versus progressive waves. Knopoff (loc. cit.) discusses the related definitions which are identical for homogeneous and isotropic media.

In his earlier article, Knopoff (1956) included Q in the differential equation of motion of a medium possessing solid friction. Simplified to the case of plane compressional waves propagating in the z-direction, the equation of motion becomes

$$\left[ 1 + \frac{1}{|\omega| Q} \frac{\partial}{\partial t} \right] \frac{\partial^2 w}{\partial z^2} = \frac{1}{c^2} \frac{\partial^2 w}{\partial t^2} \quad , \tag{3.1}$$

where $\omega$ is the angular frequency whose absolute value is taken to guarantee absorption of both positive and negative frequency components of the Fourier spectrum, w is the displacement of a particle and c is the wave velocity had the losses been assumed to be absent,

$$c = \left( \frac{\lambda + 2\mu}{\rho} \right)^{1/2} .$$

Here $\lambda$ and $\mu$ are the Lamé elastic constants and $\rho$ is the density. If it is assumed that $w = We^{i\omega t}$, equation (3.1) becomes

$$\left[ 1 + \frac{i\omega}{|\omega| Q} \right] \frac{d^2 W}{dz^2} + \frac{\omega^2}{c^2} W = 0 \quad ,$$

which has the solution

$$w = \exp \left[ iwt - i \frac{\omega}{c} \left( 1 + \frac{i\omega}{|\omega| Q} \right)^{-1/2} z \right] .$$

If $Q >> 1$, the factor in parentheses can be expanded by the binomial expansion (omitting $\omega/|\omega|$) :

$$w = \exp \{ i\omega t - \frac{i\omega z}{c} - \frac{\omega z}{2cQ} - \frac{i\omega z}{c} \left[ - \frac{3}{8Q^2} + O\left( \frac{1}{Q^4} \right) \right] - \frac{\omega z}{2cQ} O\left( \frac{1}{Q^2} \right) \} . \quad (3.2)$$

Equation (3.2) shows that the attenuation is approximately expressed by $e^{-\frac{\omega z}{2cQ}}$ and if the spatial attenuation factor is denoted in the usual manner by $e^{-\alpha z}$, then the value of $\alpha$ is given by

$$\alpha = \frac{\omega}{2cQ} . \quad (3.3)$$

In this manner, the specific attenuation factor, Q, is related to the spatial attenuation coefficient, $\alpha$, for travelling waves. Q can also be related to other parameters for different observational data. In fact, the determination of the Q-structure of the earth is an important study to provide an additional quantity from which the physical and chemical state of the earth's interior may be inferred. Sato (1967) has given a comprehensive review of Q and its determination from observational data.

In contrast to the large amount of attention which has recently been given to fundamental studies of Q in the earth's interior, there has been relatively little application of the analysis in generating synthetic reflection seismograms. The synthesis of seismograms is a technique which has only been available since the 1950's when continuous velocity logs became available (see for example, Vogel, 1952 or Summers and Broding, 1952). Subsequently, Peterson et al. (1955) described an analog computer system for the generation of synthetic seismograms. They were followed by other researchers who described various methods by which seismogram

synthesis could be achieved, especially by use of digital computers (Berryman et al., 1958; Dürschner, 1958; Wuenschel, 1960 and Bois et al., 1960). Common to all these methods was an assumption of perfect elasticity. Baranov and Kunetz (1960) proceeded one step further and provided means by which depth-independent attenuation could be included. Trorey (1962) points out the limitations such assumptions impose on the theoretical seismograms and proposed a method by which frequency and depth-dependent absorption could be programmed into the computations. His time-domain solution is a modification of the ray-tracing scheme of Baranov and Kunetz (loc. cit.) in which the seismic section is divided into many layers of equal time thickness.

For the study of synthetic seismograms of the deep reflection data, it is important to be able to investigate the effects of transition zones, which may be described as layers of the earth in which the velocity increases or decreases linearly with depth. Berryman et al. (1958) developed an iterative formula for calculation of the reflection coefficient at the surface for a model section comprised of horizontal transition layers. Plane waves at normal incidence to the layers were assumed and the density was considered to be a constant. In the course of research for the present author's M.Sc. thesis, the equations deduced by Berryman et al. were programmed to calculate the transfer function of the layered system. Since the crustal section is known to attenuate seismic energy and from some observations made when the autopower spectra of the digitized seismograms were investigated (Section 2.2.), it was concluded that synthetic seismogram studies incorporating a depth-dependent attenuation factor were necessary. Consequently, the solution given by Berryman et al. (1958) has been rederived in order that

attenuation can be included in the computations.

The equation of motion for the displacement, $u = (u_1, u_2, u_3; t)$, of a point in an unbounded elastic solid due to the transmission of a time-dependent stress, $p_{ij}$, at any instant, t, can be written as

$$\rho \frac{\partial^2 u_i}{\partial t^2} = \frac{\partial p_{ij}}{\partial x_j} , \qquad (3.4)$$

where $\rho$ is a constant density and the summation convention is used. The stress is obtained from

$$Pij = \lambda \theta \delta_{ij} + 2 \mu e_{ij}$$

where $\theta$ is the cubical dilatation,

$$\theta = \frac{\partial u_i}{\partial x_i} ,$$

and $e_{ij}$ is the strain tensor,

$$e_{ij} = \frac{1}{2} \left( \frac{\partial u_j}{\partial x_i} + \frac{\partial u_i}{\partial x_j} \right) .$$

In addition, it is assumed that $\lambda = \lambda (x_1, x_2, x_3)$ and $\mu = \mu (x_1, x_2, x_3)$ are spatially dependent. Substituting into (3.4) and neglecting the second and higher derivatives of the Lamé functions gives the equation

$$\rho \underline{\ddot{u}} = (\lambda+\mu) \underline{\nabla} \theta + \theta \underline{\nabla} \lambda + \mu \nabla^2 \underline{u} + (\underline{\nabla} \mu . \underline{\nabla}) \underline{u} + \underline{\nabla} (\underline{\nabla} \mu . u) . \qquad (3.5)$$

When studying reflection data at near-vertical incidence, a useful approximation is an assumption that plane waves propagate only in the z-direction. In this case, the only displacement is $u_3 \equiv w$ and only derivatives with respect to $x_3 \equiv z$ are non-zero and need to be considered. By again neglecting the second derivative of $\mu$, equation (3.5) becomes

$$\rho \frac{\partial^2 w}{\partial t^2} = \frac{\partial}{\partial z} \{ [\lambda(z) + \mu(z)] \frac{\partial w}{\partial z} \} + \frac{\partial}{\partial z} \mu \frac{\partial w}{\partial z}$$

or

$$\frac{\partial^2 w}{\partial t^2} = \frac{\partial}{\partial z} \left[ \frac{\lambda(z) + 2\mu(z)}{\rho} \frac{\partial w}{\partial z} \right] . \qquad (3.6)$$

Let $$w(z,t) = W(z)e^{i\omega t} \quad .$$

Substituting into equation (3.6) gives

$$-\omega^2 W(z) = \frac{d}{dz}\left[\frac{\lambda(z) + 2\mu(z)}{\rho}\right]\frac{dW}{dz} + \left[\frac{\lambda(z) + 2\mu(z)}{\rho}\right]\frac{d^2W}{dz^2} \quad , \tag{3.7}$$

where the total differential is written because W, $\lambda$ and $\mu$ are functions of z only. In order to introduce attenuation into the problem, $\lambda$ and $\mu$ are formally expressed as complex quantities (Sato, 1967):

$$\lambda = \lambda^R + i\lambda^I$$

$$\mu = \mu^R + i\mu^I \quad .$$

As the density is constant, all the attenuation is associated with these complex elastic modulii and the square of a complex velocity, v, can thus be written:

$$v^2 = \frac{\lambda^R + 2\mu^R + i(\lambda^I + 2\mu^I)}{\rho} \quad . \tag{3.8}$$

Substituting this into equation (3.7) gives

$$-\omega^2 W = \frac{d}{dz}\left[v^2(z)\right]\frac{dW}{dz} + v^2(z)\frac{d^2W}{dz^2}$$

$$= \frac{d}{dz}\left[v^2(z)\frac{dW}{dz}\right] \quad .$$

Upon rewriting, the equation becomes

$$\frac{d}{dz}\left(v^2\frac{dW}{dz}\right) + \omega^2 W = 0 \quad . \tag{3.9}$$

Consider a layered medium comprised of N+1 transition layers. The complex velocity in the $j^{th}$ layer may be written as a linear function of depth:

$$\begin{aligned} v(z) &= v_j + b_j\,(z-z_j) \\ &= v_j^R + i\,v_j^I + b_j\,(z-z_j). \end{aligned} \qquad z_j \leq z \leq z_{j+1} \tag{3.10}$$

For the zeroth layer, there is no upper boundary so $z_0$ is arbitrarily set equal to zero. In this model the initial velocity is a constant, $v_0 = v_1$. The $N^{th}$ layer is an infinite half-space of velocity $v_N$. Thus for a given layer, the real part of the velocity, representing the travelling wave, has a linear gradient and the imaginary part of the velocity, representing the attenuation, is constant.

Writing equation (3.9) for the $j^{th}$ layer yields

$$\frac{d}{dz}\left\{\left[(v_j^R + iv_j^I) + b_j(z-z_j)\right]^2 \frac{dW_j}{dz}\right\} + \omega^2 W_j = 0. \qquad (3.11)$$

Equation (3.11) is similar to equation (5) of Berryman et al. (1958) except that $v_j$ is complex:

$$v_j = v_j^R + iv_j^I \quad . \qquad (3.12)$$

The development in their paper may then be followed step-by-step to produce the reflection coefficient $R_{j-1}$ for the (j-1)th layer in terms of $R_j$.

$$R_{j-1} = \frac{b_{j-1}\beta_{j-1} + (b_j - b_{j-1}) - b_j\beta_j\left(\frac{1-R_j}{1+R_j}\right)}{b_{j-1}\beta_{j-1} - (b_j - b_{j-1}) + b_j\beta_j\left(\frac{1-R_j}{1+R_j}\right)} \exp\left\{-\beta_{j-1} \ln\left[\frac{v_j^R + iv_j^I}{v_{j-1}^R + iv_{j-1}^I}\right]\right\} \qquad (3.13)$$

where $$\beta_j = \left[1 - 4\omega^2/b_j^2\right]^{1/2} .$$

For the $N^{th}$ layer there is only a transmitted wave, so $R_N = 0$. On a digital computer, equation (3.13) can be iterated from $R_N$ to produce $R_o$ which represents the ratio of the amplitude of the reflected wave at the 'surface' to that of the incident wave. When determined for all frequencies, this constitutes the transfer function for reflected waves at vertical incidence for the entire layered system. All multiple reflections are inherent in the computed result.

In the practical application of equation (3.13), some questions might be raised as to what constitutes the complex velocity. The available data are continuous velocity logs for the sedimentary section, supplemented by velocity and depth determinations in the deeper crust. These values give the phase velocities for propagation of seismic waves. Equation (3.13) requires the complex velocities so a relation between the specific attenuation factor, Q, and the real and imaginary parts of the velocity is necessary. In general, the wave equation has a solution of the form $\exp [i\omega (z/v - t)]$ where $v = v_R + i\, v_I$. (For the sake of the following discussion, the designations for the real and imaginary terms have been changed to subscript form.) The phase velocity, c, and the attenuation coefficient, $\alpha$, can be obtained from the complex velocity:

$$\frac{1}{c} = \mathrm{Re}\left[\frac{1}{v_R + i v_I}\right]; \quad \alpha = \omega\, \mathrm{Im}\left[\frac{1}{v_R + i v_I}\right] . \tag{3.14}$$

In equation (3.3), it was established for progressive waves that

$$\frac{1}{Q} = \frac{2\alpha c}{\omega} . \tag{3.15}$$

Using (3.14) and (3.15),

$$\mathrm{Im}\,\frac{1}{v} = \mathrm{Re}\,\frac{1}{v} \,/\, 2\,Q . \tag{3.16}$$

Rationalizing the reciprocal of the complex velocity gives

$$\frac{1}{v} = \frac{v_R}{v_R^2 + v_I^2} - i\,\frac{v_I}{v_R^2 + v_I^2} . \tag{3.17}$$

From (3.16) and (3.17),

$$-\frac{v_I}{v_R^2 + v_I^2} = \frac{1}{2Q}\,\frac{v_R}{(v_R^2 + v_I^2)} ,$$

which gives

$$v_I = -\frac{v_R}{2Q} . \tag{3.18}$$

Thus the imaginary part of the complex velocity is related to the real part and the specific attenuation factor.

Although equation (3.14) shows that Re (1/v) = 1/c, (3.17) indicates that $v_R$ cannot be evaluated without prior knowledge of $v_I$, a conflict with equation (3.18). To solve this problem, it can be shown that $v_R \simeq c$. From (3.14), (3.15) and (3.17)

$$\text{Re}\ \frac{1}{v} = \frac{v_R}{v_R^2 + v_I^2} = \frac{1}{c} \qquad (3.19)$$

and

$$\text{Im}\ \frac{1}{v} = \frac{-v_I}{v_R^2 + v_I^2} = \frac{1}{2cQ} \quad . \qquad (3.20)$$

From (3.19),

$$v_R = \frac{v_R^2}{c} + \frac{v_I^2}{c}$$

and solving for $v_I$,

$$v_I = (cv_R - v_R^2)^{1/2} \quad .$$

Substituting into (3.20),

$$\frac{-(c\,v_R - v_R^2)^{1/2}}{v_R^2 + c\,v_R - v_R^2} = \frac{1}{2cQ} \quad .$$

Multiplying by $c\,v_R$ and squaring yields

$$c - v_R = \frac{v_R}{4\,Q^2} \quad .$$

Solving for $v_R$,

$$v_R = c\,\frac{4Q^2}{(4Q^2+1)} \quad .$$

Since $Q >> 1$, the approximate relation

$$v_R \simeq c \qquad (3.21)$$

is established.

Equation (3.13) has been programmed to generate the reflection response of the layered medium as a function of frequency. Some form of pulse representing the input waveform must also be produced. In the program written, the pulse normally used was generated by setting its amplitude response in the frequency domain to be constant over a specified

range of frequencies. In the time domain, this produces a spiked pulse. The reflection response and Fourier spectrum of the input waveform are multiplied in the frequency domain. A fast Fourier algorithm (Gentleman and Sande, 1966) is used to take the inverse transform of the product, this output containing the amplitude values of the synthetic seismogram. To enable comparison of such a recording with the observational data, a facility was included in the program to obtain the autopower spectrum of any desired time interval of the theoretical seismogram. All outputs from the various steps in the program were plotted on the CALCOMP plotter. The Appendix contains a FORTRAN source listing of the program used to generate synthetic seismograms with spatial attenuation.

## 3.2 Q of the crust

The attenuation of waves in elastic media has been measured for many years, but it is only within the past half decade that sufficiently precise measurements and analytical techniques have been achieved to enable computations of the distribution of Q within the earth (Anderson and Archambeau, 1964; Kovach and Anderson, 1964; Ben-Menahem, 1965 and others). These studies generally rely on earthquake-generated body and surface wave data or free oscillations of the earth. Measurements of attenuation have thus been made on long-period waves which have travelled over long distances. The resultant models of Q are only reliable for the mantle and not for the crust. Knopoff (1964) and Sato (1967) provide comprehensive reviews of the entire Q-determination problem.

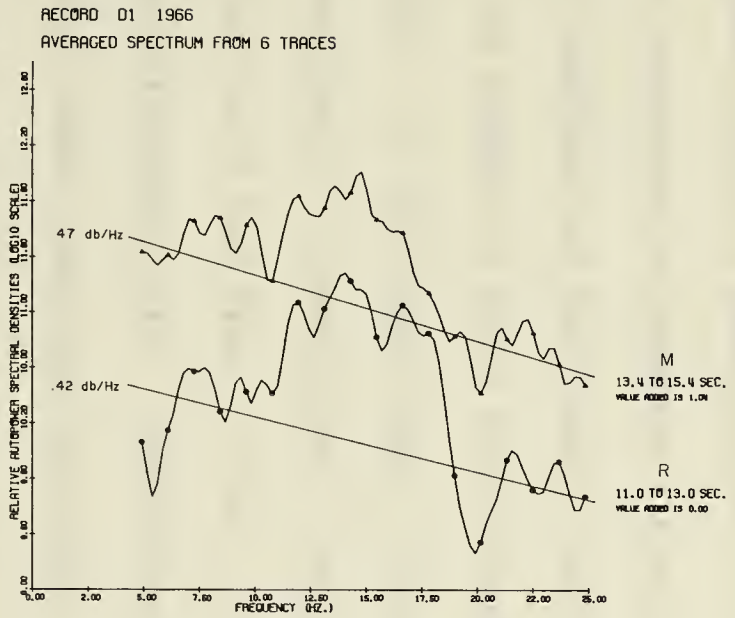
In contrast to the relatively large amount of literature concerning the study of Q in the upper mantle, very few results relating to the values of Q in the crust have been published. Press (1964) determined an average value of Q = 450 from the propagation of Lg waves from

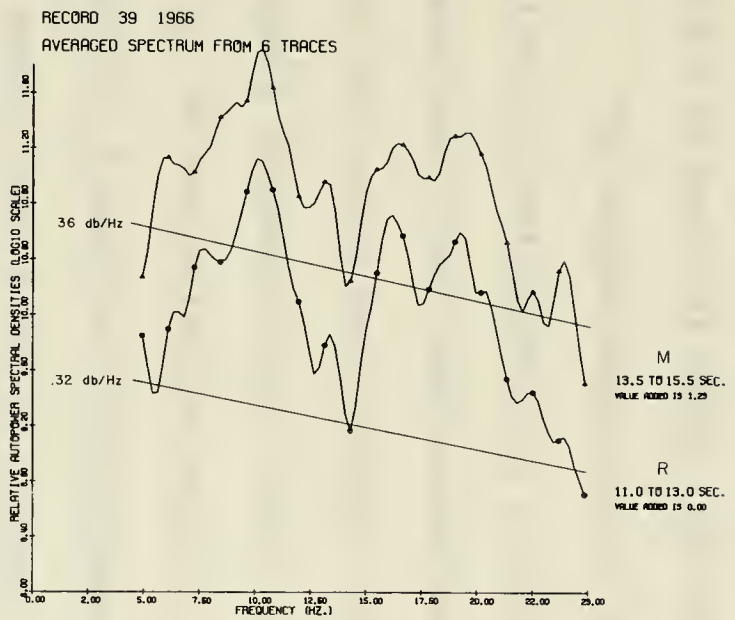
nuclear explosions in Nevada. His average value, Q = 260, for Pg waves was lower, but this he attributed to P-wave energy loss by mode conversion. From a measurement of amplitude decay for Love and Rayleigh waves of periods 50 to 300 seconds, Anderson et al. (1965) estimate a Q for P-waves of about 1000 for the crustal section to a depth of 38 kilometers. At this depth, they postulate a reduction in Q to a value of 135, this Q extending for a further 22 kilometers. For comparison with his own observations, Sumner (1967) calculates a "grouped" (or average) Q of 290 for Anderson et al.'s model to a depth of 180 kilometers. He points out the disagreement with his Q of greater than 1000 for frequencies from 1.5 to 15 Hz. and depths from the surface to 180 kilometers. This Q was established from a study of local earthquakes in southern Peru. From a study of shear waves propagating in the uppermost mantle and for paths distributed throughout the world, Molnar and Oliver (1969) show there is a significant lateral variation of upper mantle attenuating properties. They demonstrate that the shear waves are propagated efficiently throughout the stable regions of the earth, but inefficiently through active regions such as island arcs and ocean ridges. Thus reported values of Q can be highly dependent on the regions in which the seismic measurements were made.

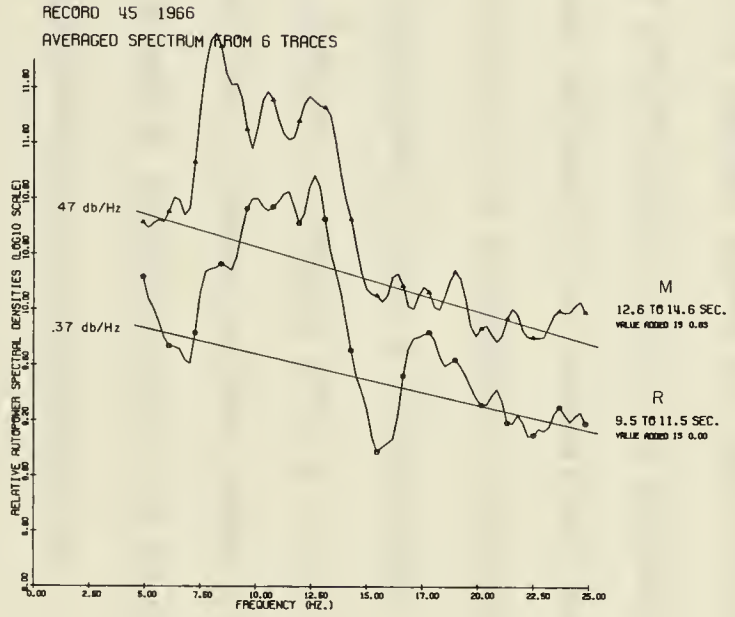
In the present research, an attempt is made to derive a Q-structure for the continental crust in southern Alberta from an analysis of the autopower spectra of reflections from the deep crust and the results from theoretical seismograms incorporating spatially dependent attenuation. A description of the autopower spectra for deep reflections on a number of seismograms was included in Section 2.2. Such spectra were computed over traveltime intervals including

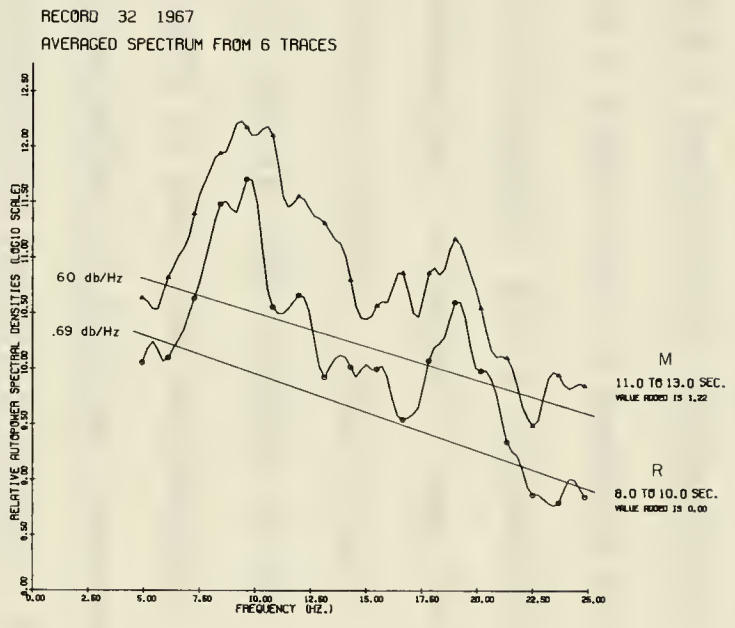
the R and M reflections for most available digitized seismograms. One characteristic which was noted for many of these spectra was a general trend toward less power at the higher frequencies within the 5 to 25 Hz. interval studied. Assuming that the trend was due primarily to the intrinsic attenuation of seismic energy as it propagated through the crustal rocks, it was decided to examine the rate of such attenuation. In order to ensure that reflected energy was being considered, only those autopower spectra for which the quality of the reflections in the lower crust at two separate time intervals was fairly good were used in the analysis. Figure 3.1 illustrates several autopower spectra for a two-second interval centered about the R or M reflection times. It should be noted that the instrument responses have been removed from these curves. The straight lines drawn across the individual spectra indicate the general trend toward less power for the higher frequency components of the reflected wave trains. To the left of each curve, the slope of the line is given. The sole purpose in presenting this linear relationship is to provide a means of comparing the rate of attenuation on the spectra of observed reflected wavelets with similar quantities determined from the autopower spectra of synthetic seismograms. This method of analysis presupposes a flat source spectrum over the frequency interval studied. The examples were chosen to show the manner in which the slopes are measured and to illustrate typical variations in the autopower spectra. Record 39, 1966 illustrates one of the lower slope values measured; Record 32, 1967 provides an example of one of the higher calculated rates. The attenuation rates of Records 01 and 45, 1966 represent more usual values. By making such measurements on many autopower spectra, an indication of the characteristic values is obtained. Figure 3.2 is a histogram of the rates

Figure 3.1 *Autopower spectra for selected time intervals on four field seismograms. The straight lines indicate the rates at which the frequency components are being attenuated.*


RECORD D1 1966
AVERAGED SPECTRUM FROM 6 TRACES
.47 db/Hz
.42 db/Hz
M
13.4 TO 15.4 SEC.
VALUE ADDED IS 1.04
R
11.0 TO 13.0 SEC.
VALUE ADDED IS 0.00
RELATIVE AUTOPOWER SPECTRAL DENSITIES (LOG10 SCALE)
FREQUENCY (HZ.)


RECORD 39 1966
AVERAGED SPECTRUM FROM 6 TRACES
.36 db/Hz
.32 db/Hz
M
13.5 TO 15.5 SEC.
VALUE ADDED IS 1.29
R
11.0 TO 13.0 SEC.
VALUE ADDED IS 0.00
RELATIVE AUTOPOWER SPECTRAL DENSITIES (LOG10 SCALE)
FREQUENCY (HZ.)


RECORD 45 1966
AVERAGED SPECTRUM FROM 6 TRACES
.47 db/Hz
.37 db/Hz
M
12.6 TO 14.6 SEC.
VALUE ADDED IS 0.85
R
9.5 TO 11.5 SEC.
VALUE ADDED IS 0.00
RELATIVE AUTOPOWER SPECTRAL DENSITIES (LOG10 SCALE)
FREQUENCY (HZ.)


RECORD 32 1967
AVERAGED SPECTRUM FROM 6 TRACES
.60 db/Hz
.69 db/Hz
M
11.0 TO 13.0 SEC.
VALUE ADDED IS 1.22
R
8.0 TO 10.0 SEC.
VALUE ADDED IS 0.00
RELATIVE AUTOPOWER SPECTRAL DENSITIES (LOG10 SCALE)
FREQUENCY (HZ.)

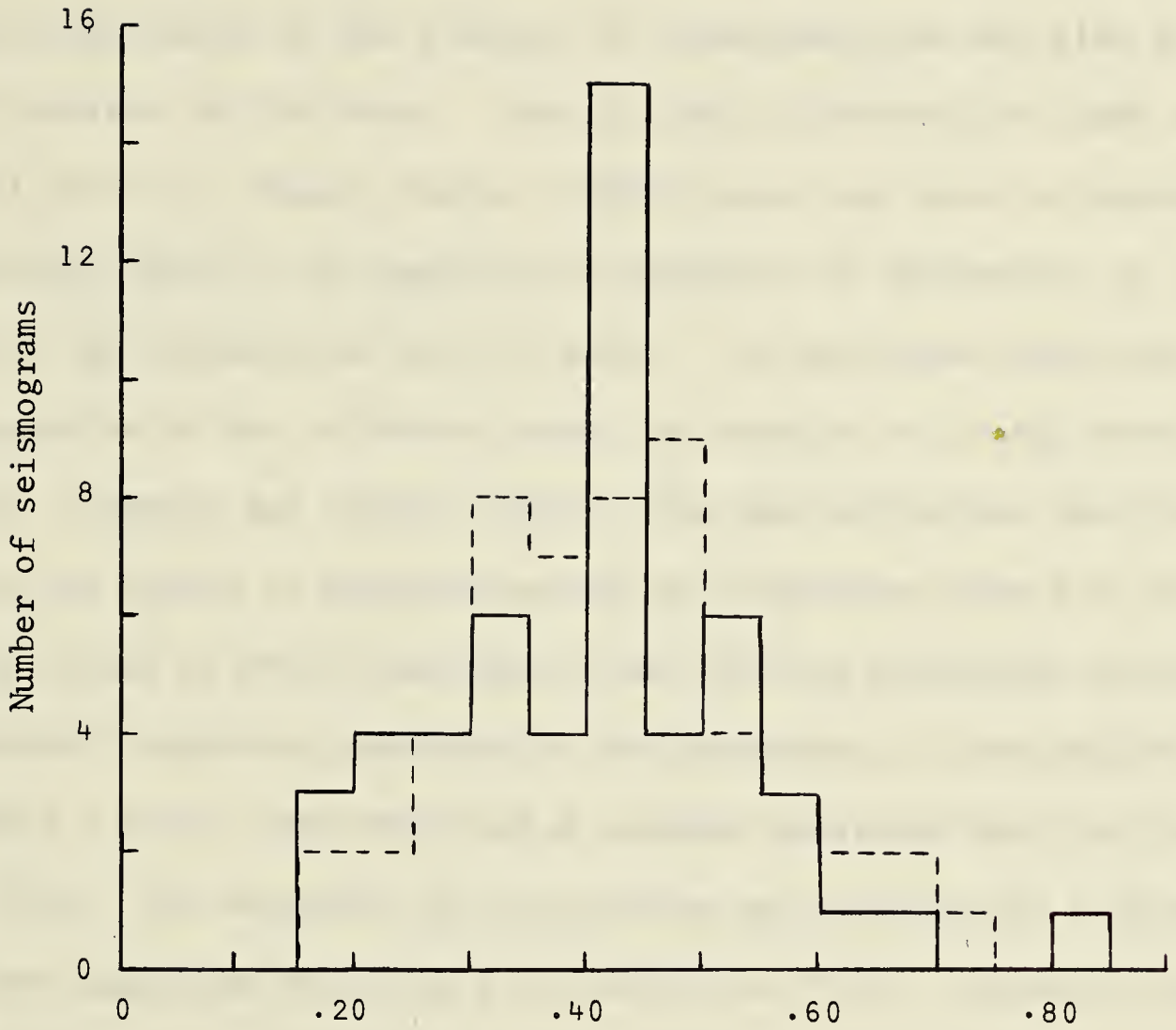


of attenuation for data from 52 seismograms. The figure shows that most of the measurements give values ranging from 0.30 to 0.55 db/Hz. as the basic rate at which power is being lost in the higher frequencies. At the bottom of the diagram, the average slope for the M and R traveltime intervals is given. The two rates of attenuation are nearly identical, being 0.42 and 0.41 db/Hz. for the M and R reflections, respectively.

The method described in Section 3.1 was used to generate the reflection coefficients as a function of frequency for a horizontally layered earth with depth-dependent attenuation. A velocity log, for which the values were averaged over 20 foot intervals, from a well (Tenneco Eyremore 10-15, Lsd.10, Sec.15, Twp.18, Rge.19 W4M) in the region of the reflection profiles was used to model the sedimentary strata to a depth of 1.68 kilometers, the extent of the log. Because the method used does not generate reflections at the free surface, a near-surface velocity contrast of 1.22 to 2.29 km/sec (4000 to 7500 ft/sec) was introduced to produce the multiple reflections from this boundary. The remainder of the crustal section was defined by a transition zone at the depths of the R (34 kilometers) and M (47 kilometers) discontinuities. In the first case, this was considered to be a first-order discontinuity in which the velocities abruptly changed from 6.5 to 7.3 km/sec for R and from 7.4 to 8.3 km/sec for M, these values being inferred from refraction data. Specification of the Q structure for the desired crustal model completed the input data necessary to determine the crustal reflection response.

It is also necessary to specify an input waveform in order to generate the synthetic seismogram for plane waves at normal incidence.

Figure 3.2 *Histogram of the rates of attenuation of frequency as measured from 52 seismograms.*




Rate of attenuation of frequency

( db per Hz. )

--- M (52 seismograms): average = 0.42 db/Hz.

—— R (52 seismograms): average = 0.41 db/Hz.

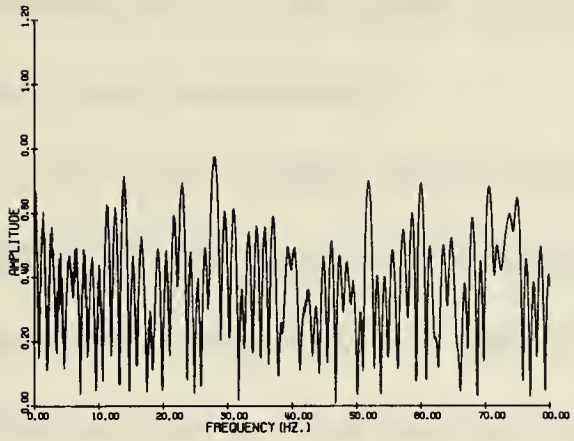


The frequency content of energy generated by an explosion in a borehole is not well known. Some indication of the spectral characteristics from an explosive source in a homogeneous medium may be obtained from studies of Sharpe (1942*a* and 1942*b*) and Heelan (1953). However, the lower frequencies have probably been enhanced over the theoretical case in our field experiments by the presence of inhomogeneities and also the use of a pattern of five holes. From a study of observations made near a small (1/8 lb.) charge, Sharpe (1942*b*) notes that even in competent material, there is an observable dissipation of frequencies as low as 150 Hz. at distances of only 60 meters. In petroleum exploration, the frequencies of the reflected energy are usually in a range from 30 to 80 Hz. (Jakosky and Jakosky, 1952). The deep reflection data from this study and others is comprised mainly of frequencies from 7 to 30 Hz. Since we had no prior knowledge of the relative amplitudes of different frequency components generated by the explosions, it was decided to produce a pulse input which had a constant amplitude spectrum from 7 to 70 Hz. The remainder of the spectrum was specified by a decrease to zero amplitude from 7 to 0 Hz. and 70 to 77 Hz. Figure 3.3 shows the input pulse resulting from such frequency specifications together with its amplitude spectrum.

The general character of the transfer function of the layered media is included in Figure 3.3, although the details change depending upon the particular model chosen. An inverse Fourier transform of the product of the complex spectra of the incident pulse and layered medium produces the synthetic seismogram shown on the lower right part of the figure. A variable gain control factor has been applied only to the plotted seismogram to provide reasonable amplitude values for display.

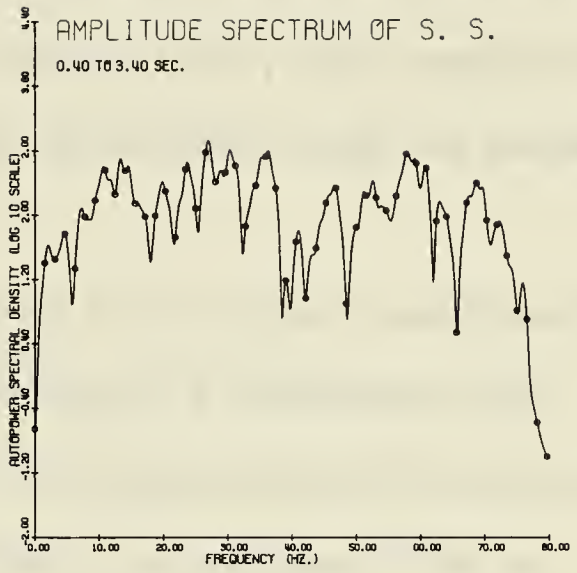
Figure 3.3 *Various quantities computed by the synthetic seismogram program. An inverse Fourier transform of the product of the complex spectrum of the input pulse and the transfer function of the layered media generates the synthetic seismogram. The autopower spectrum of the latter for the interval 0.4 to 3.4 seconds is also given.*

TRANSFER FUNCTION OF LAYERED MEDIA

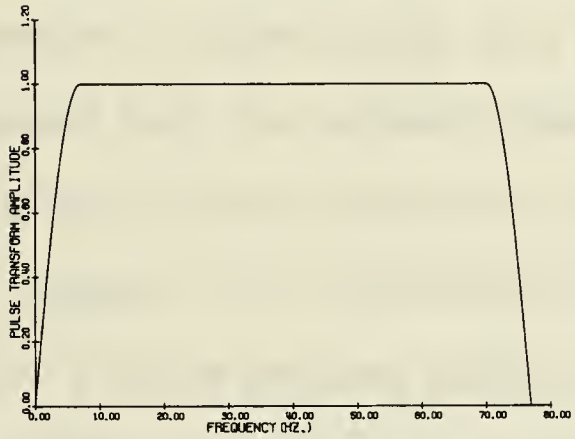



AMPLITUDE SPECTRUM OF S. S.

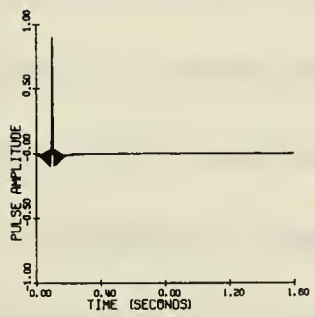
0.40 TO 3.40 SEC.

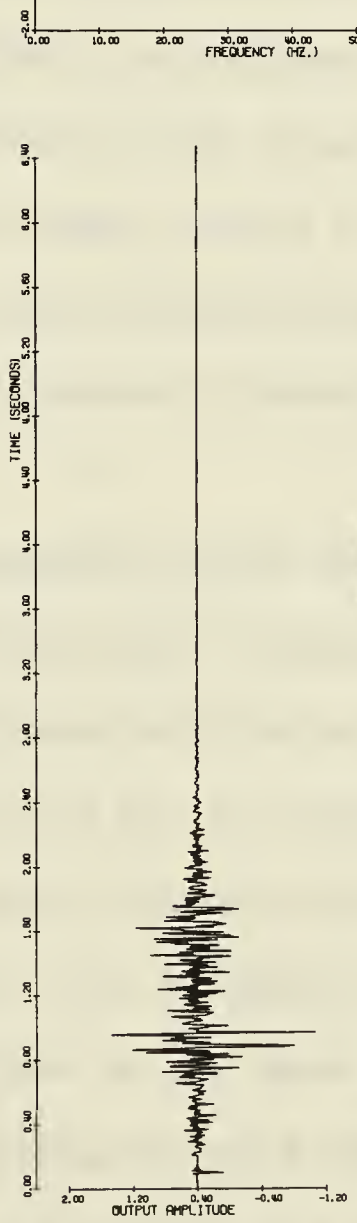


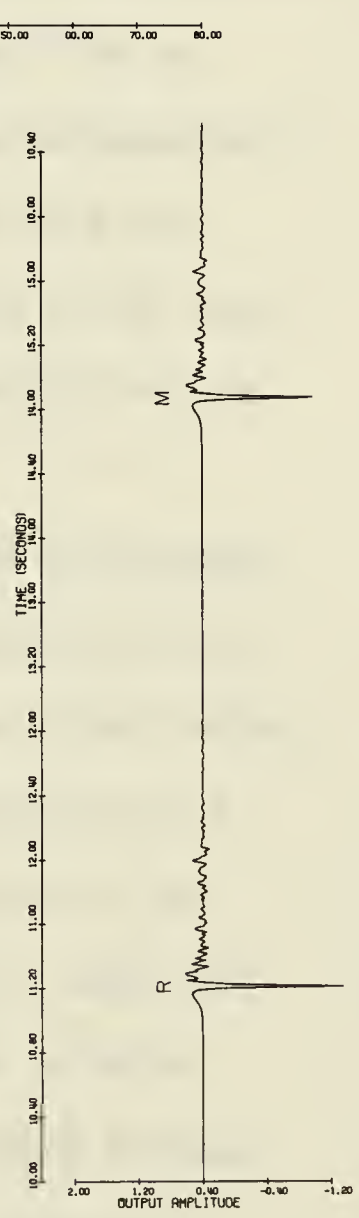

AMPLITUDE SPECTRUM OF INPUT PULSE




INPUT PULSE




SYNTHETIC SEISMOGRAM

In the upper right section of the illustration, the autopower spectral density of the synthetic seismogram from 0.4 to 3.4 seconds is plotted. For all calculations of autopower spectra, the amplitudes not modified by the gain control were used. Since only the Q values of the upper section were varied in the following investigations, this spectrum is representative of the power estimates of reflections from the sediments for any case considered.

The first model chosen consisted of first-order discontinuities at depths of the R and M interfaces. Different Q structures were attempted to determine the effects of this attenuation on the autopower spectrum of the reflections on the synthetic seismograms. For an effective Q of infinity throughout the crust, that is no attenuation, the general trend showed no decrease of energy content with higher frequencies. Finite values of Q were then introduced and it was soon discovered that the dominant trend for frequency attenuation was controlled by Q in the sedimentary layers.

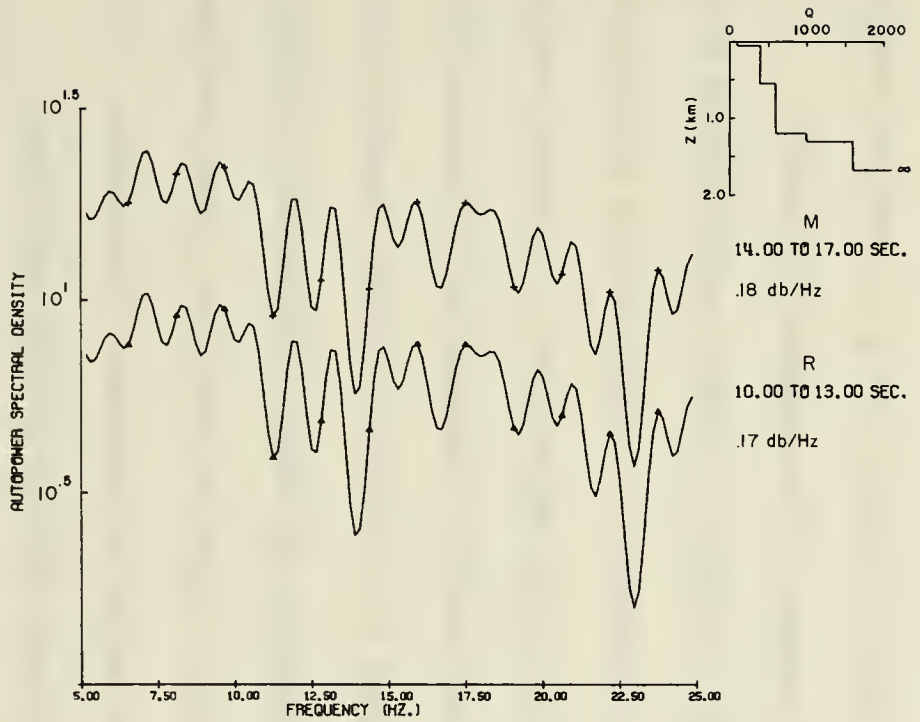
Figure 3.4 illustrates the autopower spectra for reflections from the R and M horizons modelled as first-order discontinuities for three different Q structures in the sediments with an infinite Q below. The depth extent to which each Q applied was set to correspond with the major velocity changes observed on the continuous velocity log. The first Q, extending over only 5 meters, was included to model the effects of the surface layer. A comparison of the rates at which higher frequency components are being attenuated can be made between the histogram of Figure 3.2 and the slopes measured and noted in Figure 3.4. The distributions of Q represented by the models in the upper two figures generate rates of attenuation which are lower than

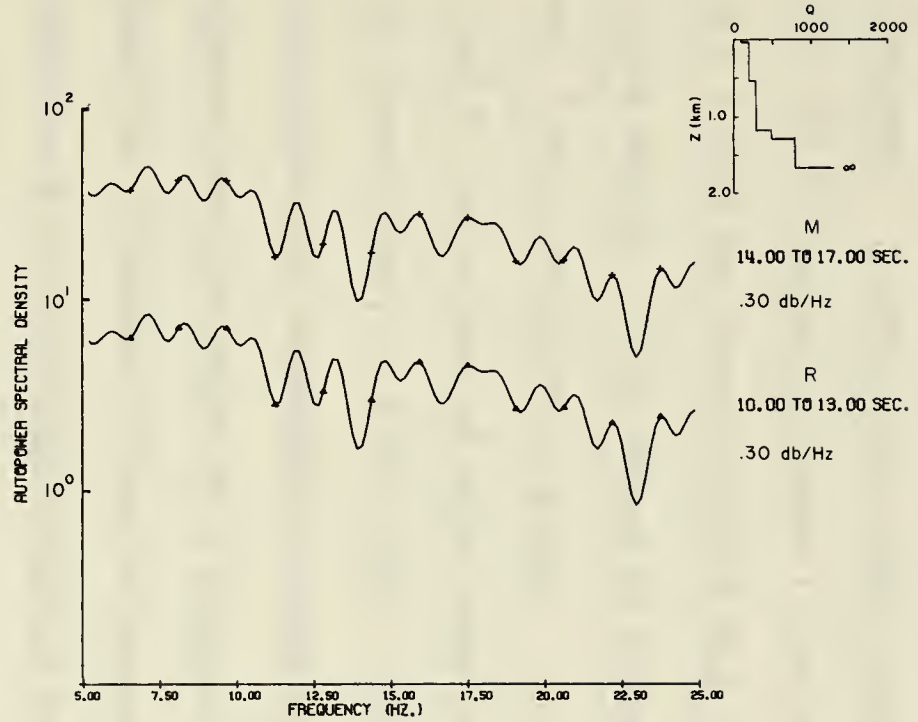
Figure 3.4 *Effects of different distributions of Q on the rates of attenuation of frequency for reflections centered about the R and M horizons modelled as first order discontinuities.*

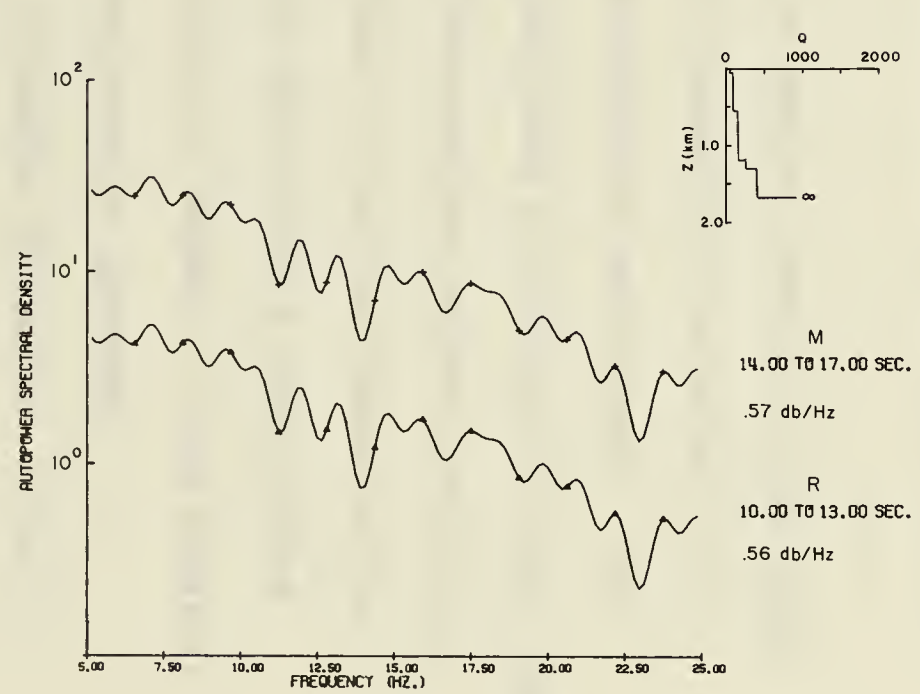
R discontinuity: *6.50 to 7.31 km/sec at a depth of 34 kilometers.*

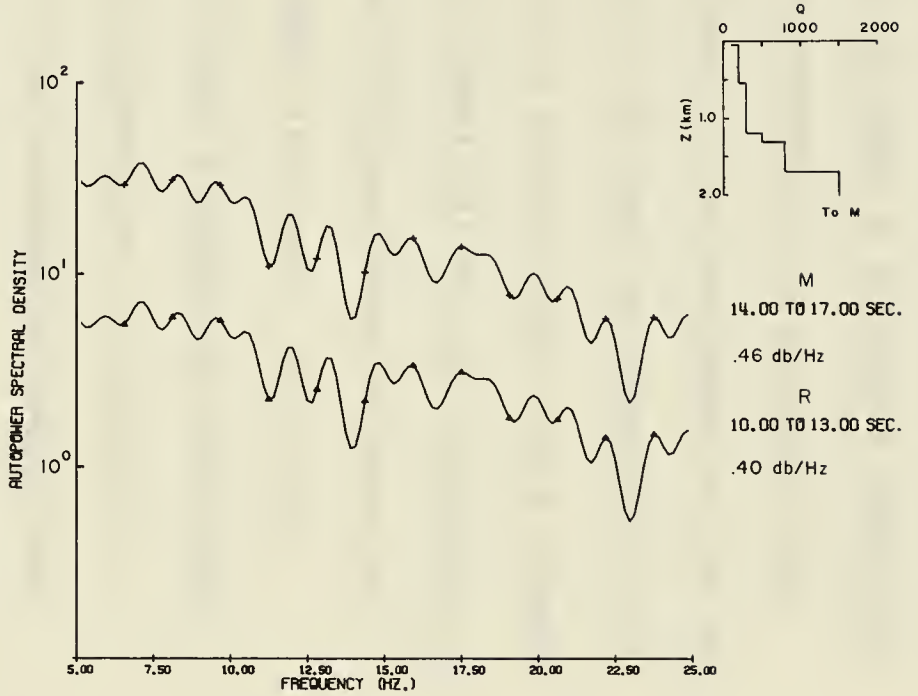
M discontinuity: *7.36 to 8.25 km/sec at a depth of 47 kilometers.*

*The variation of Q with depth for each model is shown in the upper right corner of each plot. The rates of attenuation in db/Hz. are also indicated.*


AUTOPOWER SPECTRAL DENSITY
$10^{1.5}$
$10^{1}$
$10^{-.5}$
5.00 7.50 10.00 12.50 15.00 17.50 20.00 22.50 25.00
FREQUENCY (HZ.)
Q
0 1000 2000
Z (km)
1.0
2.0
∞
M
14.00 TO 17.00 SEC.
.18 db/Hz
R
10.00 TO 13.00 SEC.
.17 db/Hz


AUTOPOWER SPECTRAL DENSITY
$10^{2}$
$10^{1}$
$10^{0}$
5.00 7.50 10.00 12.50 15.00 17.50 20.00 22.50 25.00
FREQUENCY (HZ.)
Q
0 1000 2000
Z (km)
1.0
2.0
∞
M
14.00 TO 17.00 SEC.
.30 db/Hz
R
10.00 TO 13.00 SEC.
.30 db/Hz


AUTOPOWER SPECTRAL DENSITY
$10^{2}$
$10^{1}$
$10^{0}$
5.00 7.50 10.00 12.50 15.00 17.50 20.00 22.50 25.00
FREQUENCY (HZ.)
Q
0 1000 2000
Z (km)
1.0
2.0
∞
M
14.00 TO 17.00 SEC.
.57 db/Hz
R
10.00 TO 13.00 SEC.
.56 db/Hz


AUTOPOWER SPECTRAL DENSITY
$10^{2}$
$10^{1}$
$10^{0}$
5.00 7.50 10.00 12.50 15.00 17.50 20.00 22.50 25.00
FREQUENCY (HZ.)
Q
0 1000 2000
Z (km)
1.0
2.0
To M
M
14.00 TO 17.00 SEC.
.46 db/Hz
R
10.00 TO 13.00 SEC.
.40 db/Hz

those generally observed. For the model of the lower left part of the figure, for which Q values are one half those in the upper right, it is seen that the slopes have become higher than the average given on the histogram. In the lower right diagram, an upper Q structure identical with the illustration above it has been assumed but a constant value of Q = 1500 has been included from the base of the sediments to the top of the mantle. This causes an increase in the rate of attenuation for both R and M reflection groups. A relative change in the rates between R and M, the values of which were nearly identical for no attenuation in the lower crust, is also noted. But the histogram shows evidence indicating that the attenuation rates are about the same. This would suggest that the value of Q between the R and M groups of reflections should be increased. From the preceding discussion, a possible Q structure has an average value of 290 in the sedimentary rocks, the crystalline basement has a Q of about 1500 and the lower crust would appear to have a Q in excess of 1500.

The only example of Q values for a shallow section is that given in a hypothetical case by Trorey (1962) to exemplify the effects of absorption on the first 2.5 seconds of exploration seismograms. The values chosen in this study are not inconsistent with Trorey's if one takes into account the generally higher velocities and thus higher Q values in the southern Alberta section. A comparison in the time domain of the synthetic seismogram from the sedimentary layers with a field record from the area, obtained through the courtesy of Tenneco Oil and Minerals, Ltd., indicates a reasonable degree of qualitative agreement.

One point which follows from the preceding discussion is the necessity of having wide-band recording of reflections from the post-Precambrian layers. If power spectra of such data could be obtained,

then more precise Q models for the sedimentary strata could be achieved. This would enable Q's for the lower crust to be specified with more reliability. It must also be recalled that the foregoing results were based on an assumption of a single first-order discontinuity for both the R and M transition zones. It is shown in the next section that such a model does not agree with observational results. When more complex velocity models for the transition zones are considered, it is found that by their very nature such zones may selectively enhance or decrease certain frequency components, thus introducing an apparent attenuation.

## 3.3 Properties of the crustal reflectors

On the basis of the results in Germany (Dohr and Fuchs, 1967), in the Soviet Union (Beloussov et al., 1962) and in the present study, it is well established that the deep crust is reflecting seismic energy. A question concerning the properties of these reflecting zones within the crustal section can be justifiably raised. Fuchs (1969) has recently pointed out that the classical model of a simple layered crust is not concordant with a number of observations from the deep reflection work in Germany. Such observations include reflections which rarely correlate over more than a few kilometers, the band character of the reflected signals, the apparent existence of a lower cut-off frequency and the recording of amplitudes larger than would be expected from a first-order discontinuity. To explain these observations, Fuchs postulates that the reflecting regions are best represented by laminated transition zones in which there is a series of abrupt velocity increases and decreases over small depth intervals of less than 120 meters. He shows that the reflection coefficients for such models are relatively large over certain ranges of frequency and that the reflected wavelets do

exhibit a band character.

A few remarks can be made concerning the deep reflection observations which Fuchs used to postulate such transition zones. We have previously shown that some deep crustal reflections may be continuously correlated over many tens of kilometers (Clowes et al., 1968). In the previous chapter, a comment was made concerning the generation of seismograms with an oscillatory appearance when the original data were filtered by a narrow band-pass filter. Finally, it might be noted that part of the reason that near-vertical incidence reflections with frequencies below 5 Hz. have not been successfully recorded might be due to source conditions. Sharpe (1942$\alpha$) notes that an important frequency component generated from the application of an explosive pressure within a spherical cavity in an elastic medium will be

$$f = \frac{\omega}{2\pi} = \frac{\sqrt{2}}{3\pi}\,\frac{v}{R_s} \quad ,$$

where v is the velocity of the medium and $R_s$ is the radius of the cavity. This implies that to produce a dominant component of 5 Hz. in a medium of velocity 1 km/sec, the cavity radius, which in a real medium may be approximately equivalent to the radius at which the stress produced equals the strength of the material, would be about 30 meters. To generate lower frequencies would require a medium with unusually low velocities or a very large effective cavity. Thus it is possible that the small explosions typically used in boreholes may not generate much energy at the lower frequencies.

The synthesis of seismograms with attenuation as described in Section 3.1 has been used to provide a means by which transition zones can be studied. Autopower spectra of selected time intervals on such

data may be computed and compared with those calculated from the field seismograms. Figure 3.5 illustrates the autopower spectral densities of theoretical seismograms over a three-second interval for three different types of transition zones at the depths of the R and M reflecting horizons. For display purposes, the spectrum for M in models B and C has been raised by about one order of magnitude above that for R. The characteristics of the assumed Q distribution, the type of transition zones and the form of the reflected wavelet for each model are given in Figure 3.6. Note that the peak values of the spectra for models B and C are approximately one and two orders of magnitude, respectively, greater than the maximum value for model A. This has an important bearing on the acceptance of a proposed model for it relates to the amplitudes of the reflected wavelets. From the synthetic seismogram for the sedimentary layers, the average peak power in the interval 0.4 to 3.4 seconds is about $10^{2.7}$ in relative units (Figure 3.3). It should be recalled that the synthetic seismograms generated are for plane waves at normal incidence in a horizontally layered medium. Thus the spherical spreading factor (1/r) is not taken into account. The dominant reflector within the sedimentary section has a two-way depth of three kilometers while the two-way depths to the R and M interfaces are approximately 60 and 80 kilometers. Assuming a decrease of power at a rate of $1/r^2$, it is found that the R and M reflections are attenuated by factors of $10^{-2.6}$ and $10^{-2.9}$, respectively, relative to the shallow reflector.

During the course of the field program, a few attempts were made to obtain reflections from the sedimentary layers with the same recording procedure used for the deep reflection work, except that only one

Figure 3.5 *Autopower spectra for three-second time intervals centered about the R and M reflections on synthetic seismograms. The ordinate scales are in arbitrary units. In (B) and (C), the curve for M has been raised by about one order of magnitude for display purposes. The types of model for the R and M horizons and the Q-structures which were used in generating the theoretical seismograms are given in Figure 3.6.*

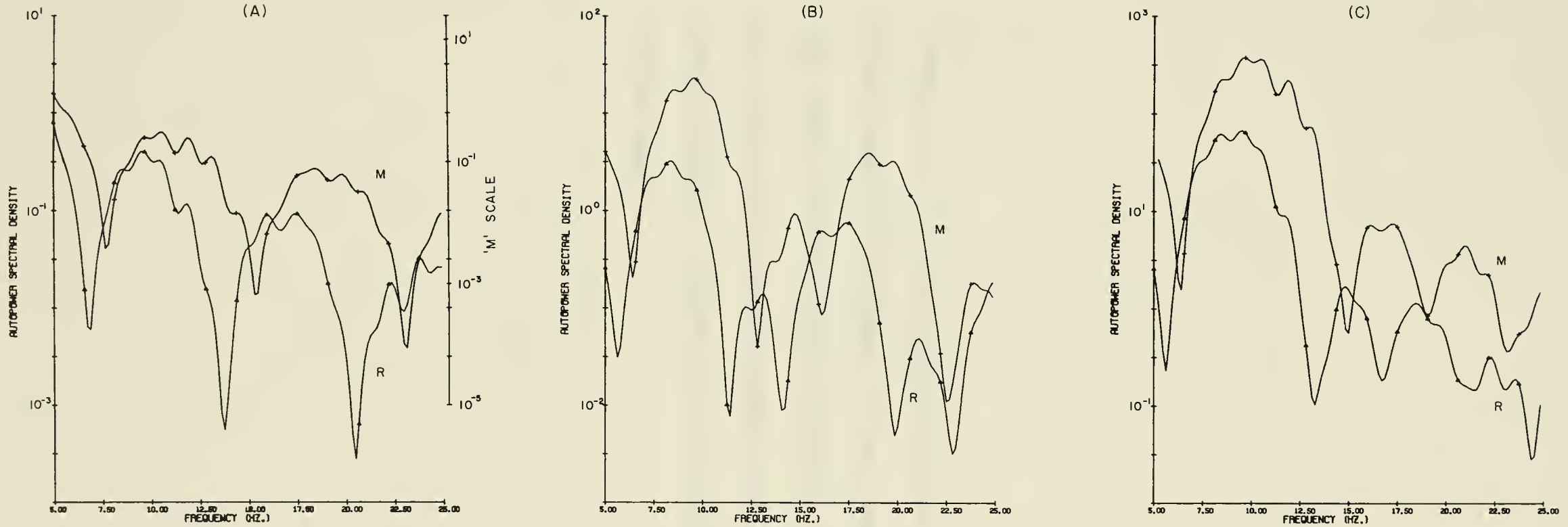
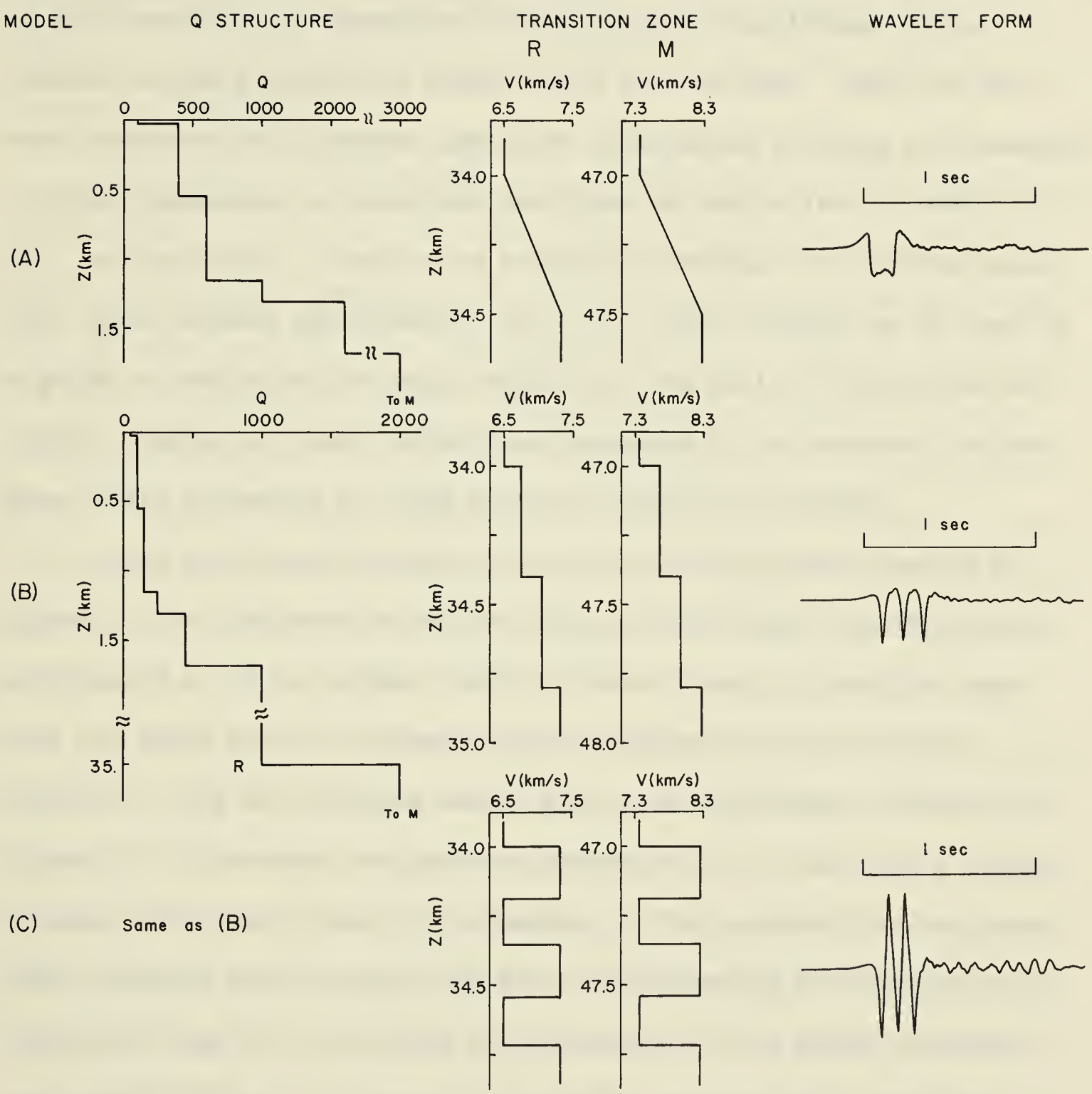

(A)
(B)
(C)
AUTOPOWER SPECTRAL DENSITY
'M' SCALE
M
R
FREQUENCY (HZ.)
5.00
7.50
10.00
12.50
15.00
17.50
20.00
22.50
25.00

Figure 3.6 *Details of the models for which the auto-power spectra of Figure 3.5 are computed. The shape of the wavelet reflected from the indicated transition zone, for a pulse input waveform (Figure 3.3), is also illustrated.*


MODEL
Q STRUCTURE
TRANSITION ZONE
R
M
WAVELET FORM
(A)
Q
0
500
1000
2000
3000
Z(km)
0.5
1.5
V(km/s)
6.5
7.5
7.3
8.3
34.0
34.5
47.0
47.5
1 sec
(B)
To M
35.
R
35.0
48.0
(C)
Same as (B)



five-pound charge in one hole was used. These attempts were generally unsuccessful because the field techniques were not optimized. However, in one instance, a seismogram with identifiable reflections from about the top of the Paleozoic and one deeper horizon was recorded. A normal deep reflection seismogram was also recorded for the same positions of the detectors. A comparison of the relative amplitudes of the shallow and deep reflection events could thus be made. When the data were corrected for different amplifier attenuation settings and assuming a linear dependence of resultant amplitude on charge size, a ratio of 53:1 was calculated. Squared to provide an estimate of relative power, this ratio becomes approximately $10^{3.4}$:1. Such a figure can be used as a guide in evaluating the applicability of the ratio of power spectra for the shallow and deep reflections generated in the synthetic seismogram, after allowance has been made for spherical spreading.

From the characteristics of the observed autopower spectra of Figure 3.1 and the spectra for the case of first-order discontinuities in Figure 3.4, it is evident that the latter form of transition zone does not yield spectral characteristics similar in form to those observed. Thus more complex models had to be constructed. Model A of Figure 3.5 illustrates the spectral densities for a zone with a linear increase of velocity over 0.5 kilometers. This produces the two peaks often observed but even with the model incorporating a distribution of relatively high Q's, the rates of attenuation of the higher frequency components (.70 and 1.0 db/Hz. for R and M, respectively) are much larger than the observed values. The shape of the reflected wavelet for a pulse input bears no relation to any observed reflections. Because the peak power of the curve for R is about $10^{-0.6}$, the ratio

of energy in the shallow reflections to that in the R reflections is $10^{5.9}$:1, after allowance has been made for the effects of spherical spreading. This compares to the observed ratio of $10^{3.4}$:1. It can be noted that a gradient over only 0.25 kilometers was also tried, but the shape of the curve, rate of attenuation and relative amplitudes did not agree with observation. For these reasons, the possibility of a linear increase in velocity with depth as a model for transition zones can probably be eliminated.

The second transition model, B, of Figure 3.5 comprises three equal step increases in velocity, the total extent of the zone being 0.8 kilometers. The general shapes of the computed spectra correlate well with those for some observed data. Although the measured rates of attenuation (.60 and .77 db/Hz. for R and M, respectively) are somewhat high, the assumed distribution of Q was low so that attenuation was considerable. The pulse input reflected from such a zone produces a sequence of pulses with strong amplitudes in one direction only. However, this wavelet form bears a closer resemblance to observed reflections than does that of model A. Comparing the power in the shallow reflections with the peak value for the R curve, and considering the effects of spherical spreading, the ratio is $10^{4.8}$:1 which is more than one order of magnitude greater than that measured from the recorded seismograms. If the depth extent of the transition zone is lessened, everything else remaining constant, the effect is a shift of the frequencies at which the spectral peaks occur, but the slopes and power spectrum ratio are relatively unaffected. Thus a step transition zone as described by model B can only be considered to have a low probability of modelling the deep reflectors.

Model C is based on the preferred solution for the deep reflecting zones as described by Fuchs (1969). It consists of a series of sharp

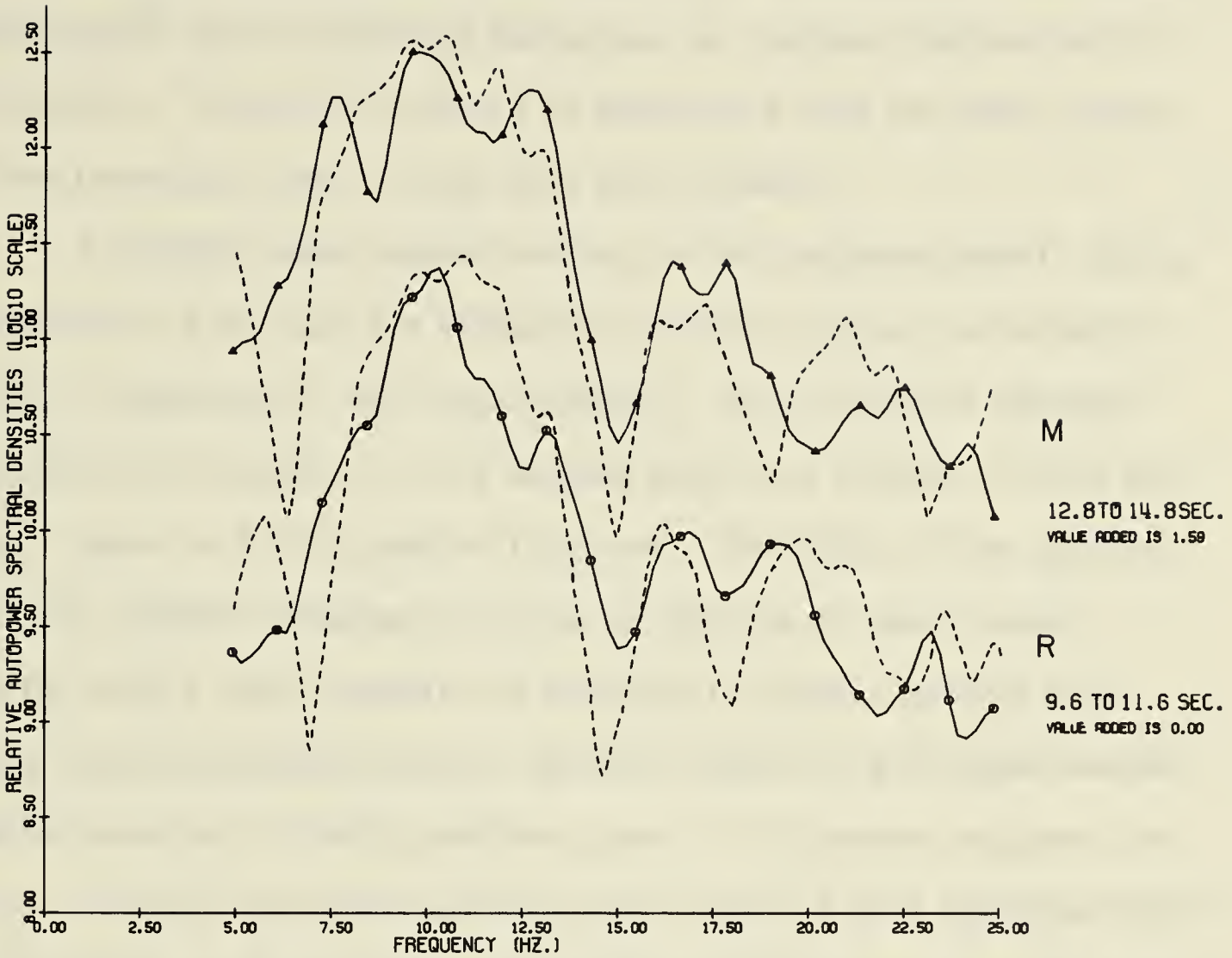
increases and decreases of velocity, for which the thickness of the individual layers is 180 meters. The shapes of the spectral curves bear a good similarity to many of those computed from the deep reflection seimograms. As measured from the spectrum, the rates of attenuation of frequency for the R and M curves are .52 and .53 db/Hz., respectively. These rates are in the range of those given in the histogram of Figure 3.2. It is seen that the attenuation included in this case is relatively high since the Q's are low. From the shape of the reflected wavelet, it is evident that the transition region of model C produces an oscillatory sequence of reflected pulses from a single input pulse. The ratio of the power in the spectrum of the shallow reflections to the peak power in that of the R reflection, allowing for the effects of spherical spreading, is $10^{3.5}$:1. This agrees favorably with the calculated ratio of $10^{3.4}$:1 for observed reflections on the field seismograms. The model of a reflecting interface consisting of thin, multiple layers of high and low velocities best satisfies all the observational data.

In Figure 3.7, a comparison of the autopower spectral densities for a two-second interval centered about the R and M reflection times of a recorded seismogram (solid curves) is made with the spectra computed from a synthetic seismogram (dashed curves). The transition model for both the R and M reflecting zones and the specified structure of Q are given in the lower part of the figure. The agreement between the observational and theoretical curves is quite good. In terms of the frequencies at which the spectra have their peak values, the depth extent of the individual high and low velocity zones is critical. For example, if the depth interval of the R zone was reduced to 0.12 from

Figure 3.7 *Comparison of the autopower spectra for two-second intervals centered about the R and M reflections on field seismograms (solid curves) with spectra computed from reflections on synthetic seismograms (dashed curves). The ordinate scale is in relative units. The variation of Q with depth and the characteristics of the transition zone models are shown in the lower part of the figure.*

RECORD 43 1966

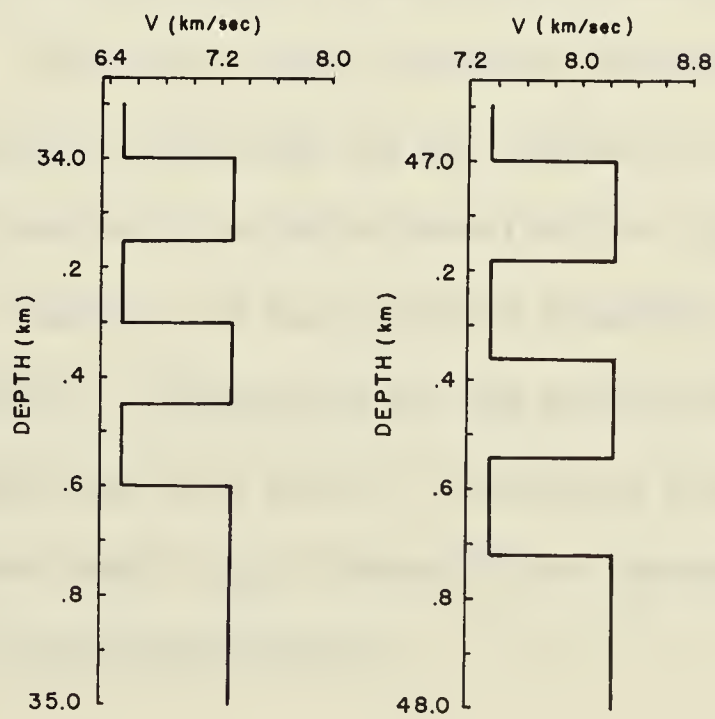
AVERAGED SPECTRUM FROM 6 TRACES




ATTENUATION




TRANSITION ZONES







0.15 kilometers, the resultant spectrum would peak at about 15 Hz. A variation in the individual thicknesses of the velocity lenses can thus account for the observed variations in the peak frequencies of the spectra. However, it should be emphasized that the total extent of the transition zone is less than one kilometer.

A slightly more complex version of the laminated model, having thicknesses of 0.1 and 0.2 kilometers for the high and low velocity layers, respectively, has been attempted. This yielded a spectrum for which the frequency of the maximum power was similar to that for equal layers of 0.15-kilometer thickness. The width of the spectral peak was somewhat broadened relative to the case of equal layers. Similar models could probably be designed to produce spectra which would closely approach observed spectral densities with broad maxima. Another version, in which gradients over 0.2 kilometers replaced the abrupt velocity increases and decreases, resulted in a spectrum which had slightly lower amplitudes, a high rate of attenuation and a form not very similar to the observed ones. One further effect was investigated. Two sets of identical lenticular transition zones were modelled to produce two sequences of reflected pulses separated by about one second of two-way traveltime. The first-order multiples generated between these zones had negligible amplitudes on the synthetic seismogram. An autopower spectrum over both reflected wavelets was calculated and showed that all the basic features of the spectrum from just one of the pulse sequences was retained. Irrespective of the particular details for any one model, it was found that some form of transition zone which included velocity reversals over small depth intervals was necessary to produce results concordant with observations.

Because the autopower spectra of the two-second time intervals, centered about reflections interpreted as being from the M discontinuity, include effects of crustal properties over a depth extent of about seven kilometers, these spectra do not represent just the M itself. In Chapter 4, it is shown that a number of reflections appear to come from within the deepest part of the crust, so that much of the character of the computed spectra from the field seismograms might be attributed to effects near the base of the crust. Thus the form of the M reflector illustrated in Figure 3.7 does not necessarily represent the Mohorovičić discontinuity, but may model a number of reflecting zones at depths near the Moho. However, it can be reiterated that on the basis of a detailed study of wide angle reflections from the M discontinuity, Meissner (1967*a*) proposed a laminated structure with individual layers less than 0.15 kilometers thick.

The model of a deep crustal reflector which has alternating lenses of low and high velocity material poses the problem of how such a zone could be formed by natural processes. It could possibly represent a series of intermittently occurring lava flows in which sediments, since metamorphosed, were deposited during periods of quiescence. Perhaps it represents the effects of partial melting and the segregation of more basic, high velocity material from lower velocity, acidic rocks. From petrological studies, Ringwood and Green (1966) give evidence that mineral assemblages, which are stable under the pressure-temperature conditions of the lower continental crust and which are likely to exist there, have densities and seismic velocities that are much higher than values believed to be characteristic of the lower crust. They suggest that in this region there exist large quantities of minerals of

relatively low seismic velocity to counterbalance the higher velocities of the other rocks. Such a hypothesis could have some relation to the postulated deep crustal reflectors.

# CHAPTER 4

## INTERPRETATION OF THE DATA

### 4.1 The analog reflection seismograms

In the last chapter, it was demonstrated that inherent on the recorded seismograms was information relating to the nature of the reflecting horizons and to the elastic properties of the crustal section. However, the primary intent of the experimental research, and the philosophy behind the design of the project, was an investigation of possible structural features in the lower crust. To this end, more than one hundred deep reflection seismograms from the Lomond and Blackfoot profiles were carefully processed and analysed to provide as comprehensive an interpretation as possible. Since a considerable time lag often existed between the data acquisition in the field and the subsequent digitization in the laboratory, an analysis of the photographically recorded seismograms was considered necessary and important. Usually the quality of these data was sufficiently good to enable a preliminary interpretation of the lower crustal structure.

For such an interpretation, the seismograms were examined to identify most coherent phases which could possibly be identified with reflected energy. Because the field method employed was continuous profiling, two traces on adjacent records had reflected energy which ideally followed the same travel path but in opposite directions, thus allowing a time correlation (time-tying) of reflected events between these records. Phase correlation of the seismograms also proved possible. In this manner, many reflecting events were correlated, some over much of the entire profile, others over only a few kilometers. A preliminary time cross section of the profile was plotted, with each reflection being

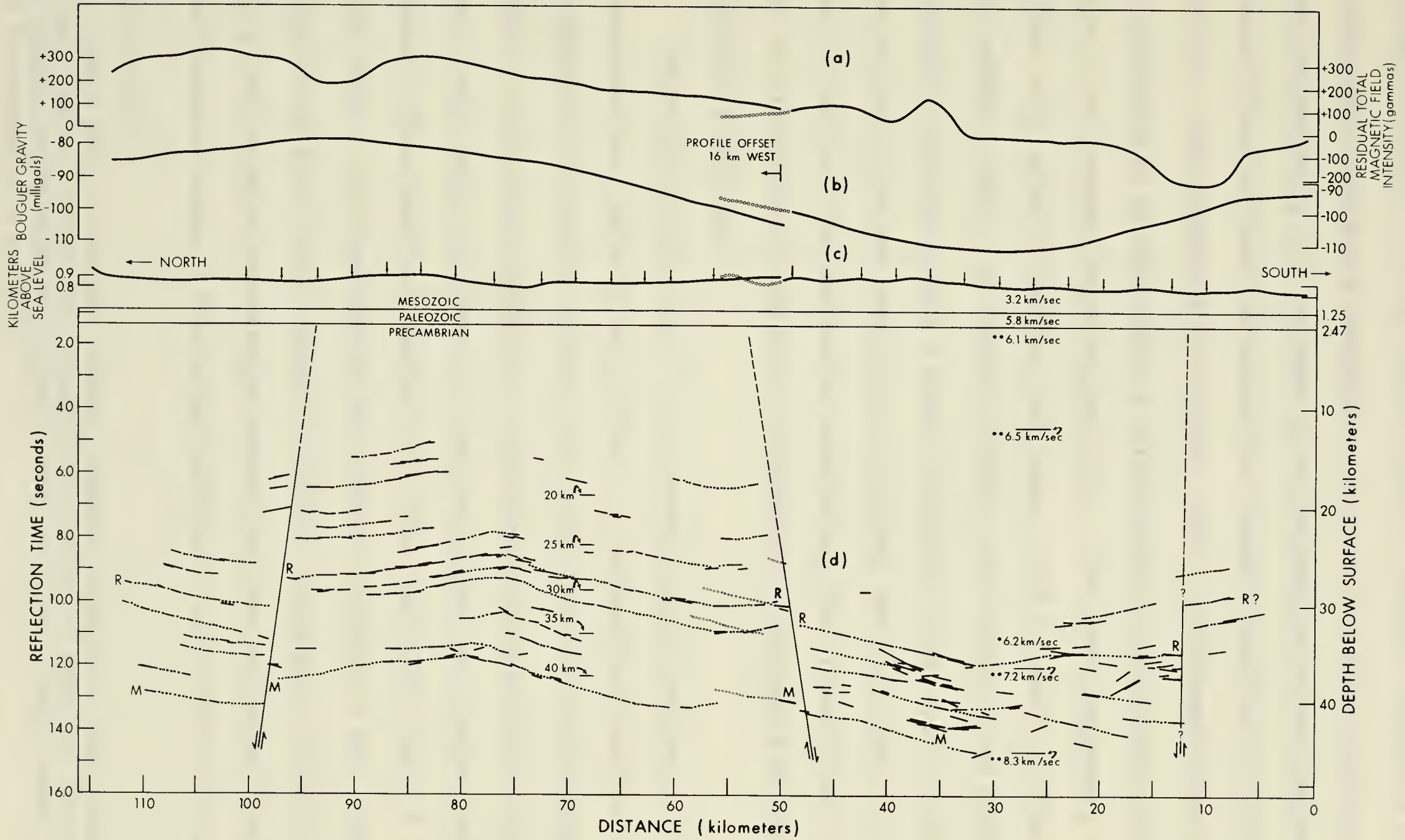
placed directly below the surface region at which it was recorded. From the steep dips which could be seen, it was evident that all reflections would have to be migrated in order to display the reflecting horizons in their true subsurface positions. For this purpose, a wavefront migration chart was generated following the method described by Gaby (1945). A velocity function consisting of five layers of constant velocity was used. In the post-Precambrian layers, the velocities were determined from continuous velocity logs of wells in the vicinity, while refraction and reflection data were utilized in the lower section (Cumming and Kanasewich, 1966). In Figure 4.1, the migrated seismic cross section is plotted as a function of two-way traveltime on an approximately 1:1 scale. A depth scale has been appended to the section to aid interpretation but it must be remembered that along the section the depth scale varies due to variations in average velocity as the thickness of the layers changes. The depth on the right applies to the deepest part of the structure; that near the middle applies to the highest part.

The lack of reflections between 0 and 6 to 9 seconds is due to a combination of factors. As mentioned previously, the instrumentation incorporates no automatic gain control so that the signals received between 0 and 4 seconds generally exceeded the dynamic range of the amplifiers. Additionally, large amplitude surface waves generated by the explosion often obscure reflected energy up to times of 6 or 9 seconds. As evidenced by the figure, this problem was more severe for the southern profile than for the northern profile, where coherent events from shallower events were observed.

The reflection labelled R was the one with the largest amplitude on most seismograms and appeared to correlate across nearly the entire

Figure 4.1 (a) *and* (b): *Residual total magnetic intensity and Bouguer gravity, respectively, along the seismic profiles.* (c) *Surface topography along the profiles. The vertical exaggeration is about ten times. Arrows indicate shot point locations.* (d) *Reflection seismic cross section. Depths and velocities of refracting horizons (**) from an east-west survey are superimposed at the position of intersection. The "*6.2 km/sec" velocity is an average vertical velocity between the top of the Paleozoic and the Riel* (R) *discontinuity as obtained from reflection data. Correlation of the reflecting events is indicated by dots.*

*Note the east-west offset of 16 kilometers between the two halves of the section.*


(a)
(b)
(c)
(d)
BOUGUER GRAVITY (milligals)
+300
+200
+100
0
-80
-90
-100
-110
PROFILE OFFSET
16 km WEST
RESIDUAL TOTAL MAGNETIC FIELD INTENSITY (gammas)
+300
+200
+100
0
-100
-200
-90
-100
-110
KILOMETERS ABOVE SEA LEVEL
NORTH
SOUTH
0.9
0.8
MESOZOIC
PALEOZOIC
PRECAMBRIAN
3.2 km/sec
5.8 km/sec
••6.1 km/sec
1.25
2.47
••6.5 km/sec
20 km
25 km
30 km
35 km
40 km
R
M
•6.2 km/sec
••7.2 km/sec
••8.3 km/sec
R?
REFLECTION TIME (seconds)
2.0
4.0
6.0
8.0
10.0
12.0
14.0
16.0
DEPTH BELOW SURFACE (kilometers)
10
20
30
40
110
100
90
80
70
60
50
40
30
20
10
0
DISTANCE (kilometers)

90-kilometer profile. At the position where a reversed refraction survey had been made (Cumming and Kanasewich, loc. cit.) the depth to this reflector corresponded with the depth of an intermediate refracting horizon. Previously this interface was termed the "Conrad" discontinuity (Richards and Walker, 1959; Kanasewich and Cumming, 1965). This nomenclature has been criticized as it could imply a stratigraphic or petrologic correlation with the European Conrad discontinuity. The latter represents an interface with velocity changing from about 5.6 to 6.2 km/sec (Conrad, 1925; Jeffreys, 1926). In southern Alberta, the refracting and reflecting intermediate layer represents a change in velocity from 6.5 to 7.2 km/sec. Since the velocities are substantially different and since there is no desire to imply an intercontinental correlation, the present study will refer to this horizon as the Riel[1] discontinuity as suggested by Professor D. H. Hall of Manitoba.

The reflection labelled M was of erratic quality but could still be correlated over parts of the profile. At the position where the east-west refraction survey was recorded, the reflecting horizon corresponded in depth to that of the Mohorovičić discontinuity as determined by that survey. Other quasi-continuous horizons were generally of poorer quality and some of these exhibited contrary dip. One event which lies 0.9 seconds deeper than R and mirrors the latter's structure is most certainly of multiple origin. This is shown in synthetic seismogram studies (Clowes et al., 1968) where a reverberation between the free surface and the top of the Paleozoic causes a first-order multiple to occur about 0.9 seconds

---

[1]Louis Riel, a colorful western Canadian intellectual and pioneer of French-Indian ancestry who brought the province of Manitoba into union with Canada, became a member of parliament, and finally led a revolt which ended his career on a scaffold.

after the primary event.

Intermingled groups of many closely spaced reflections at some positions probably show the effects of three-dimensional structure projected on a two-dimensional cross section. Some steeply dipping events could be due to energy scattered from steep structural features or faults. Some indication of three-dimensional structure was obtained from a 2.4 kilometer east-west profile located at the 17-kilometer distance on the diagram. Good continuous reflections which corresponded to events at similar times on the major profile were recorded. All reflecting horizons showed considerable west dip, this amounting to about 12 degrees for the Riel discontinuity. Such results emphasize the need for detailed investigations and imply that one should interpret two-dimensional sections with caution when the true structure probably has major three-dimensional complications.

Structural relief, as indicated by the cross section of Figure 4.1, is of considerable magnitude. The horizon interpreted as the M discontinuity varies from a depth of 47 to 38 kilometers. At the same time, the Riel discontinuity changes from a maximum depth of 37 kilometers to a minimum of 26 kilometers. The latter variation represents relief of 11 kilometers over a horizontal distance of only 50 kilometers. Considering that for most refraction interpretations in stable areas, the Moho is assumed to be planar with either little or no dip, it is surprising and enlightening that the deeper horizon shows comparable relief to the shallower one. The profile suggests that the isopach, R to M, is increasing toward the north, as it should to agree with depths calculated by Richards and Walker (1959) for a reversed refraction profile centered about 60 kilometers to the northwest. Evidence for the faults could be

seen on some seismograms where good quality reflections within about one second of each other and having similar character but opposing stepouts could be picked. When these events were migrated to their true reflecting positions, the hypothesis of faulting was further strengthened. Although this initial interpretation was expected to be somewhat preliminary, it has stood up well in light of much further evidence.

## 4.2 The digitally processed seismograms

The dips of the structures indicated on the two-dimensional profile presented in the last section are manifested on the recorded seismograms as reflection events with varying apparent velocities. Consequently the form of digital filter described in Section 2.4—the velocity filter which selectively enhances reflections within a specified pass range of apparent velocities—is admirably suited for delineating any possible coherent reflected energy which may be arriving from dipping structures.

Filters of this type have been applied to the entire suite of digitized reflection seismograms except for cases where one of the two individual recordings necessary for the filtering process was not available. In general, the beam-forming filter was applied with three different pass bands: -11.7 to -35.2 km/sec, -35.2 to +35.2 km/sec and +35.2 to +11.7 km/sec. If these values are converted to time stepout per trace, the total range of such moveout is from -25 to +25 milliseconds per trace (subsurface dips of about -17° to 0° to +17° at the level of the Riel). Whenever plots of the original data or filtered output suggested that apparent velocities other than those generally used might be significant, a filter with different characteristics would be applied. In a few cases a search for coherent energy with very low apparent velocities was made, but this provided few correlatable events.

By carefully analysing the velocity filtered seismograms, a complete record section along the Lomond and Blackfoot profiles has been obtained. Frequently it was found that one of the three filtered outputs showed coherent reflection phases with greater amplitudes than either of the remaining two. In such cases, it was easy to choose an appropriate filtered record for using in the section. However quite often it was found that one, two or all three filtered outputs would have some reflections with good signal-to-noise ratios. Usually these would be at different traveltimes and it was necessary to piece together a composite record to represent all the reflection events. Of course the choice of which filtered seismogram provided the best data was not always simple. Complications arising from the simultaneous arrival of energy representing reflections from horizons of opposing dips could be found on some recordings. To further confuse the interpreter, the effects of three-dimensional structure producing some coherent reflected energy must be considered.

In Figure 4.2, the total reflection record section compiled from the velocity filtered seismograms is presented. Because of the large quantity of data, the profile has been divided into six sections and the illustration continues for six pages. The record section progresses from south to north, from the Lomond to the Blackfoot profile. In order to provide continuity, the last record on each page of the section is duplicated as the first record of the succeeding page (except for 4.2B to 4.2C where there was one set of seismograms unavailable). As an aid for comparison with the cross section of Figure 4.1, the caption for the present diagram lists the approximate distance ranges according to the scale of Figure 4.1 for each part of the illustration. Blank spaces

Figure 4.2 *Velocity filtered reflection record section along a 90-kilometer profile. On the labels to the left of each seismogram, the first two numbers refer to the records which were filtered. The numbers following* "VF" *give the range of apparent velocities for the pass band of the velocity filter. If the results from more than one pass band have been considered, this is indicated at the appropriate position above the seismogram.*

*The illustration continues for six pages and the appropriate part of the cross-section of Figure 4.1 to which each page refers is shown below according to the distance scale of Figure 4.1.*

4.2A *10 to 24 kilometers.*

4.2B *22 to 35 kilometers.*

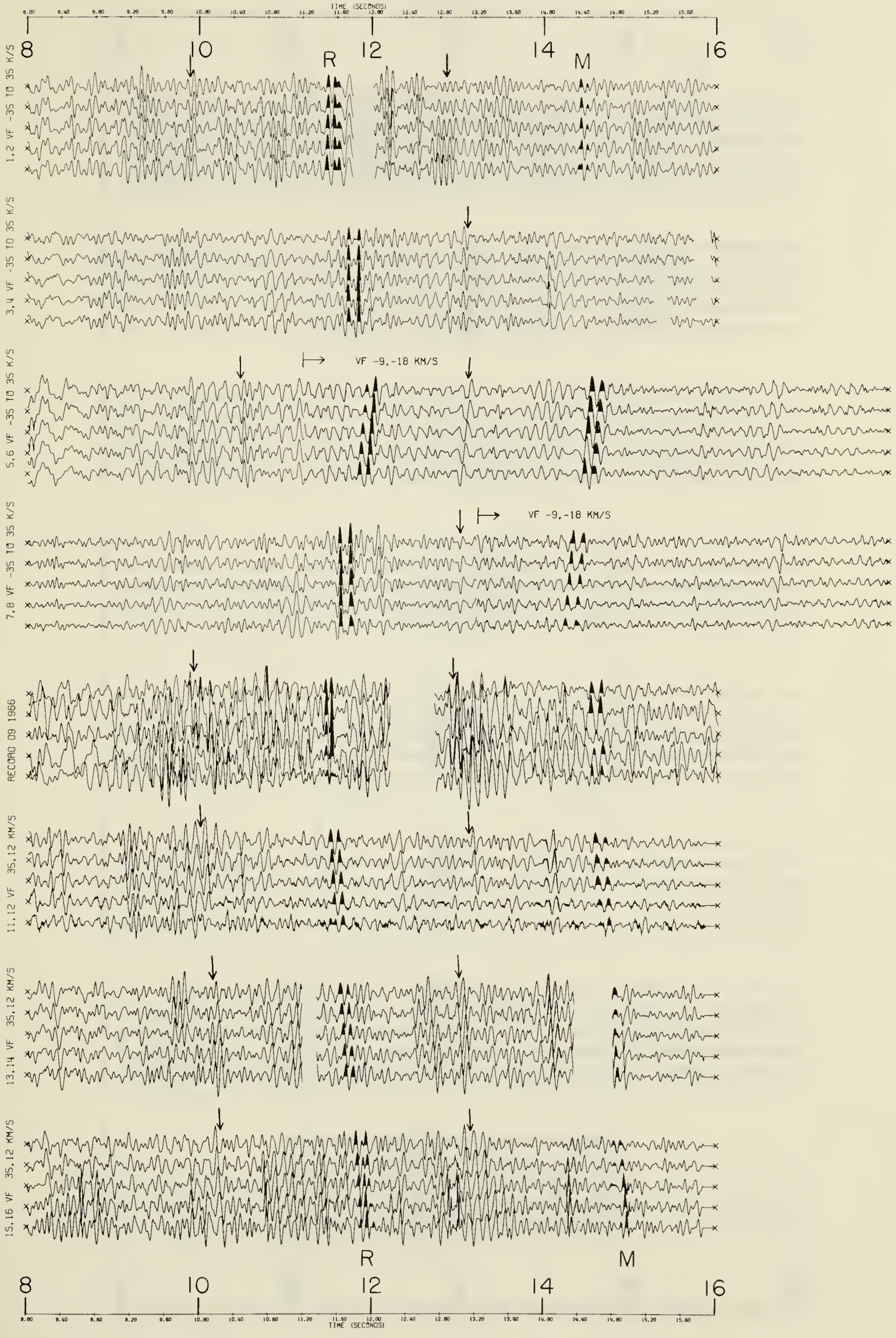
4.2C *36 to 50 kilometers.*

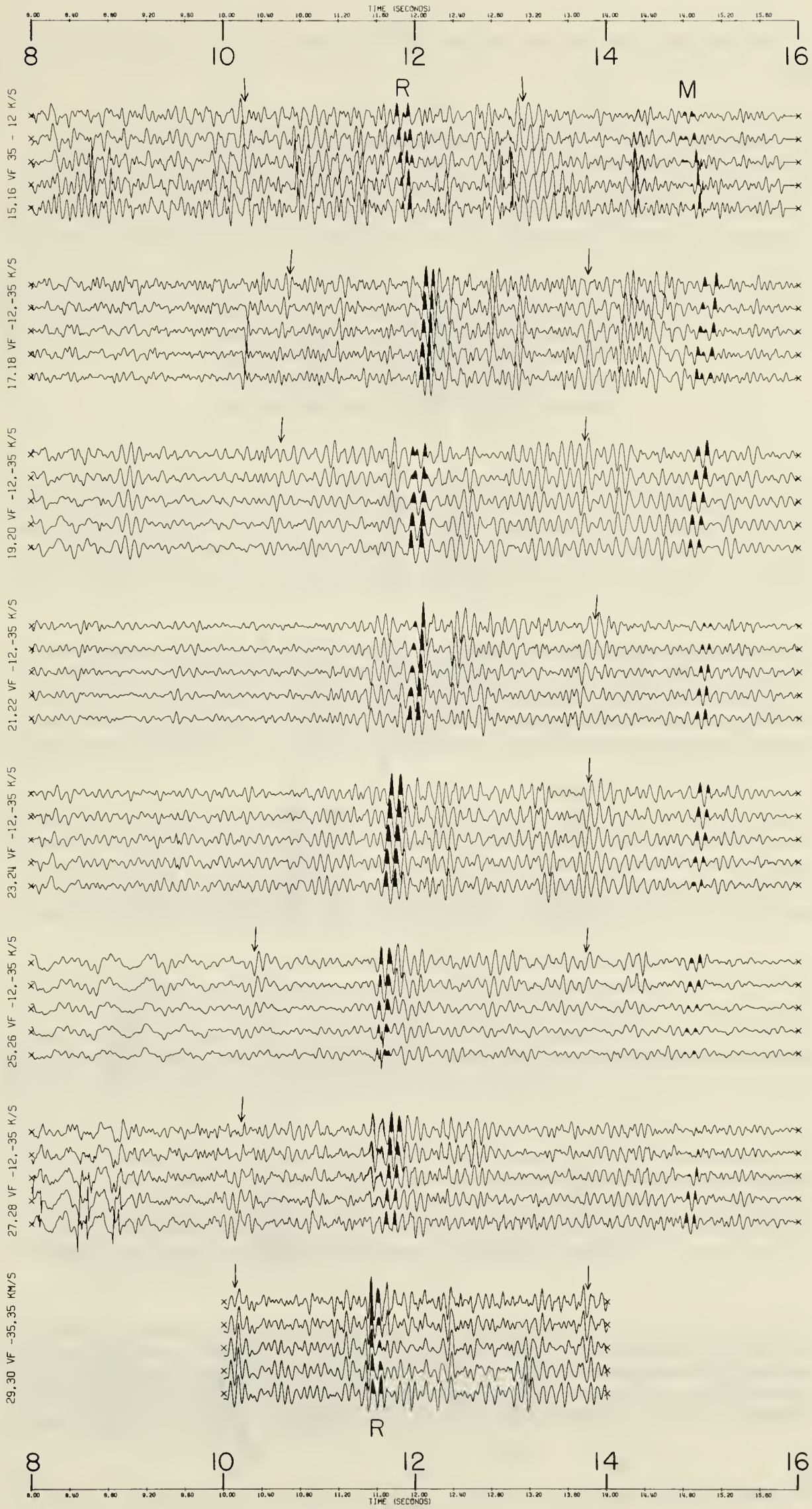
4.2D *50 to 71 kilometers.*

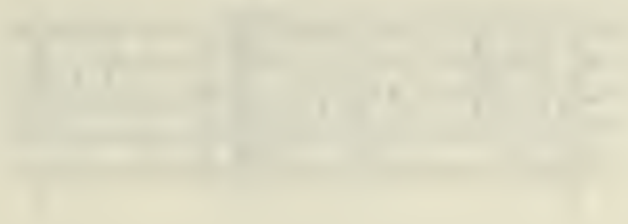
4.2E *69 to 87 kilometers.*

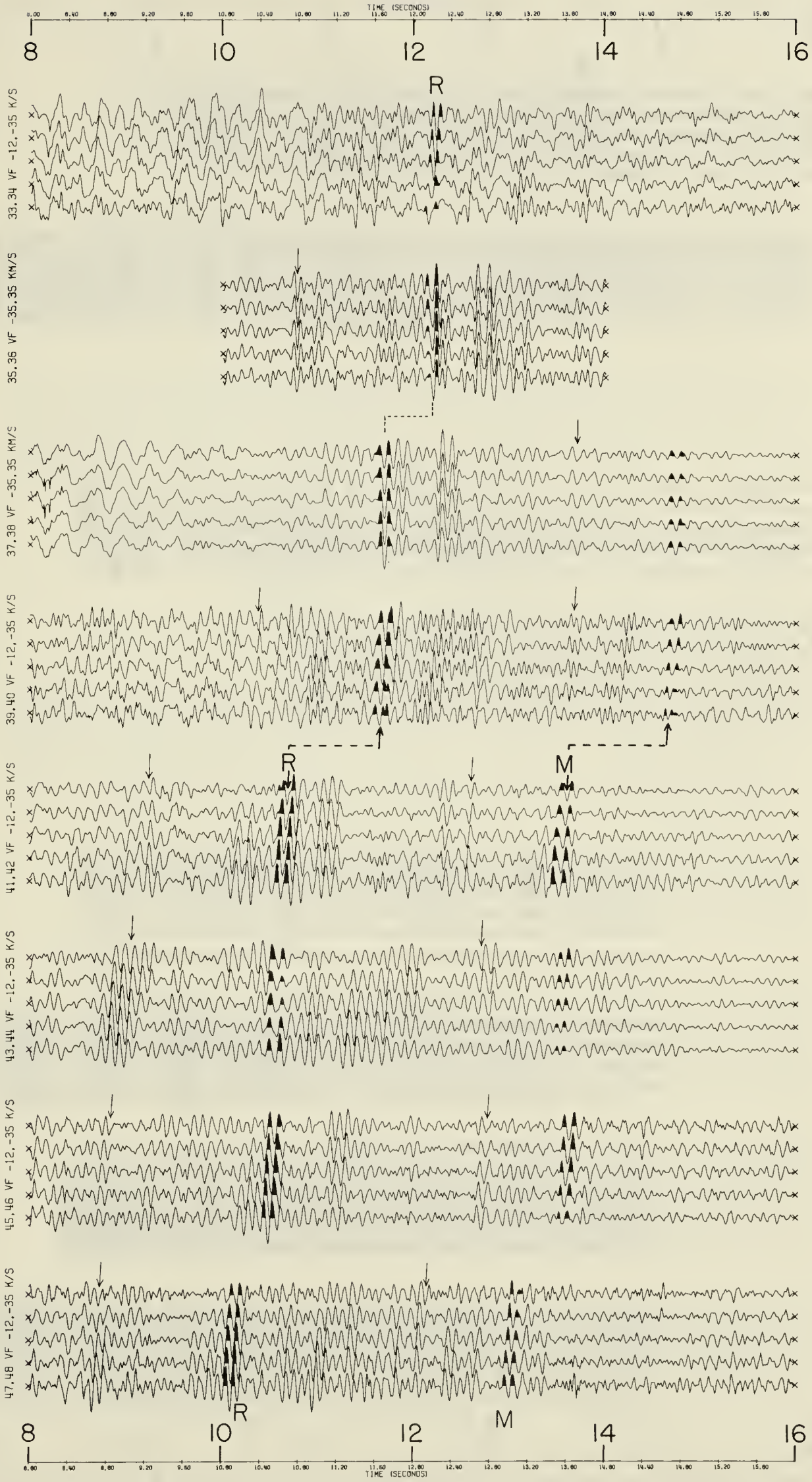
4.2F *85 to 102 kilometers.*

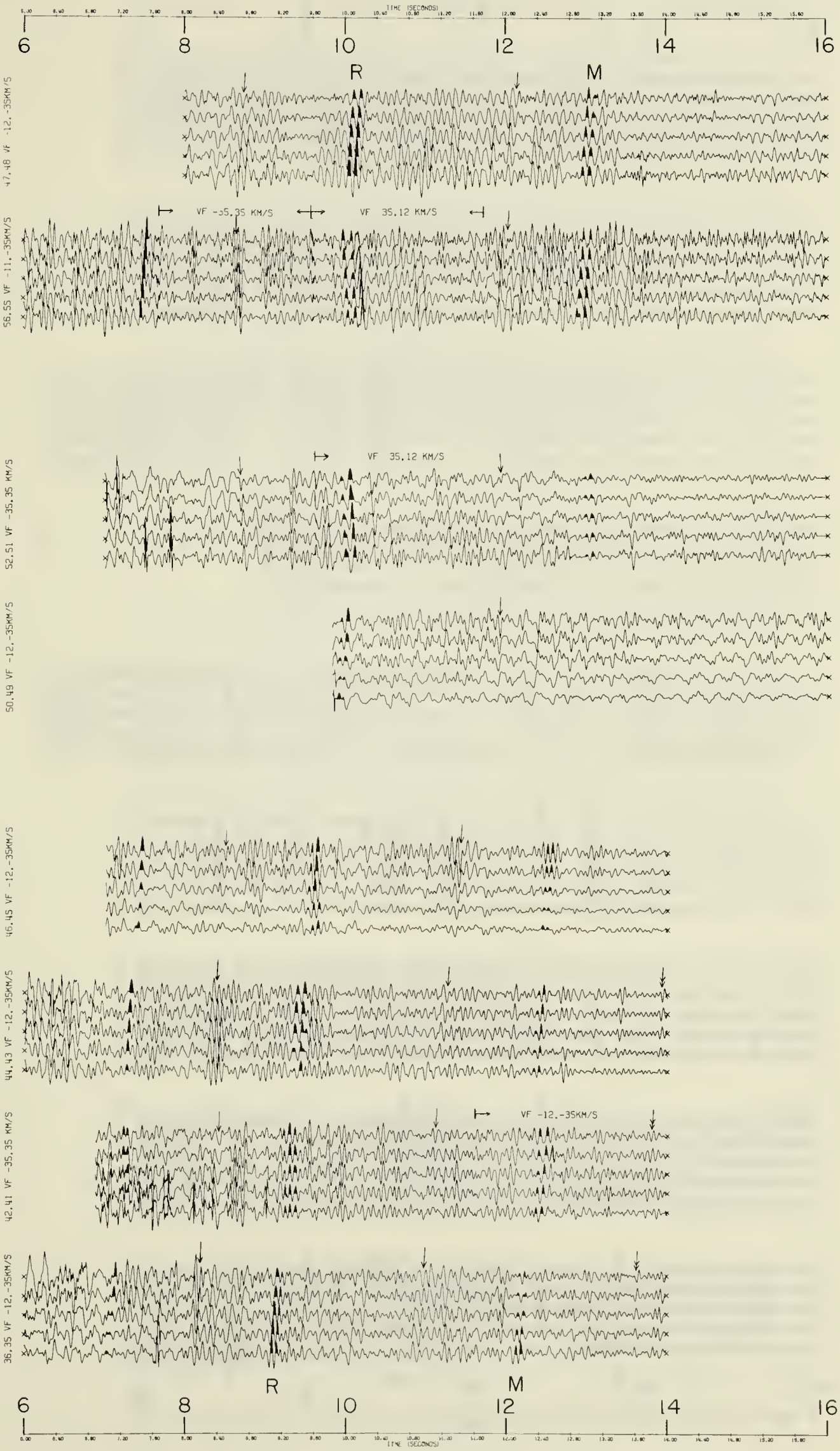
*Note that Figure 4.1 is a migrated structure section while the foregoing distances refer to the surface recording locations.*

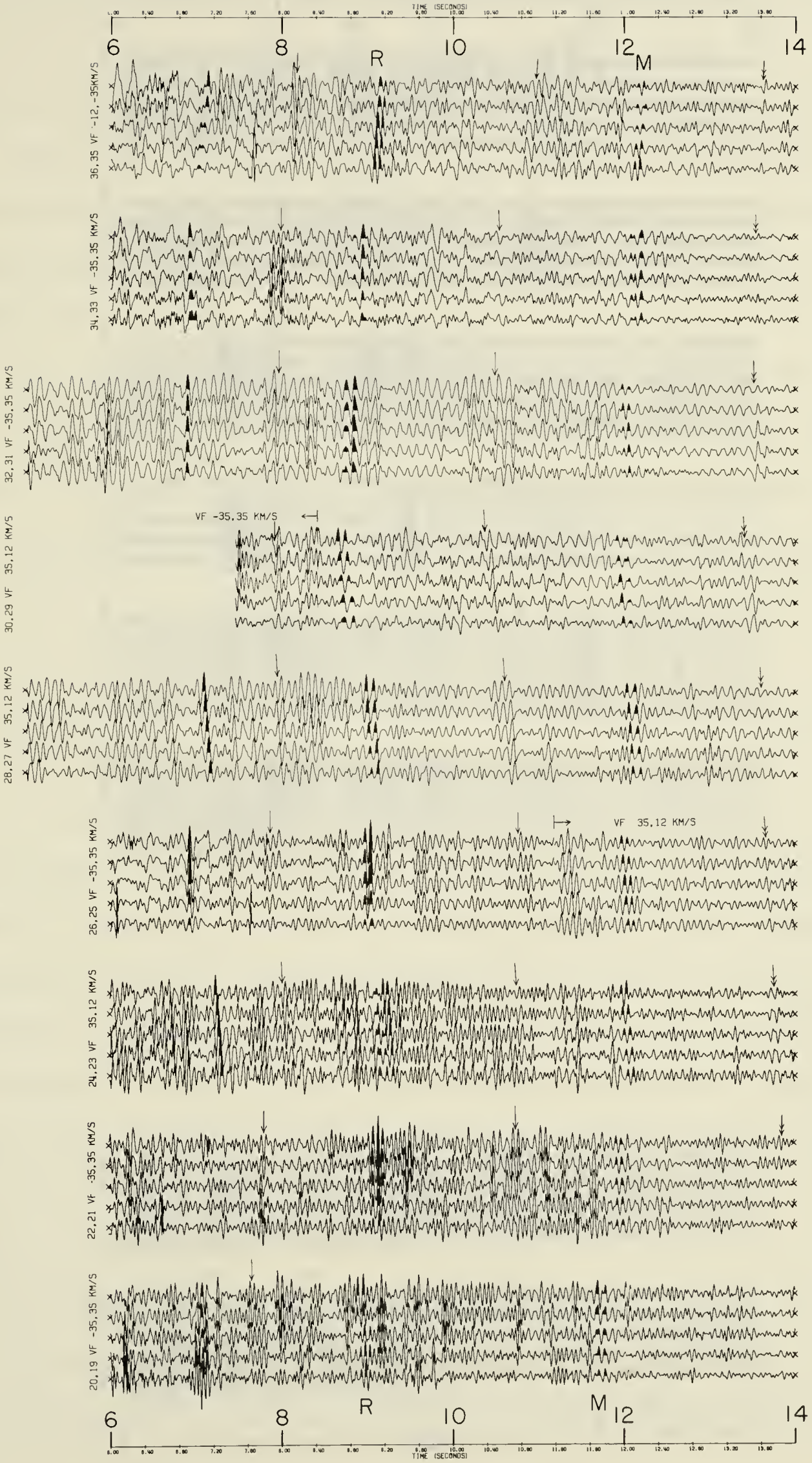

TIME (SECONDS)
8.00 8.40 8.80 9.20 9.60 10.00 10.40 10.80 11.20 11.60 12.00 12.40 12.80 13.20 13.60 14.00 14.40 14.80 15.20 15.60
8
10
12
14
16
R
M
1,2 VF -35 TO 35 K/S
3,4 VF -35 TO 35 K/S
5,6 VF -35 TO 35 K/S
7,8 VF -35 TO 35 K/S
VF -9,-18 KM/S
VF -9,-18 KM/S
RECORD 09 1966
11,12 VF 35,12 KM/S
13,14 VF 35,12 KM/S
15,16 VF 35,12 KM/S
R
M
8
10
12
14
16
8.00 8.40 8.80 9.20 9.60 10.00 10.40 10.80 11.20 11.60 12.00 12.40 12.80 13.20 13.60 14.00 14.40 14.80 15.20 15.60
TIME (SECONDS)


TIME (SECONDS)
8
10
12
14
16
R
M
15,16 VF 35 - 12 K/S
17,18 VF -12,-35 K/S
19,20 VF -12,-35 K/S
21,22 VF -12,-35 K/S
23,24 VF -12,-35 K/S
25,26 VF -12,-35 K/S
27,28 VF -12,-35 K/S
29,30 VF -35,35 KM/S
R
TIME (SECONDS)




TIME (SECONDS)
8
10
12
14
16
R
M
33,34 VF -12,-35 K/S
35,36 VF -35,35 KM/S
37,38 VF -35,35 KM/S
39,40 VF -12,-35 K/S
41,42 VF -12,-35 K/S
43,44 VF -12,-35 K/S
45,46 VF -12,-35 K/S
47,48 VF -12,-35 K/S


TIME (SECONDS)
6
8
10
12
14
16
R
M
47.48 VF -12.-35KM/S
56.55 VF -11.-35KM/S
VF -35.35 KM/S
VF 35.12 KM/S
52.51 VF -35.35 KM/S
VF 35.12 KM/S
50.49 VF -12.-35KM/S
46.45 VF -12.-35KM/S
44.43 VF -12.-35KM/S
42.41 VF -35.35 KM/S
VF -12.-35KM/S
36.35 VF -12.-35KM/S
R
M
6
8
10
12
14
16
TIME (SECONDS)


TIME (SECONDS)
6
8
R
10
12
M
14
36,35 VF -12,-35KM/S
34,33 VF -35,35 KM/S
32,31 VF -35,35 KM/S
30,29 VF 35,12 KM/S
VF -35,35 KM/S
28,27 VF 35,12 KM/S
26,25 VF -35,35 KM/S
VF 35,12 KM/S
24,23 VF 35,12 KM/S
22,21 VF -35,35 KM/S
20,19 VF -35,35 KM/S
6
8
R
10
M
12
14
TIME (SECONDS)


TIME (SECONDS)
6
8
R
10
M
12
14
20,19 VF -35,35 KM/S
-35,35 KM/S
18,17 VF 35,12 KM/S
VF -12,-35KM/S
16,15 VF 35,12 KM/S
VF -12,-35KM/S
14,13 VF -35,35 KM/S
VF -12,-35KM/S
12,11 VF -35,35 KM/S
10,09 VF -35,35 KM/S
VF -35,35 KM/S
04,03 VF -12,-35KM/S
VF -35,35 KM/S
02,01 VF -12,-35KM/S
6
8
R
10
12
M
14
TIME (SECONDS)

on the seismograms represent time ranges for which there were instrumental difficulties or large amplitude low frequency waves. The few cases where the latter interference effects have been left in the illustration are obvious from their low frequency and unusual character. In one instance (Record 09, 1966 of Figure 4.2A) where only one of the two seismograms necessary for filtering was available, the original unfiltered data has been substituted for the sake of continuity.

While making a correlation across the fan-pass filtered seismograms, it must be recalled that the filtering process reduces the number of traces from twelve to five. If the original traces were numbered 1 to 12 to reference their surface position, the filtered channels would be labelled 4.5 to 8.5 in which the trace at 4.5 is a weighted composite of traces 1 to 8, the one at 5.5 of traces 2 to 9, etc. On the basis of the horizontal separation between station locations, the spacing between adjacent seismograms should be 2.4 times greater than that depicted to present a true scaled section. This fact should be noted when correlations are being made. In addition, consideration should also be given to the results concerning transition zones which were discussed in Chapter 3. It is possible that the largest amplitude peak in a given reflected signal sequence could shift from record to record depending on the thickness of the transition zone. However, since this must occur within a depth interval of less than one kilometer, for any reasonable velocity values chosen the oscillations of the pulse series should be negligible within less than 0.4 seconds.

The reflection, R, from the Riel discontinuity is usually distinguished as the most prominent event on the seismograms and as such, it could be correlated most easily across the entire section. Two peaks

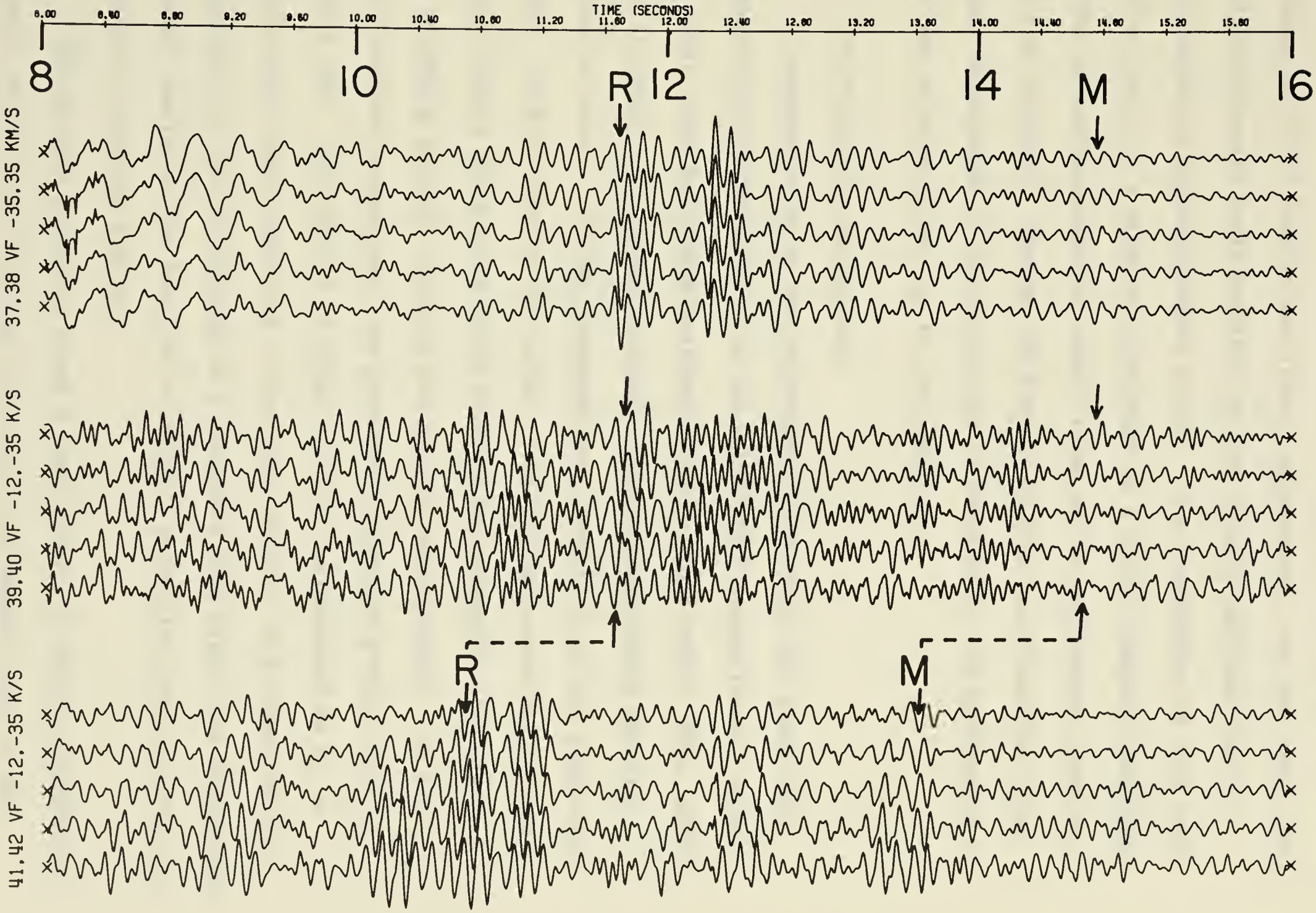
of the pulse sequence associated with R have been darkened to more clearly show the correlation. In many cases, these are followed by another large amplitude pulse about one second later and this is most likely of multiple origin. With only a few exceptions, a reflection, M, interpreted as being from the Mohorovičić discontinuity has also been correlated across the suite of records. While in many cases signal-to-noise ratios were only slightly greater than one, the correlation is aided by considering other sequences of pulses and their variation from record to record. Peaks from this event have also been darkened for emphasis. For both R and M, correlations at the northern end of the Blackfoot profile (Figures 4.2E and 4.2F) were more ambiguous and a definitive interpretation is difficult.

One of the most obvious results to be derived from the record section is the large number of events which have been revealed by the velocity filtering process. Some of these could be correlated over much of the profile. Two of the more continuous sequences, one in the interval between R and M and one about 1.5 seconds prior to R, have been designated by single-headed arrows. In most cases the existence of these reflections is quite clear and in a few instances an excellent quality reflected pulse has been delineated. On some seismograms for which the dynamic range of the instrumentation was not exceeded and surface waves were negligible, much shallower reflections were detected. In two such cases (Records 32,31 and 28,27 of Figure 4.2E), a good quality reflection was obtained just five seconds after the shot instant. On the part of the record section where the structure reaches its maximum height (Figures 4.2D and E), indication of a continuously correlatable pulse can be detected at about 13.8 seconds, nearly two seconds later than the reflection attributed to the M discontinuity. Over the ten seismograms

on which it is quite clear, the pulse has been marked with a double-headed arrow. Further evidence for reflected energy from below the Moho is given on Records 05,06 and 07,08 (Figure 4.2A) near the southern end of the profile. A good amplitude event is seen at a two-way reflection time of about 16.8 seconds. Beloussov et al. (1962) and Khalevin et al. (1966) have reported similar observations from the deep seismic sounding program in the Soviet Union where good reflections as late as 18 seconds have been observed. It is possible that the late-arriving, steeply dipping event could be associated with diffracted energy from the fault postulated at the southern end of the Lomond profile. On the other hand, some of the relfections from low dipping interfaces may be from skills within the upper mantle.

The velocity filtered data have confirmed the gross structural features of the cross section derived in Section 4.1 and have provided additional details. For example, the R and M horizons have been more reliably correlated across the profile and indicate that the structure of the horizons is less smooth than depicted. The correlation of other reflections across much of the profile provides evidence of more extended layering than is usually considered within the deep crust. These horizons also exhibit similar structural variations. Some support has been obtained for the possible existence of reflecting interfaces below the M discontinuity. As well, some evidence is given for block-faulting in contrast to the single fault plane interpreted in the original cross section. For clarity, Figure 4.3 illustrates three filtered seismograms which show the good correlation across the central fault of the section. The offset represents a time difference of about one second. This interpretation is consistent with refraction data which is discussed in the following section.

Figure 4.3 *Velocity filtered seismograms from Figure 4.2C. Good evidence for the central fault in Figure 4.1 is shown.*


TIME (SECONDS)
8.00 8.40 8.80 9.20 9.60 10.00 10.40 10.80 11.20 11.60 12.00 12.40 12.80 13.20 13.60 14.00 14.40 14.80 15.20 15.80
8
10
R
12
14
M
16
37,38 VF -35,35 KM/S
39,40 VF -12,-35 K/S
41,42 VF -12,-35 K/S
R
M



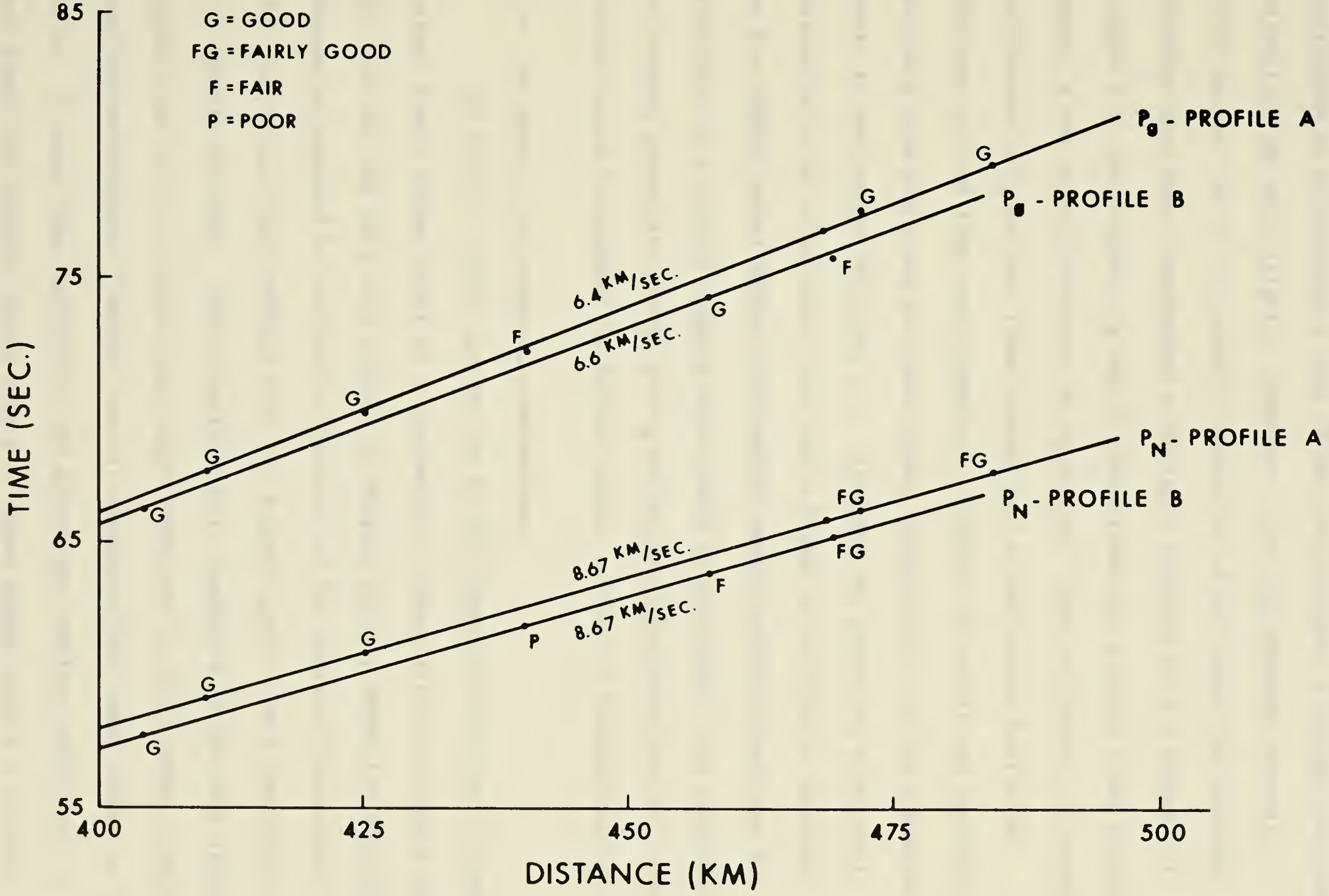
Even without band-pass filtering, some of the fan-pass filtered seismograms still have an oscillatory appearance. For such cases the reflection events could possibly be more clearly distinguished by utilization of dereverberation filters. The application of this suggestion would be a difficult procedure as a fairly complete knowledge of the reflection-producing capabilities of the sedimentary layering would be required. However the present section has shown that significant improvement in record quality is rendered by the application of just the velocity filter to the observed data.

## 4.3 The refraction seismograms

Interpretation of the reflection observations has shown that large-sized structures exist on the Mohorovičić discontinuity, within the lower crust and probably extend into the upper crust. This implies that it should be possible to detect such features with a detailed refraction study. For the broadside arc, Profile C, of the refraction survey, the positions of the seismic detectors were selected to most clearly detail those areas where faulting was suspected (see Figure 1.1 for recording station locations and profile designations). On the twelve useable seismograms, two prominent refraction events could be clearly seen. The earlier of these arrivals corresponded to $P_n$, a compressional wave travelling in the upper mantle. The second arrival, designated $P_g$, was interpreted as a head wave from within the Precambrian basement complex on the basis of a reversed refraction profile previously obtained in southern Alberta.

The in-line profiles, A and B, were chosen to observe differences in phase velocity and intercept times over the deepest part of the structure and on the highest part to the north. Figure 4.4 shows the

Figure 4.4 *Traveltime curves for* $P_g$ *and* $P_n$ *from profiles* A *and* B *(Figure 1.1). For Profile A recorded along the center of the deep part of the structure, the arrivals are about one second later than for Profile B recorded along the structural high.*


G = GOOD
FG = FAIRLY GOOD
F = FAIR
P = POOR
$P_g$ - PROFILE A
$P_g$ - PROFILE B
6.4 KM/SEC.
6.6 KM/SEC.
$P_N$ - PROFILE A
$P_N$ - PROFILE B
8.67 KM/SEC.
8.67 KM/SEC.
85
75
65
55
400
425
450
475
500
TIME (SEC.)
DISTANCE (KM)

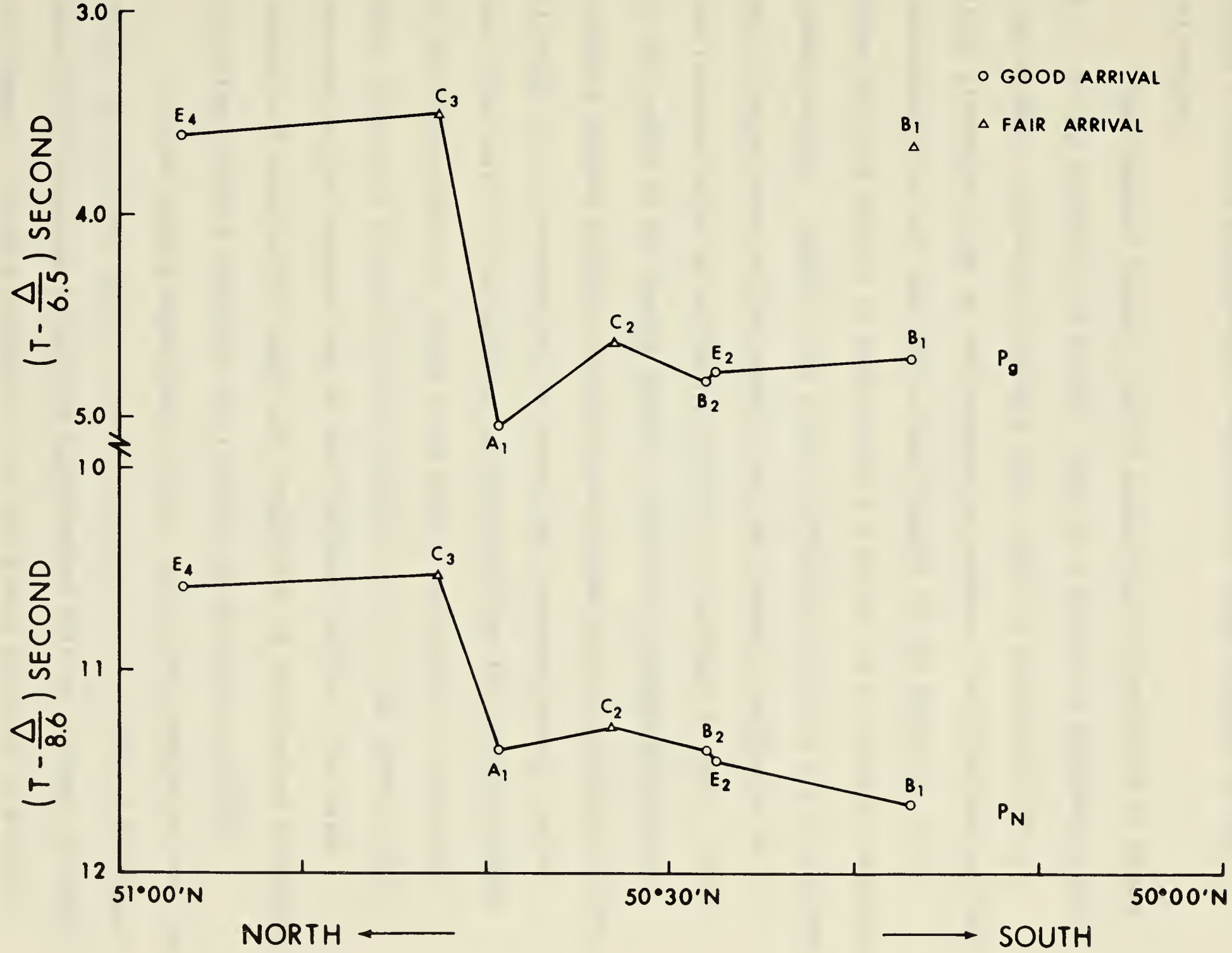


traveltime curves for $P_g$ and $P_n$. It is noted that there is a distinct difference in the intercept time of the two profiles, although the phase velocities are only slightly different. The high apparent velocity (8.67 km/sec) for $P_n$ is probably indicative of dip since the reversed profiles have been interpreted as having a velocity of 8.3 km/sec. In Figure 4.5, the residual $P_g$ and $P_n$ traveltimes for Profile C are plotted. Nearly a one-second difference in $P_n$ arrival times and about 1.3 seconds difference in $P_g$ arrival times occurs over a north-south horizontal distance of less than ten kilometers. Stations C3 and A1 are recording arrivals from the upper and lower sides, respectively, of the postulated fault in the center of Figure 4.1. Although the amount of structural variation to be interpreted from such a change is critically dependent on the crustal model chosen, the general result certainly confirms the existence of a steeply dipping major fault in the crust. The similarity in reduced traveltime curves for $P_g$ and $P_n$ indicates that the fault does indeed extend throughout the entire crustal section of Precambrian age.

## 4.4 The gravity and magnetic observations

The gravity survey carried out by the Geophysics Division recorded values from a Worden Model XP 0 gravimeter. Normal field procedures were followed and the data were reduced to Bouguer gravity anomalies following the method adopted by the Gravity Division of the Dominion Observatory. This survey was then combined with the Bouguer gravity data provided by the Gravity Division. Their compilation is comprised of the base stations established by the Division plus values submitted by Gulf Canada, Limited and Chevron Standard, Limited, two oil companies that have worked in the area. In cases where university and government stations coincided, it was found that Bouguer values from the former agreed within a fraction

Figure 4.5 *Residual* $P_g$ *and* $P_n$ *traveltime curves for Profile C (Figure 1.1). The horizontal distance between stations* C3 *and* A1 *is less than ten kilometers.*


3.0
4.0
5.0
10
11
12
$(T-\frac{\Delta}{6.5})$ SECOND
$(T-\frac{\Delta}{8.6})$ SECOND
E4
C3
A1
C2
E2
B2
B1
PS
PN
GOOD ARRIVAL
FAIR ARRIVAL
51°00'N
50°30'N
50°00'N
NORTH
SOUTH



of one milligal with those listed by the government. All gravity station locations which were used in compiling the map are indicated on Figure 4.6, with approximately one-third of these occupied by the university.

The complete Bouguer gravity anomaly map is presented in Figure 4.7. To the northeast of Brooks, there is a small but prominent positive anomaly, called the Princess high, which is associated with a local structural high on the Precambrian surface. This feature has been penetrated by a well and, from a small sample of the material, it is known that the density is high—about 3.0 $gm/cm^3$ (R.M. Burwash, personal communication). However, the seismic reflection profiles are a considerable distance west of this anomaly and are probably unaffected by it. Two features relative to these profiles are important to note. First, in the region of the Lomond profile, there is a pronounced east-west trending Bouguer gravity low which cuts across most of southern Alberta, although it is distorted by the local high discussed above. To the west, the course of the anomaly is intercepted by the gravity effects of the Rocky Mountains, which trend nearly north-south. The second major feature of interest for this project is the broad gravity high centered on the northern end of the Blackfoot profile. Its large expanse and considerable magnitude, suggestive of deep-seated structural variations, helped determine the location of the latter profile.

For the ground magnetometer survey run by the Geophysics Division, values of the total magnetic field intensity were read from a Barringer Model GM-102A nuclear precession magnetometer with an accuracy of about ten gammas. The data recorded in the field were adjusted to minimize any differences in readings at repeated stations. By computing

Figure 4.6 *Gravity station locations for the map of Figure 4.7. The heavy lines show the location of the Lomond and Blackfoot profiles and the east-west expanding spread profile. The dashed lines outline the assumed boundaries of the ancient rift valley (Section 4.5) as traced from magnetic and gravity trends.*

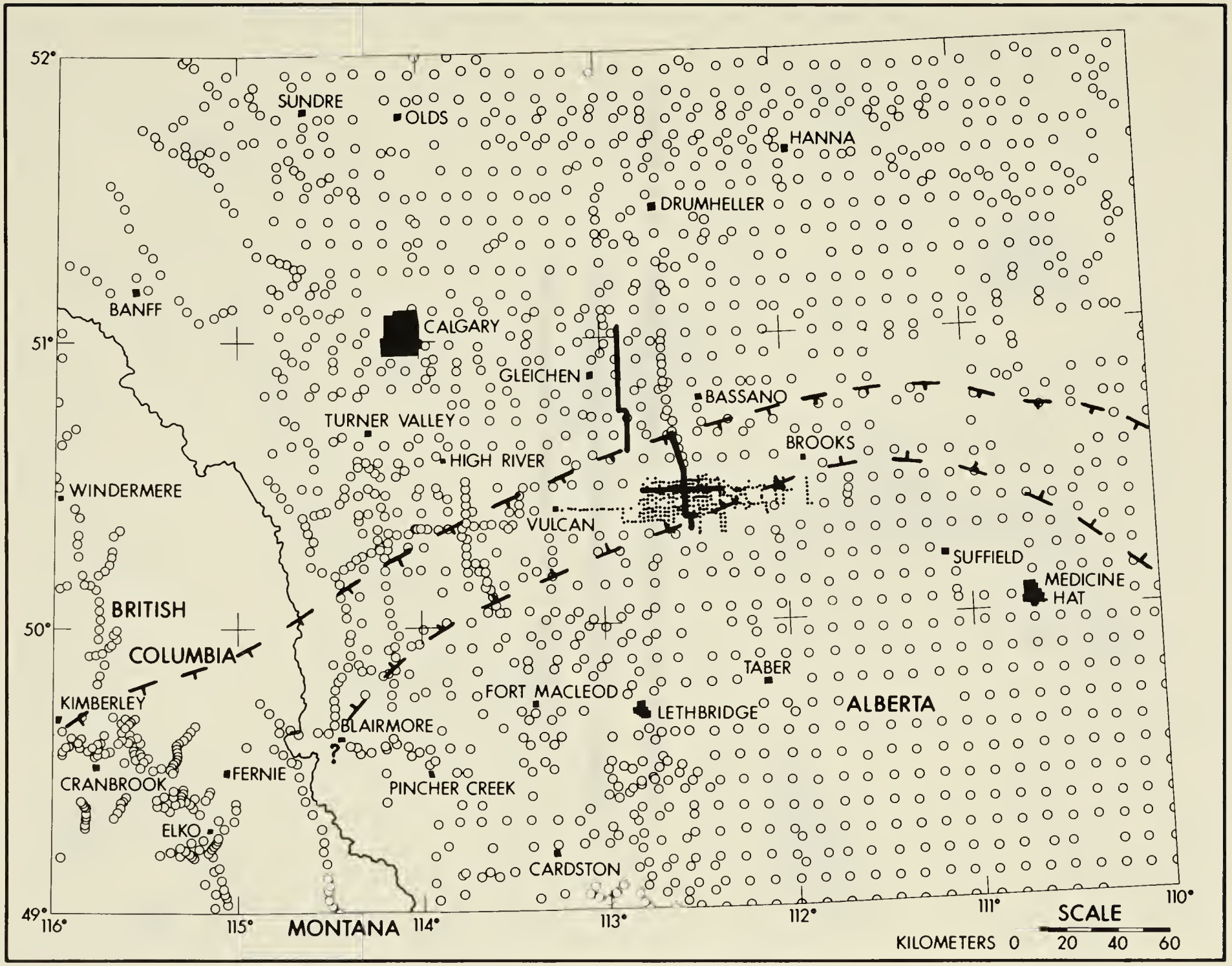
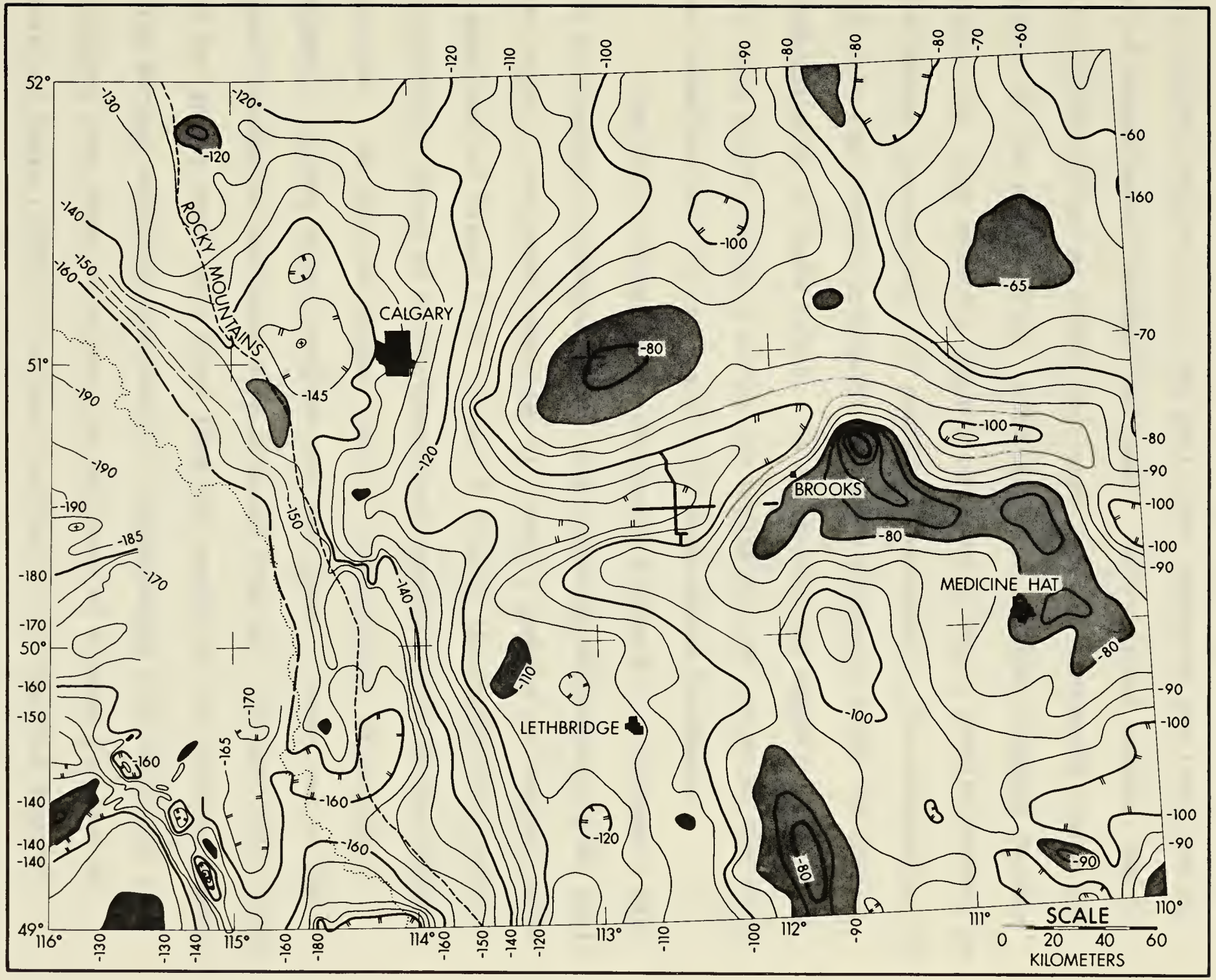

52°
SUNDRE
OLDS
HANNA
DRUMHELLER
BANFF
51°
CALGARY
GLEICHEN
BASSANO
TURNER VALLEY
BROOKS
HIGH RIVER
WINDERMERE
VULCAN
SUFFIELD
MEDICINE HAT
BRITISH COLUMBIA
50°
TABER
FORT MACLEOD
ALBERTA
KIMBERLEY
LETHBRIDGE
BLAIRMORE
?
FERNIE
CRANBROOK
PINCHER CREEK
ELKO
CARDSTON
49°
116°
115°
MONTANA
114°
113°
112°
111°
110°
SCALE
KILOMETERS 0 20 40 60



Figure 4.7 *Bouguer gravity anomaly map for southern Alberta and southeastern British Columbia. The contour interval is 5 milligals.*


CALGARY
ROCKY MOUNTAINS
BROOKS
MEDICINE HAT
LETHBRIDGE
SCALE
0 20 40 60
KILOMETERS



the magnetic field due to dipole and higher order effects by means of a seventh-degree spherical harmonic analysis, then subtracting these values from the observed ones, a residual total magnetic intensity map was derived (Figure 4.8). The small dots represent the locations at which magnetometer readings were made. This residual magnetic map is also characterized by strong east-west trending lineaments across the region of the two profiles. Although it is centered slightly further south, the large negative anomaly corresponds with a similar feature on the Bouguer gravity map. Of particular interest is the continuation of the east-west trends underneath the Rocky Mountains which lie almost perpendicular to these trends. It shows that the magnetic effects of the more recent mountain system are negligible and causes of the residual anomalies must be associated with deep-seated phenomena.

On the structure cross section of Figure 4.1, the deepest part of the features corresponds with both a gravity and magnetic low, while the horst to the north coincides with both a gravity and magnetic high (upper part of Figure 4.1). Figure 4.9 shows the results of gravity calculations based on a two-dimensional generalization of the seismic section. The observed Bouguer gravity (solid curve) and residual magnetic (dashed curve) profiles are also given. Velocities in the post-Precambrian sediments were obtained from well log data while those in the deeper crust were taken from the results of the reversed refraction surveys mentioned previously. Corresponding rock densities were selected from these velocities on the basis of a model proposed by Nafe and Drake (1959). The small circles on the observed Bouguer profile show the fit of the proposed crustal section. By seismic means, the existence of the fault in the central part of the section has been

Figure 4.8 *Residual total magnetic field intensity map for southern Alberta and southeastern British Columbia.*

# RESIDUAL TOTAL MAGNETIC FIELD INTENSITY

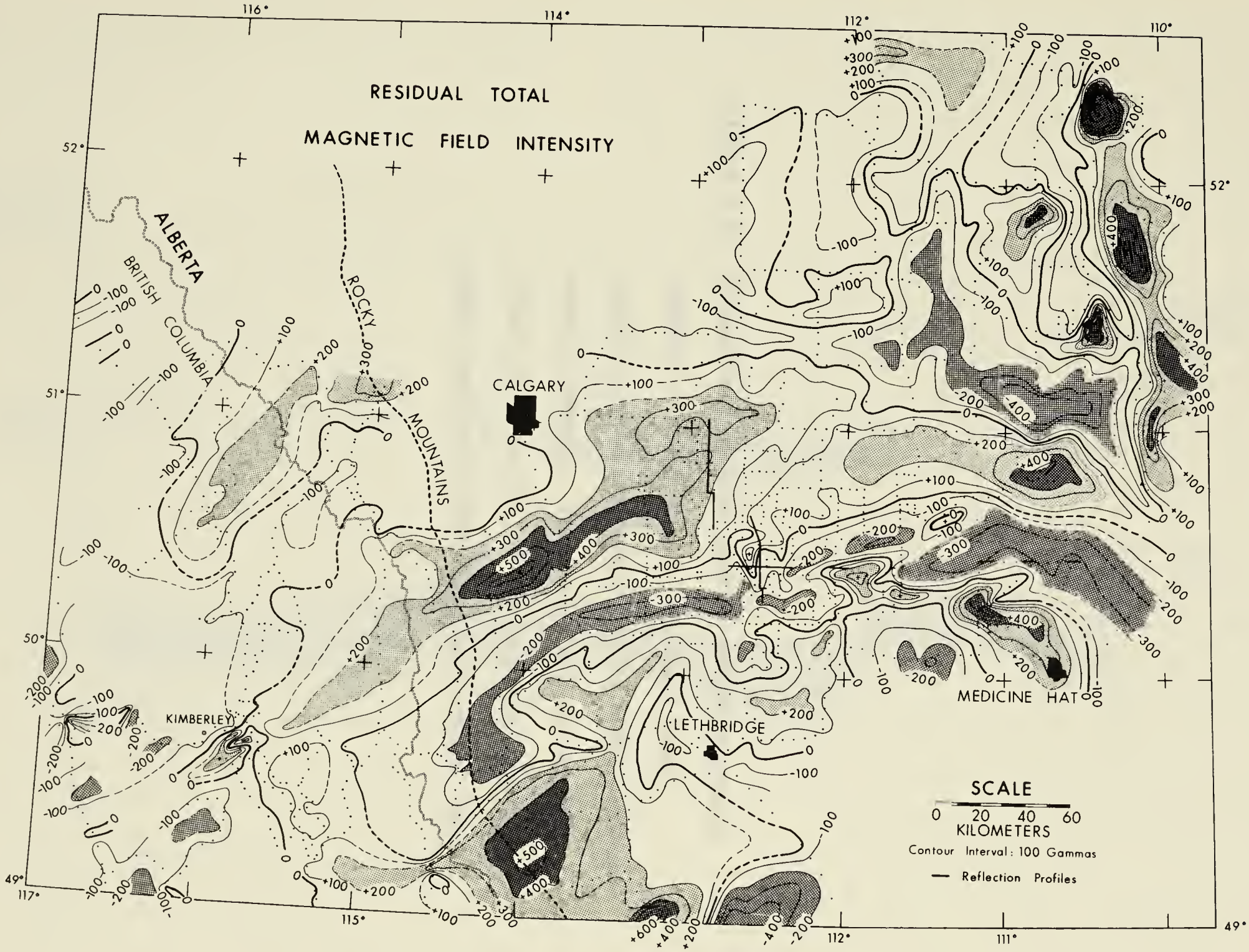
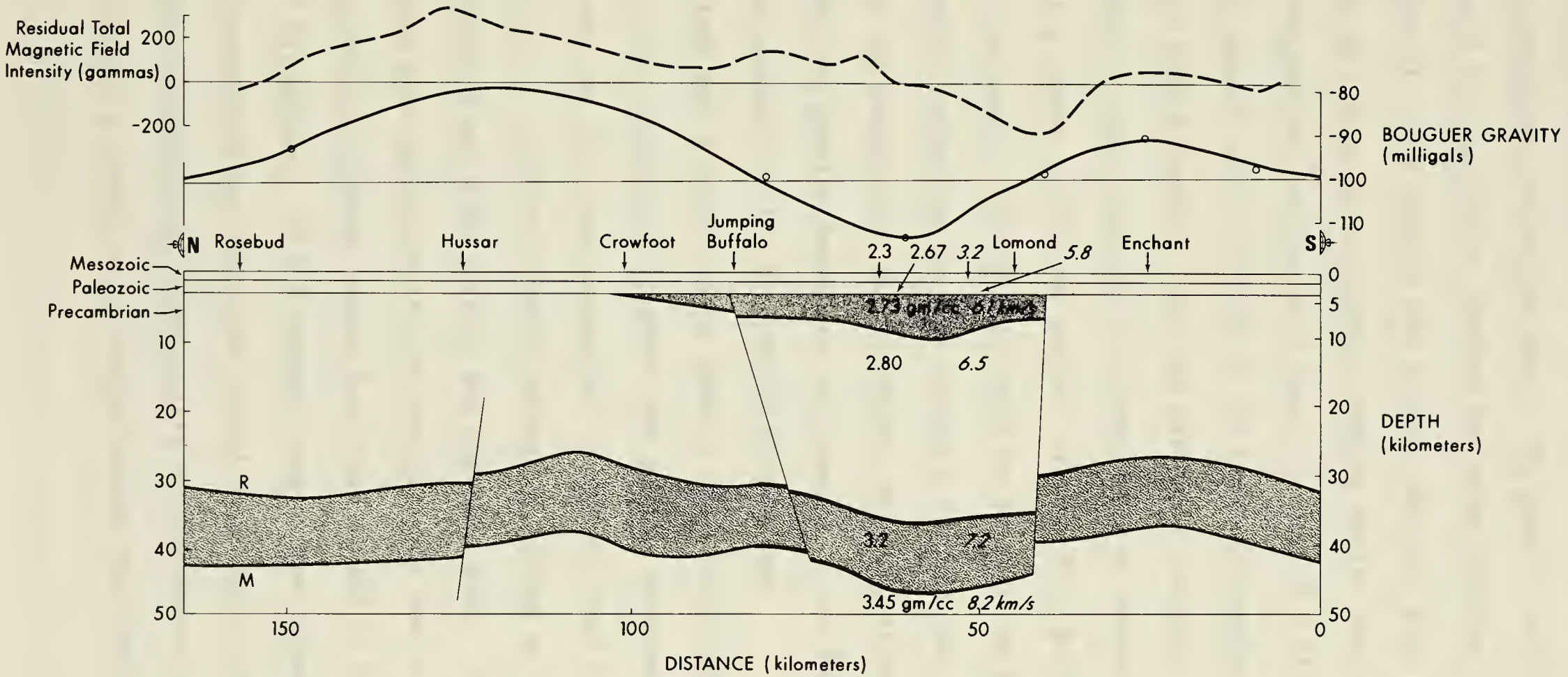




Figure 4.9 *Generalized crustal section across southern Alberta. Dashed curve: residual total magnetic field intensity. Solid curve: Bouguer gravity anomaly. The small circles on the latter show the fit of the proposed crustal model depicted in the lower half of the figure.*


Residual Total Magnetic Field Intensity (gammas)
200
0
-200
-80
-90
-100
-110
BOUGUER GRAVITY (milligals)
N
Rosebud
Hussar
Crowfoot
Jumping Buffalo
2.3
2.67
3.2
Lomond
5.8
Enchant
S
Mesozoic
Paleozoic
Precambrian
2.73 gm/cc 6.1 km/s
2.80
6.5
10
20
30
40
50
R
M
3.2
7.2
3.45 gm/cc 8.2 km/s
0
5
10
20
30
40
50
DEPTH (kilometers)
150
100
50
0
DISTANCE (kilometers)



confirmed, but the postulated fault on the southern end of the profile was based on ambiguous reflection data. The gravity calculation shows that this fault is required to produce the steep gradient observed directly above it. The gravity and seismic data are best fitted if the two fractures are taken to be steeply dipping faults that extend to the top of the Precambrian section at a depth of about 2.5 kilometers. On the basis of several wells drilled to the basement complex, it is known that no major faults continue into the Paleozoic sediments. From these considerations it seems reasonable to describe the deepest part of the structure as a graben within the ancient crust. This graben must be filled with low density Precambrian rocks to satisfy the gravity low and an upper crustal refracting horizon having a low apparent velocity. At the level of the Mohorovičić discontinuity, mass variations do not have a great effect on gravity models so the premise of low density fill is necessary to account for the pronounced gravity low.

Garland and Burwash (1959) found a correlation between the lithology of the Precambrian basement and gravity observations in central Alberta. From the data just presented, it appears that a similar correlation exists in southern Alberta between lithology as suggested by seismic velocities and both gravity and magnetic data. The seismic section indicates that such correlations are directly due to deep crustal structure in which different blocks have been raised or lowered by as much as ten kilometers. In the present case, there appears to be a graben of Precambrian age which was filled with lighter density rocks having a lower proportion of magnetically susceptible mineralization. Thus there exists a direct relationship between the gravity and magnetic profiles.

## 4.5 A buried Precambrian rift

The most prominent feature of the generalized crustal profile presented in the last section is a graben coinciding with gravity and magnetic lows which form part of an east-west trending lineation. From this correlation, the graben appears to be a major east-west structure extending at least 450 kilometers across southern Alberta and passing at right angles to the strike of the more recent Rocky Mountain system. The latter are underlaid by a peneplaned and gently westward sloping crystalline basement (Bally et al., 1966) which has potassium-argon dates of 1.5 to 2.0 billion years (Burwash et al., 1962) and forms a portion of the Churchill geological province (Kanasewich, 1965). From the evidence of its great elongation on the gravity and magnetic maps, the graben may best be described as a rift. Since post-Middle Cambrian sediments are not known to be affected by the faulting, it seems reasonable to conclude that this structure represents a buried Precambrian rift. The probable location of this feature as traced with the aid of the gravity and magnetic lineaments is sketched in Figure 4.6.

While the existence of Precambrian rifting has not previously been established, there are good examples of more recently developed continental fractures such as the East African, Rhinegraben and Lake Baikal rift systems. The rift valleys of East Africa have been extensively discussed (Gregory, 1896 and 1921), but only limited geophysical studies have been made (see Irvine, 1966). Both the Rhinegraben (see Rothe and Sauer, 1967) and the Lake Baikal (see Bulmasov, 1960; Zorin, 1966; Reisner, 1966; and Ladynin, 1966) rift systems have undergone more extensive geophysical analyses. Thus some comparisons of the recent rifts can be made with the Precambrian rift in western Canada.

Freund (1966) notes that most continental and oceanic rifts have widths ranging from 30 to 70 kilometers, although there are exceptions. The width of the rift whose outlines are traced in Figure 4.6 averages about 40 kilometers. At Lake Baikal, the maximum overall depth of the rift, from the highest mountain crest to the surface of the sediment fill, is greater than 4.1 kilometers (Hope, 1967). A similar value, 4.4. kilometers, is established by Illies (1967) for the total throw of the faulting in the Rhinegraben. In the structure sections of Figures 4.1 and 4.9, the offsets along the fault amount to about 3 to 5 kilometers. With regard to the sedimentary fill, Illies (loc. cit.) estimates a maximum depth extent of 3.4 kilometers, while Florensov (1966) places the total thickness of sediments in the Baikal rift zone at about 5 to 6 kilometers. On the basis of gravity and refraction surveys, the graben fill of Figure 4.9 varies in thickness from about 3 to 7 kilometers. From an analysis of deep reflection seismograms, Demnati and Dohr (1965) concluded that the Conrad discontinuity was depressed beneath the Upper Rhine valley and suggested about 5 kilometers of relief. From geophysical work on the delta of the Selenga River and surface geological mapping, Florensov (loc. cit.) places the total amplitude of crustal displacement at about 5 to 7 kilometers. These estimates are not dissimilar from the 10 kilometers of total displacement obtained for the rift system in southern Alberta on much stronger geophysical evidence. Thus it is seen that in terms of physical magnitudes, the characteristics of the Precambrian rift bear a remarkable similarity to those determined for the Rhinegraben and Lake Baikal rift zones. It is unfortunate that more comprehensive geophysical analyses, including detailed seismic investigations, have not been made in the

region of the East African, Rhinegraben and Lake Baikal rifts in order that a better comparison of such physical characteristics could be made.

However, both gravity and magnetic features of the recent rifts have a similar expression over the ancient one. In all three cases, a pronounced gravity low parallels the central region of the rifting. Closs and Plaumann (1967) give a relative magnitude of -20 to -50 milligals for the depression in the Rhinegraben, values which fit well with the data given in Figure 4.7. From a consideration of two-dimensional models, they conclude that the Bouguer anomaly across the graben can be fully explained on the basis of the sedimentary fill in the upper crust, and it is not necessary to invoke causes of the anomaly being situated in the lower crust or upper mantle. Zorin (1966) reaches a similar conclusion for the observed anomalies at Lake Baikal and additionally shows that the edges of the rift are bounded by strong positive anomalies. All these characteristics were noted from the gravity study in the region of the Precambrian rift. Just as with the gravitational field, the magnetic field above the Rhinegraben and Lake Baikal is characterized by linear trending anomalies, parallel to the strike of the rifts. Bosum and Hahn (1967) find that in the graben negative anomalies exist and are bounded by greater amplitude positive values of the magnetic field. Over the Baikal folded region, Bulmasov (1960) finds a regional field which is negative although strong linear positive anomalies stand out against this. These, he argues, are caused by intrusions of basic rocks along faults located below the surface (depth-faults). A strong positive magnetic field exists on one side of the rift zone. On the residual magnetic field map of Figure 4.8, negative anomalies are evident above the Precambrian rift with positive residuals bounding it on either side.

The entire map is dominated by the east-west trending lineaments associated with the rift. Thus it is found that the prevalent gravity and magnetic features of the Rhinegraben and Lake Baikal bear a striking resemblance to those associated with the rift in southern Alberta.

That a rift in the geologically ancient crustal section has been discovered possesses some significance, for DeSitter (1959) notes that "the great rift valleys of the earth are all relatively young, or rejuvenated structures . . . . The reason for the fact that no large rift valleys of Hercynian or earlier age are known remains obscure." The recognition of these recent rift valleys is generally based on their spectacular geomorphological features and not on geologic structure. However, there is now some geological evidence for the existence of Precambrian rifting in East Africa (McConnell, 1967). In the present research, the buried Precambrian rift has been identified on the basis of geophysical studies. This has shown evidence for large amounts of relief with steeply dipping surfaces on the Precambrian terrain. If it is assumed that the Precambrian terrain exposed in many shield areas has undergone similar amounts of warping during the long period of tectonic evolution, then the evidence from this study indicates that in some places on an ancient peneplaned craton, it is possible to observe directly the rocks ten kilometers deeper on one section than on an adjacent one.

# CHAPTER 5

# CONCLUSION

This thesis has demonstrated that, by careful design of field procedures including the use of patterns of holes and arrays of seismometers, near-vertical incidence reflected energy from within and at the base of the earth's crust can be successfully recorded. Velocity filtering techniques proved to be an effective method of enhancing individual reflection events and thus made correlations over longer distances more reliable. Not only do the observed reflections provide detailed knowledge concerning structural variations, but inherent in the reflected events is information relating to the intrinsic properties of the material through which the seismic waves have propagated.

The interpretation of the recorded seismograms has revealed the presence of large-scale structural features and steeply dipping faults within the lower crustal section of southern Alberta. By combining gravity and magnetic data with the seismic results, a major east-west rift of Precambrian origin has been discovered. Under 2.5 kilometers of younger sediments, the feature extends for over 450 kilometers and has 11 kilometers of relief from the highest to the lowest part. Geomorphological features and geophysical characteristics of this ancient rift bear a remarkable similarity to those of more recently developed continental rift valleys.

On the basis of the discovery of the Precambrian rift described in this study, and from other data, Kanasewich (1968) suggested a possible origin for the lead-zinc field near Kimberley, British Columbia and the Coeur d'Alene mining district of Idaho. He postulated that

these ore bodies were deposited in the Precambrian rift under conditions closely related to those prevailing in the present Red Sea rift, where three pools of hot acidic brines with extremely high concentrations of heavy-metals have been found.

The importance of crustal effects on seismic arrivals recorded at the LASA array in Montana has been demonstrated by Mack (1969). He considered a simplified version of the crustal section in southern Alberta (Clowes et al., 1968) to show that such deep crustal relief could cause a plane wave, incident from below, to produce interference patterns at the surface. Similar effects may explain the variation in character of the seismic arrivals at individual subarrays.

The identification of reflections from depths corresponding to the Mohorovičić discontinuity has an important bearing on the controversy surrounding the nature of the crust-mantle boundary. Almost since the time of A. Mohorovičić's discovery in 1909 of a refracting interface at depths of a few tens of kilometers, two hypotheses have been advanced concerning the mineralogy at the base of the crust. One holds that the Moho is a chemical boundary separating the basic rocks (predominantly basalt) of the lower crust from the ultrabasic rocks (peridotite) of the upper mantle. The second assumes that the boundary represents an isochemical phase change from basalt to eclogite. In recent years, Lovering (1958), Kennedy (1959), MacDonald and Ness (1960), Stishov (1963) and others have advocated the hypothesis of a phase change for the continental crust-mantle boundary. Bullard and Griggs (1961), Nakamura and Howell (1964), Ringwood and Green (1964), Ringwood (1966) and others have opposed this idea and argue in favor of a chemical transition. If the Moho is a phase transformation, it is generally accepted that the

velocity transition would occur over a vertical distance of at least a few kilometers and possibly as much as 15 kilometers. This is contrary to the evidence presented in this study in which near-vertical incidence reflections are obtained from depths corresponding to that of the refracting discontinuity. Such data support the hypothesis that the base of the crust is a sharp boundary, less than one kilometer thick, representing a change in chemical composition.

This study contains the first attempt at obtaining the specific attenuation factor, Q, as a function of depth from reflected seismic waves. On the basis of a comparison of autopower spectral densities of field records and synthetic seismograms, an acceptable Q structure appears to require considerable variation in the sedimentary layers, but having an average value of nearly 300. In the crystalline basement, the magnitude of Q is approximately 1500 and probably increases with depth. In order to provide values which have more reliability and precision, wide-band recording of reflections from within the sediments, with similar instrumentation and field procedures as that used for the deep reflections, would be valuable. Indeed, it is likely that one may be able to determine the distribution of Q with depth and also map lateral variations from an average model.

Initial attempts at determining the nature of deep crustal reflectors has met with more success than was originally anticipated. Autopower spectra and synthetic seismograms have been utilized to specify models of transition zones with acceptable characteristics. The parameters used for the study included the shapes of the spectra, the relative rates of attenuation of frequency components, the forms of reflected wavelets for a pulse input and the ratios of the power in the

spectra of shallow reflections to that in the deeper ones. Models incorporating a first-order discontinuity in velocity, a linear increase of velocity with depth or step increases in velocity did not satisfy all the observational data. Thin layers, less than 200 meters thick, of alternating velocity increases and decreases over a total depth extent of less than one kilometer provided a model which was acceptable on the basis of observed results.

Thus the import of seismic reflection crustal studies is already being realized. The method can provide the details of deep crustal structure necessary for the interpretation of a much wider range of data. It is hoped that this research has contributed significantly toward the establishment of the seismic reflection technique as a recognized and viable method of crustal research.

# BIBLIOGRAPHY


Alpaslan, T., 1968. *Spectral behaviour of short period body waves and the synthesis of crustal structure in western Canada.* M.Sc. thesis, Edmonton: University of Alberta, Department of Physics.

Anderson, D. L. and C. B. Archambeau, 1964. The anelasticity of the earth. *J. Geophys. Res.*, v.69, p.2071-2084.

Anderson, D. L., A. Ben-Menahem and C. B. Archambeau, 1965. Attenuation of seismic energy in the upper mantle. *J. Geophys. Res.*, v.70, p.1441-1448.

Bally, A. W., P. L. Gordy and G. A. Stewart, 1966. Structure, seismic data, and orogenic evolution of southern Canadian Rocky Mountains. *Bull. Can. Petrol. Geol.*, v.14, p.337-381.

Baranov, V. and G. Kunetz, 1960. Film synthetique avec réflexions multiples theorie et calcul pratique. *Geophys. Prosp.*, v.8, p.315-325.

Båth, M. and E. Tryggvason, 1962. Deep seismic reflection experiments at Kiruna. *Geof. Pura Appl.*, v.51, p.79-90.

Beloussov, V. G., B. S. Vol'vovski, I. S. Vol'vovski and V. Z. Ryaboĭ, 1962. Experimental investigation of the recording of deep reflected waves. *Bull. (Izvestiya), Acad. Sci., U.S.S.R., Geophys. Ser.*, English Translation, No. 8, 1962, p.662-669.

Ben-Menahem, A., 1965. Observed attenuation and Q values of seismic surface waves in the upper mantle. *J. Geophys. Res.*, v.70, p.4641-4651.

Berryman, L. H., P. L. Goupillaud and K. H. Waters, 1958. Reflections from multiple transition layers. Part I - Theoretical results. *Geophysics*, v.23, p.223-243.

Bois, P., J. Chauveau, G. Grau and M. Lavergne, 1960. Seismogrammes synthetiques; possibilités, techniques de réalisation et limitations. *Geophys. Prosp.*, v.8, p.260-314.

Bosum, W. and A. Hahn, 1967. Aeromagnetic surveying in the upper Rhinegraben. In *The Rhinegraben progress report 1967*, J. P. Rothe and K. Sauer (eds.), International Upper Mantle Project, Scientific Report No. 13, Freiburg i Br./Strasbourg: Rota-Druck Johannes Krause Buchbinderei, p.89-91.

Brown, R. J. S., 1969. Normal move-out and velocity relations for flat and dipping beds and for long offsets. *Geophysics*, v.34, p.180-195.

Bullard, E. C. and D. T. Griggs, 1961. The nature of the Mohorovičić discontinuity. *Geophys. J. Roy. Astron. Soc.*, v.6, p.118-123.

Bulmasov, A. P., 1960. Magnetic and gravitational fields of the Baikal region as related to its seismicity. *Biull. Soveta po Seismologiyi AN SSSR (Bull. of the Seismological Council, Acad. Sci., USSR)*, no.10, p.49-58. (Translated by E. R. Hope, T435R, Ottawa: Defence Research Board, 1967.)

Burwash, R. A., H. Baadsgaard and Z. E. Peterman, 1962. Precambrian K-Ar dates from the western Canada sedimentary basin. *J. Geophys. Res.*, v.67, p.1617-1625.

Chamo, S., 1962. Study of the deep geologic structure of the Earth's crust by the reflection method. *Razvedochnaya i Promyslovaya Geofizika*, no.46, p.130-138. (Abstract: *Geophys. Abst.* no.206, 206-301, p.235, 1964.)

Closs, H. and S. Plaumann, 1967. On the gravity of the upper Rhinegraben. In *The Rhinegraben progress report 1967*, J. P. Rothe and K. Sauer (eds.), International Upper Mantle Project, Scientific Report No. 13, Freiburg i Br./Strasbourg: Rota-Druck Johannes Krause Buchbinderei, p.92-93.

Clowes, R. M., 1966. *Deep crustal seismic reflections at near-vertical incidence*. M.Sc. thesis, Edmonton: University of Alberta, Department of Physics.

Clowes, R. M. and E. R. Kanasewich, 1969. Digital analysis of deep crustal seismic reflections (Abstract). *Trans. Am. Geophys. Union*, v.50, p.239.

Clowes, R. M., E. R. Kanasewich and G. L. Cumming, 1968. Deep crustal seismic reflections at near-vertical incidence. *Geophysics*, v.33, p.441-451.

Conrad, V., 1925. Laufzeitkurven des Tauernbebens vom 28. November, 1923. *Mitt. Erdbeben-Kommission Wiener Akad. Wiss.*, N.F., No.59.

Cumming, G. L., G. D. Garland and K. Vozoff, 1962. *Seismological measurements in southern Alberta*. Vela Uniform Project 8652, Geophysics Research Directorate, AFCRL, Bedford, Mass.

Cumming, G. L. and E. R. Kanasewich, 1966. *Crustal structure in western Canada*. Project Vela-Uniform, Final Report AFCRL-66-519, Bedford, Mass.

Demnati, A. and G. Dohr, 1965. Reflexionsseismiche Tiefensondierungen im Bereich des Oberrheintalgrabens und des Kraichgaues. *Ztschr. f. Geophys.*, v.31, p.229-245.

DeSitter, L. U., 1959. *Structural geology*. London: McGraw-Hill, p.10.

Dix, C. H., 1965. Reflection seismic crustal studies. *Geophysics*, v.30, p.1068-1084.

Dohr, G., 1957. Ein Beitrag der Reflexionsseismik zur Erforschung des teiferen Untergrundes. *Geologische Rundschau*, v.46, p.17-26. (Translated by T. Gretener.)

Dohr, G. and K. Fuchs, 1967. Statistical evaluation of deep crustal reflections in Germany. *Geophysics*, v.32, p.951-967.

Dürschner, H., 1958. Synthetic seismograms from continuous velocity logs. *Geophys. Prosp.*, v.6, p.272-284.

Embree, P., J. P. Burg and M. M. Backus, 1963. Wide-band velocity filtering — the pie-slice process. *Geophysics*, v.28, p.948-974.

Fail, J. P. and G. Grau, 1963. Les filtres en éventail. *Geophys. Prosp.*, v.11, p.131-163.

Florensov, N. A., 1966. The Baikal rift zone. In *The world rift system*, T. N. Irvine (ed.), Geological Survey of Canada, Paper 66-14. Ottawa: Queen's Printer, p.173-180.

Francis, T. J. G., 1969. How necessary are large scale seismic refraction measurements? (preprint).

Freund, R., 1966. Rift valleys. In *The world rift system*, T. N. Irvine (ed.), Geological Survey of Canada, Paper 66-14. Ottawa: Queen's Printer, p.330-344.

Fuchs, K., 1968. Das Reflexions- und Transmissionsvermögen eines geschicteten Mediums mit beliebiger Tiefen-Verteilung der elastischen Moduln und der Dichte für schrägen Einfall ebener Wellen. *Ztschr. f. Geophys.*, v.34, p.389-413.

Fuchs, K., 1969. On the properties of deep crustal reflectors. *Ztschr. f. Geophys.*, v.35, p.133-149.

Fursov, A. N. and G. A. Yaroshevskaya, 1967. Experiences in recording deep waves using stations with intermediate magnetic recording. In *Problems in deep seismic sounding*, S. M. Zverev (ed.). New York: Consultants Bureau, p.1-14.

Gaby, P. P., 1945. A new type of seismic cross-section wherein accuracy of representation is rendered insensitive to velocity error. *Geophysics*, v.10, p.171-185.

Garland, G. D. and R. A. Burwash, 1959. Geophysical and petrological study of Precambrian of central Alberta, Canada. *Bull. Amer. Assoc. Petrol. Geol.*, v.43, p.790-806.

Garland, G. D., E. R. Kanasewich and T. L. Thompson, 1961. Gravity measurements over the southern Rocky Mountain trench area of British Columbia. *J. Geophys. Res.*, v.66, p.2495-2505.

Gentleman, W. M. and G. Sande, 1966. Fast Fourier transforms — for fun and profit. *Proc. of the Fall Joint Computer Conference*, San Francisco, p.563-578.

German Research Group for Explosion Seismology, 1964. Crustal structure in western Germany. *Ztschr. f. Geophys.*, v.30, p.209-234.

German Research Group for Explosion Seismology, 1966. Seismic wide angle measurements in the Bavarian Molasse Basin. *Geophys. Prosp.*, v.14, p.1-6.

Gregory, J. W., 1896. *The great rift valley.* London: John Murray, 422 p.

Gregory, J. W., 1921. *The rift valleys and geology of East Africa.* London: Seeley, 479 p.

Heelan, P. A., 1953. Radiation from a cylindrical source of finite length. *Geophysics*, v.18, p.685-696.

Hope, E. R., 1967. *The Baikalian rift system.* T435R. Ottawa: Defence Research Board.

Illies, J. H., 1967. Development and tectonic pattern of the Rhinegraben. In *The Rhinegraben progress report 1967*, J. P. Rothe and K. Sauer (eds.), International Upper Mantle Project, Scientific Report No. 13, Freiburg i Br./Strasbourg: Rota-Druck Johannes Krause Buchbinderei, p.7-9.

Irvine, T. N. (ed.), 1966. *The world rift system.* Geological Survey of Canada, Paper 66-14. Ottawa: Queen's Printer, 471 p.

Jakosky, J. Jay and John J. Jakosky, 1952. Frequency analysis of seismic waves. *Geophysics*, v.17, p.721-738.

James, D. E. and J. S. Steinhart, 1966. Structure beneath continents: A critical review of explosion studies 1960-65. In *The earth beneath the continents*, J. S. Steinhart and T. J. Smith (eds.). Washington: American Geophysical Union, p.293-333.

Jeffreys, H., 1926. On near earthquakes. *Mon. Not. R. Astr. Soc., Geophys. Suppl.*, v.1, p.385-402.

Junger, A., 1951. Deep basement reflections in Big Horn County, Montana. *Geophysics*, v.16, p.499-510.

Kanasewich, E. R., 1965. Seismicity and other properties of geological provinces. *Nature*, v.208, p.1275-1278.

Kanasewich, E. R., 1968. Precambrian rift: genesis of strata-bound ore deposits. *Science*, v.161, p.1002-1005.

Kanasewich, E. R. and R. M. Clowes, 1968. Geophysical studies of the earth's crust and upper mantle in western Canada. *XXIII Session, International Geological Congress*, v.1, K. Beneš (ed.). Prague: Academia, p.239-247.

Kanasewich, E. R., R. M. Clowes and C. H. McCloughan, 1969. A buried Precambrian rift in western Canada. *Rev. Geophys.*, (in press).

Kanasewich, E. R. and G. L. Cumming, 1965. Near-vertical-incidence seismic reflections from the 'Conrad' discontinuity. *J. Geophys. Res.*, v.70, p.3441-3446.

Kennedy, G. C., 1959. The origin of continents, mountain ranges and ocean basins. *Am. Scientist*, v.47, p.491-504.

Khalevin, N. I., V. S. Druzhinin, V. M. Rybalka, E. A. Nezoienova and L. N. Chudakova, 1966. The results of deep seismic sounding of the earth's crust in the Middle Urals. *Physics of the Solid Earth*, 1966, p.226-232.

Knopoff, L., 1956. The seismic pulse in material possessing solid friction: I. Plane waves. *Bull. Seism. Soc. Amer.*, v.46, p.175-183.

Knopoff, L., 1964. Q. *Rev. Geophys.*, v.2, p.625-660.

Knopoff, L., 1969. The upper mantle of the earth. *Science*, v.163, p.1277-1287.

Kosminskaya, I. P., 1964. On layering of the earth's crust. *J. Geophys. Res.*, v.69, p.802-804.

Kosminskaya, I. P., 1965. Problems of deep seismic sounding of the earth's crust and upper mantle at the 7th conference of geophysicists of the Eurasian region. *Physics of the Solid Earth*, 1965, p.420-423.

Kosminskaya, I. P. and Y. V. Riznichenko, 1964. Seismic studies of the earth's crust in Eurasia. In *Research in Geophysics*, v.2, H. Odishaw (ed.). Cambridge: The M.I.T. Press, p.81-122.

Kovach, R. L. and D. L. Anderson, 1964. Attenuation of shear waves in the upper and lower mantle. *Bull. Seism. Soc. Amer.*, v.54, p.1855-1864.

Krey, T., G. Schmidt and K.-H. Seelis, 1961. Über die Möglichkeit, den reflexionsseismisch erfassbaren Tiefenbereich zu erweitern. *Erdöl und Kohle*, v.14, p.521-526.

Ladynin, A. V., 1966. Gravity anomalies in the Graaff-Hunter reduction and crustal isostasy, Transbaikalia. *Geolog. i Geofiz.*, no.3, p.113-120. (Translated by E. R. Hope, T465R. Ottawa: Defence Research Board, 1967.)

Lovering, J. F., 1958. The nature of the Mohorovičić discontinuity. *Trans. Am. Geophys. Union*, v.39, p.947-955.

MacDonald, G. J. F. and N. F. Ness, 1960. Stability of phase transitions within the earth. *J. Geophys. Res.*, v.65, p.2173-2190.

Mack, H., 1969. Nature of short-period P-wave signal variations at LASA. *J. Geophys. Res.*, v.74, p.3161-3170.

Maureau, G. T. F. R., 1964. *Crustal structure in western Canada.* M.Sc. thesis. Edmonton: University of Alberta, Department of Physics.

McConnell, R. B., 1967. The East African rift system. *Nature*, v.215, p.578-581.

Meissner, R., 1966. An interpretation of the wide angle measurements in the Bavarian Molasse Basin. *Geophys. Prosp.*, v.14, p.7-16.

Meissner, R., 1967*a*. Exploring deep interfaces by seismic wide-angle measurements. *Geophys. Prosp.*, v.15, p.598-617.

Meissner, R., 1967*b*. Zum Aufbau der Erdkruste. Ergebnisse der Weitwinkelmessungen im bayerischen Molasse becken. *Gerl. Beitr. z. Geophys.*, v.76, Part I: p.211-254, Part II: p.295-314.

Molnar, P. and J. Oliver, 1969. Lateral variations of attenuation in the upper mantle and discontinuities in the lithosphere. *J. Geophys. Res.*, v.74, p.2648-2682.

Musgrave, A. W., 1962. Applications of the expanding reflection spread. *Geophysics*, v.27, p.981-993.

Nafe, J. E. and C. L. Drake, 1959. (Published by Talwani, M., G. H. Sutton and J. L. Worzel.) Crustal section across the Puerto Rico Trench. *J. Geophys. Res.*, v.64, p.1545-1555.

Nakamura, Y. and B. F. Howell, Jr., 1964. Maine seismic experiment: frequency spectra of refraction arrivals and the nature of the Mohorovičić discontinuity. *Bull. Seism. Soc. Am.*, v.54, p.9-18.

Narans, H. D., Jr., J. W. Berg, Jr. and K. L. Cook, 1961. Sub-basement seismic reflections in northern Utah. *J. Geophys. Res.*, v.66, p.599-603.

Papazachos, B. C., P. E. Comninakis, J. C. Drakopoulos, 1966. Preliminary results of an investigation of crustal structure in southeastern Europe. *Bull. Seism. Soc. Am.*, v.56, p.1241-1268.

Perkins, W. E., 1969. Moho reflections on the north wall of the Puerto Rico Trench (Abstract). *Trans. Am. Geophys. Union*, v.50, p.211.

Perret, W. R., 1967. Deep reflections from a nuclear explosion in a salt dome. *J. Geophys. Res.*, v.72, p.6327-6333.

Peterson, R. A., W. R. Fillipone and F. B. Coher, 1955. The synthesis of seismograms from well-log data. *Geophysics*, v.20, p.516-538.

Phinney, R. A. and W. E. Perkins, 1969. Reflection profiling of the ocean crust. Preprint supplied by W. E. P.

Press, F., 1964. Seismic wave attenuation in the crust. *J. Geophys. Res.*, v.69, p.4417-4418.

Reisner, G. I., 1966. Multi-disciplinary research on the Baikal rift zone. *Vestnik Akad. Nauk SSSR*, no.9, p.112-114. (Translated by E. R. Hope, T472R, Ottawa: Defence Research Board, 1966.)

Richards, T. C. and D. J. Walker, 1959. Measurement of the thickness of the earth's crust in the Albertan plains of western Canada. *Geophysics*, v.24, p.262-284.

Ringwood, A. E., 1966. The chemical composition and origin of the earth. In *Advances in earth science*, P. M. Hurley (ed.), Cambridge: The M.I.T. Press, p.287-356.

Ringwood, A. E. and D. H. Green, 1964. Experimental investigations bearing on the nature of the Mohorovičić discontinuity. *Nature*, v.201, p.566-570.

Ringwood, A. E. and D. H. Green, 1966. Petrological nature of the stable continental crust. In *The earth beneath the continents*, J. S. Steinhart and T. J. Smith (eds.), Washington: American Geophysical Union, p.611-619.

Robertson, G., 1963. Intrabasement reflections in southwestern Alberta. *Geophysics*, v.28, p.910-955.

Roller, J. C., 1965. Crustal structure in the Eastern Colorado Plateaus Province from seismic-refraction measurements. *Bull. Seism. Soc. Am.*, v.55, p.107-119.

Rothe, J. P. and K. Sauer (eds.), 1967. *The Rhinegraben progress report 1967*. International Upper Mantle Project, Scientific Report No. 13, Freiburg i Br./Strasbourg: Rota-druck Johannes Krause Buchbinderei, 146 p.

Ryder, J. D., 1959. *Electronic fundamentals and applications, 2nd ed.* Englewood Cliffs: Prentice-Hall, Inc., p.285.

Sanford, A. L. and L. T. Long, 1965. Microearthquake crustal reflections, Socorro, New Mexico. *Bull. Seism. Soc. Am.*, v.55, p.579-586.

Sato, R., 1967. Attenuation of seismic waves. *J. Phys. Earth*, v.15, p.32-61.

Savit, C. H., J. T. Brustad and J. Sider, 1958. The moveout filter. *Geophysics*, v.23, p.1-25.

Schriever, W., 1952. Reflection seismograph prospecting — how it started. *Geophysics*, v.17, p.936-942.

Sengbush, R. L. and M. R. Foster, 1968. Optimum multichannel velocity filters. *Geophysics*, v.33, p.11-35.

Shanks, J. L., 1967. Recursion filters for digital processing. *Geophysics*, v.32, p.33-51.

Sharpe, J. A., 1942*a*. The production of elastic waves by explosion pressures. I. Theory and empirical field observations. *Geophysics*, v.7, p.144-154.

Sharpe, J. A., 1942*b*. The production of elastic waves by explosion pressures. II. Results of observations near an exploding charge. *Geophysics*, v.7, p.311-321.

Steinhart, J. S. and R. P. Meyer, 1961. *Explosion studies of continental structure*. Carnegie Inst. Wash. Publ. 622, Washington: The Kirby Lithographic Company, Inc., 409 p.

Stewart, S. W. and L. C. Pakiser, 1962. Crustal structure in eastern New Mexico interpreted from the GNOME explosion. *Bull. Seism. Soc. Am.*, v.52, p.1017-1030.

Stishov, S. M., 1963. The nature of the Mohorovičić discontinuity. *Bull. (Izvestiya), Acad. Sci. USSR, Geophys. Ser.*, no.1, p.28-31.

Summers, G. C. and R. A. Broding, 1952. Continuous velocity logging. *Geophysics*, v.17, p.598-614.

Sumner, R. D., 1967. Attenuation of earthquake generated P waves along the western flank of the Andes. *Bull. Seism. Soc. Am.*, v.57, p.173-190.

Treitel, S., J. L. Shanks and C. W. Frasier, 1967. Some aspects of fan filtering. *Geophysics*, v.32, p.789-800.

Trorey, A. W., 1962. Theoretical seismograms with frequency and depth dependent absorption. *Geophysics*, v.27, p.766-785.

Tucker, L. R., 1968. Geophysical activity in 1967 applied to petroleum exploration. *Geophysics*, v.33, p.885-902.

Vogel, C. B., 1952. A seismic velocity logging method. *Geophysics*, v.17, p.586-597.

White, R. E., 1969. Seismic phases recorded in South Australia and their relation to crustal structure. *Geophys. J. Roy. Astron. Soc.*, v.17, p.249-261.

Wiggins, R. A., 1966. ω-k filter design. *Geophys. Prosp.*, v.14, p.427-440.

Wuenschel, P. C., 1960. Seismogram synthesis including multiples and transmission coefficients. *Gepphysics*, v.25, p.106-129.

Zorin, Yu. A., 1966. The deep structure of the Lake Baikal depression according to geophysical findings. *Izvestiya Akad. Nauk SSSR, Geological Series*, no.7, p.75-85. (Translated by E. R. Hope, T473R, Ottawa: Defence Research Board, 1967.)

Zverev, S. M. (ed.), 1967. *Problems in deep seismic sounding*. New York: Consultants Bureau, 166 p.

# APPENDIX

## FORTRAN SOURCE LISTINGS OF COMPUTER PROGRAMS

### The velocity filter program

The velocity filter program is designed to process deep reflection seismograms with a fan-pass filter. The logic of the program follows the algorithm developed by Treitel et al. (1967). The input data, comprised of amplitude values from two seismograms, are processed using three different filter characteristics. This data and the three sets of filtered output data are plotted by the use of CALCOMP plotter subroutines. As well, the output data are written on tape.

Execution time for the program is short. If twelve vectors of 960 points are processed by three different filters which use eight of these data sets per single output vector, each filter thus producing a total of five output traces, the execution time is 0.92 minutes on the IBM 360/67 computing system.

```
C
C  THIS PROGRAM VELOCITY FILTERS SEISMIC DATA ACCORDING TO THE
C   ALGORITHM DEVELOPED BY TREITEL ET AL. (GEOPHYSICS, V. 32,
C   P. 789-800,1967).
C  THE BLOCK LENGTH OF THE INPUT DATA IS 1200 WORDS/BLOCK
C  NOTE.....FOR VELOCITY FILTERED DATA ONLY THE OUTPUT TAPE COMPRISES
C            DATA FOR WHICH THE BLOCK LENGTH IS 200 WORDS/BLOCK
C
 1000 FORMAT (16I5)
 1001 FORMAT (8F10.5)
 1002 FORMAT ('0 THE TOTAL NUMBER OF PLOTS FOR INCLUDING ON PLOT REQUEST
     1 SLIP IS',I5)
 1003 FORMAT (1H0,'POINTS 1 TO',I5,' FOR THE DATA POINTS',I5,' TO',I5,'
     1OF INPUT TRACE ',I2,' WHICH ARE TO BE FILTERED')
 1004 FORMAT (1H0, 10(1X,E11.4))
 1005 FORMAT (1H0,'POINTS 1 TO',I5,' FOR THE ',I2,'TH VELOCITY FILTERED
     1OUTPUT TRACE WHOSE POSITION IS ',F4.1,' RELATIVE TO POSITION 1')
 1006 FORMAT (1H0,I4,' BLOCKS OF 200 WORDS PER BLOCK WERE COPIED ONTO TH
     1E NEW TAPE')
 1007 FORMAT (1H1,'BLOCKS ',I5,' TO ',I5,'(200 WORDS PER BLOCK) CONTAIN
     1THE ',I2,'TH VELOCITY FILTERED OUTPUT TRACE FROM THIS DATA')
 1008 FORMAT (9I5,5A4,3F5.1)
 1009 FORMAT (1H0,5A4,' HAVE BEEN VELOCITY FILTERED TO PROVIDE',I3,' TRA
     1CES OF',I5,' POINTS/TRACE, THE LAST DATA ON TAPE'//' FILTER CENTER
     2ED AT ',I2,' DELTA T/TRACE WITH A CUTOFF OF + OR - ',I2,' DELTA T/
     3TRACE')
C
 1010 FORMAT (1H1,' NUMBER OF INPUT TRACES EQUALS ',I3//2X,'NO. OF TRACE
     1S USED IN FAN PASS OPERATION EQUALS ',I2//2X,'PASS BAND CENTERED A
     2BOUT ',I2,' DELTA T/TRACE.  CUTOFF APPARENT VELOCITY IS ',I2,' DEL
     3TA T/TRACE'//2X,'NO. OF POINTS TO BE FILTERED EQUALS ',I5//2X,'STA
     4RTING BLOCKS ON TAPE FOR INPUTTING DATA FROM 2 RECORDS ARE ',I5,'
     5AND ',I5//2X,'FOR DATA READ INTO MATRIX XDATA, THE STARTING POINT
     6FOR VELOCITY FILTERING IS',I5)
C
      COMMON/STORAG/XDATA(12,2400),BLKST(2)
      COMMON/STORE/XFILT(5,1600), SEPT, TSTART, TINCH, SCALE, COPS,
     1 RECNO(5), CENTER, NTAU
      DIMENSION SUM(1600), Y(1600), Z(1600), SPARE(200), BUFF(1536)
      INTEGER BLKST, PTSTAR, CENTER, START, ROWST, PTEND, CENT(3),TAU(3)
      EQUIVALENCE (SUM(1),SPARE(1))
      XPOS = 2.)
      YPOS = 29.0
      IP = 0
      NREAD = 0
      READ (5,1000) M, NBLK, NTR, NOUT, NCOPY, NPRINT, JPLOT
C
C  M        MUST BE EVEN (8, 10 OR 12) AND GIVES THE NO. OF TRACES TO BE
C           USED IN THE FAN PASS OPERATION
C  NBLK     NO. OF BLOCKS OF DATA OF 6 X 200 POINTS IN EACH RECORD
```

```
C  NTR      NUMBER OF INPUT TRACES WHICH ARE TO BE FILTERED
C  NOUT     THE NUMBER OF OUTPUT TRACES EXPECTED
C  NCOPY    NO. OF BLOCKS OF 200 WORDS/BLOCK TO COPY FROM UNIT 3 ONTO 2
C  NPRINT   NO. OF DATA VALUES TO LIST
C  JPLOT    = 0 AND NO PLOTTING IS DONE
C           = 1 AND THE INPUT AND VELOCITY FILTERED TRACES ARE PLOTTED
C
      READ (5,1001) SEPT, TINCH, COPS, SCALE
C
C  THIS READS IN PARAMETERS REQUIRED FOR THE PLOTVF ROUTINE
C  SEPT     SEPARATION IN INCHES BETWEEN TRACES
C  TINCH    NUMBER OF INCHES OF PAPER PER SECOND
C  COPS     NUMBER OF CONVERSIONS PER SECOND
C  SCALE    SCALE FACTOR TO REDUCE MAGNITUDE FOR PLOTTING IN INCHES
C
      IF (JPLOT.EQ.1) CALL PLOTS (BUFF(1),6144)
      NTR PT = 0
      IF (NCOPY.EQ.0) GO TO 4
      DO 2 J=1,NCOPY
      READ (3,ERR=3) SPARE
      GO TO 2
    3 READ (3) SPARE
    2 WRITE (2) SPARE
    4 WRITE (6,1006) NCOPY
      NWRIT = NCOPY
    1 READ (5,1008) ISTOP, BLKST(1), BLKST(2), (CENT(I),I=1,3), (TAU(I),
     1I=1,3), (RECNO(I),I=1,5), RSTART, TSTART, TEND
C
C  ISTOP     = 999 IN COLUMNS 3-5 STOPS THE RUN
C  BLKST    STARTING BLOCK FOR EACH GROUP OF 6 TRACES WHICH MAY BE USED
C  CENT(I) IS THE MOVEOUT IN SAMPLING INCREMENTS/TRACE ABOUT WHICH THE
C           PASS BAND IS CENTERED.  FOR 2 APPARENT VELOCITIES, CENTER
C           IS DETERMINED FROM (V2 + V1)/2.
C  TAU(I)   IS THE MOVEOUT IN SAMPLING INCREMENTS/TRACE WHICH
C           APPROXIMATES THE CUTOFF APPARENT VELOCITY.  FOR 2 VELOCITIES,
C           NTAU IS DETERMINED FROM ABS(V2 - V1)/2.
C  RECNO     ALPHAMERIC IDENTIFICATION FOR DATA BEING FILTERED
C  RSTART    TIME CORRESPONDING TO POINT 1 OF THE RECORDS
C  TSTART    TIME AT WHICH VELOCITY FILTERING AND PLOTTING BEGIN
C  TEND      TIME AT WHICH VELOCITY FILTERING AND PLOTTING END
C  TSTART - TEND MUST BE LESS THAN OR EQUAL TO 13.2 SECONDS
C
      IF (ISTOP.EQ.999) GO TO 110
      PT = (TSTART - RSTART) * COPS
      IF ((PT - IFIX(PT)).GE.0.5) PT = PT + 1.0
      PTSTAR = IFIX(PT) + 1
      PT = (TEND - RSTART) * COPS
      IF ((PT - IFIX(PT)).GE.0.5) PT = PT + 1.0
      NPEND = IFIX(PT)
      NPTS = NPEND - PTSTAR + 1
```

```
      CALL READ3(NBLK,NREAD)
C   THIS FEEDS INTO XDATA THE TRACES TO BE VELOCITY FILTERED
C
      NP = PTSTAR + NPRINT - 1
      DO 5 J=1,NTR
      WRITE (6,1003) NPRINT, PTSTAR, NPEND, J
    5 WRITE (6,1004) (XDATA(J,JA),JA=PTSTAR,NP)
      IF (JPLOT.EQ.1) CALL PLOTVF (NTR,NPTS,1,NOUT,PTSTAR, 0,NTR PT,
     1XPOS, YPOS, IP)
C   THIS USES THE CALCOMP PLOTTER TO PLOT THE INPUT TRACES TO THE V.F.
C
      DO 100 KF = 1,3
      CENTER = CENT(KF)
      NTAU = TAU(KF)
      WRITE (6,1010) NTR, M,CENTER,NTAU,NPTS,BLKST(1),BLKST(2),PTSTAR
      L = M-1
      MC = L*IABS(CENTER)
      NEND = NPEND - (L+1)*NTAU/2
      START = PTSTAR + (L-1)*NTAU/2
      IF (CENTER.LT.0) START = START + MC
      IF (CENTER.GT.0) NEND = NEND - MC
C   THE STARTING AND ENDING TIMES HAVE BEEN CHANGED SO THAT ONLY POINTS
C   IN THE TIME INTERVAL TSTART TO TEND WILL BE USED WHEN THE DATA
C   POINTS ARE TIME SHIFTED.
C
      A = 0.65465
      B = 0.98612
      C = 0.13091
      ROWST = 0
   20 ROWST = ROWST + 1
      DO 10 I=1,1600
   10 SUM(I) = 0.0
      DO 50 N=START, NEND
      NSN = N - PTSTAR + 1
      IROW = ROWST
      DO 40 J=1,M
      JA = J-1
      MU = 2*JA - L
      MUDE = (MU-1)*NTAU/2
      MUAD = (MU+1)*NTAU/2
      JB = CENTER*JA
      ICOL1 = N - MUDE + JB
      ICOL2 = N + MUAD + JB
      DIFF = (XDATA(IROW,ICOL1) - XDATA(IROW,ICOL2))/MU
      SUM(NSN) = SUM(NSN) + DIFF
   40 IROW = IROW + 1
   50 CONTINUE
      NST1 = START - PTSTAR + 1
      NEN1 = NEND - PTSTAR + 1
C   THE VECTOR 'SUM' HAS NOW BEEN FILLED WITH THE WEIGHTED SUM
```

```
C  OF THE TIME SHIFTED TRACES.
C
      DO 55 I=1,1600
      Y(I) = 0.0
      Z(I) = 0.0
   55 XFILT(ROWST,I) = 0.0
      DO 60 N=NST1,NEN1
      NA = N-1
      NB = N-2
      Y(N) = SUM(NA) - A*SUM(NB) + B*Y(NA) - C*Y(NB)
      NN = NEN1 - N + NST1
      NC = NN+1
      ND = NN+2
   60 Z(NN) = SUM(NN) - A*SUM(NC) + B*Z(NC) - C*Z(ND)
      DO 70 N=NST1,NEN1
   70 XFILT(ROWST,N) = 0.2026424*(Z(N) - Y(N))
      LL = NEN1 + 200 - MOD(NEN1,200)
C  THE RECURSIVE FILTER OPERATOR HAS JUST BEEN APPLIED TO THE DATA
C  XFILT(ROWST, ) CONTAINS THE (ROWST)TH VELOCITY FILTERED OUTPUT TRACE
C
      IF (ROWST.LT.NOUT) GO TO 20
      IF (JPLOT.EQ.1) CALL PLOTVF (ROWST,NPTS,2,NOUT,1,KF, NTR PT, XPOS,
     1 YPOS, IP)
      FM = FLOAT(M/2)
      DO 80 J=1,NOUT
      POS = FM + 0.5 + FLOAT(J-1)
      LLL = LL/200
      NW = NWRIT + 1
      NWRIT = NWRIT + LLL
      WRITE (6,1007) NW, NWRIT, J
      WRITE (6,1005) NPRINT, J, POS
      DO 75 JA = 1,LLL
      JC = 200*.A
      JB = JC - 199
   75 WRITE (2) (XFILT(J,JD),JD=JB,JC)
   80 WRITE (6,.004) (XFILT(J,JA),JA=1,NPRINT)
      WRITE (6,.009) RECNO, NOUT, LL, CENTER, NTAU
  100 CONTINUE
      GO TO 1
  110 IF (JPLOT.EQ.0) GO TO 120
      CALL PLOT (XPOS,YPOS-28.0,-3)
      IP = IP + 2
      CALL PLOT (0.0, 0.0, 999)
      WRITE (6,1002) IP
  120 END FILE 2
      REWIND 2
      STOP
      END
```

```
      SUBROUTINE READ3 (NBLK,NREAD)
C  THIS SUBROUTINE READS 12 CHANNELS, 6 FROM EACH OF 2 DIFFERENT
C  RECORDS, OF UP TO 2400 POINTS INTO XDATA
C
C  MOUNT DATA TAPE ON FTC04
C  NBLK IS THE NO. OF BLOCKS OF 6 X 200 POINTS TO BE READ IN
C  BLKST IS THE STARTING BLOCK FOR EACH GROUP OF 6 TRACES WHICH ARE USED
C
      COMMON/STORAG/XDATA(12,2400), BLKST(2)
      INTEGER BLKST
      NPTS = 200*NBLK
      DO 30 KA=1,2
      NSKIP = BLKST(KA) - NREAD - 1
      CALL SKIP (NSKIP, 4)
      NREAD = NREAD + NSKIP
   10 JB = 6*KA
      JA = JB - 5
      DO 20 J=1,NPTS,200
      JC = J + 199
      READ (4,ERR=15) ((XDATA(JD,JE),JD=JA,JB),JE=J,JC)
      GO TO 20
   15 READ (4) ((XDATA(JD,JE),JD=JA,JB),JE=J,JC)
   20 CONTINUE
      NREAD = NREAD + NBLK
   30 CONTINUE
      RETURN
      END


      SUBROUTINE SKIP (ISKIP,ITAPE)
C
C  THIS SUBROUTINE IS USED TO SKIP DOWN A TAPE TO THE DESIRED RECORD
C
      IF (ISKIP.EQ.0) RETURN
      IF (ISKIP.LT.0) GO TO 1
      DO 2 II = 1,ISKIP
      READ (ITAPE,ERR=5)
      GO TO 2
    5 READ (ITAPE)
    2 CONTINUE
      RETURN
    1 ISKIP = - ISKIP
      DO 3 I=1,ISKIP
      BACKSPACE ITAPE
    3 CONTINUE
      RETURN
      END
```

```
      SUBROUTINE PLOTVF (NTP,NPTS,INDEX,NOUT,NPSTAR,KF,NTR PT,XPOS,YPOS,
     1 IP)
C
C   THIS SUBROUTINE PLOTS THE INPUT DATA FOR THE VELOCITY FILTER AND ALL
C   DATA WHICH HAS BEEN FILTERED
C
      COMMON/STORAG/XDATA(12,2400),BLKST(2)
      COMMON/STORE/XFILT(5,1600), SEPT, TSTART, TINCH, SCALE, COPS,
     1 RECNO(5), CENTER, NTAU
      INTEGER CENTER
      WRITE (6,1001) NPTS,NTP,SEPT,TINCH,COPS,TSTART,SCALE
 1001 FORMAT (1HO,'FOR PLOTTING THE',I5,' POINTS FOR',I3,' TRACES, THE T
     1RACE SEPARATION IS',F5.2//4X,'THE PAPER SPEED IS ',F4.2,' IN./SEC
     2AND THE DIGITIZING RATE IS ',F7.2,' CONV/SEC'//4X,'THE BEGINNING T
     3IME IS ',F5.2,' AND THE SCALING FACTOR IS ',F7.1)
C
      NPEND = NPSTAR + NPTS - 1
      T = TINCH/COPS
      XLEN = FLOAT(NPTS)*T
      ABSINT = 1.0/TINCH
      MNTR = MOD (NTR PT, 2)
      GO TO (20,30), INDEX
   20 DO 27 J=1,NTP
      DO 22 JA = NPSTAR,NPEND
   22 XDATA(J,JA) = XDATA(J,JA)/SCALE
   27 CONTINUE
      CALL PLOT (XPOS,YPOS,-3)
      IP = IP+1
      CALL PLOT (0.0,-1.0,-3)
      IP = IP+1
      CALL AXIS (0.0,0.0,'TIME IN SECONDS',+15,XLEN,0.0,TSTART,ABSINT,
     110.0)
      YD = 3.5 + 5.5*SEPT
      CALL SYMBOL (-1.0,-YD,0.2,RECNO,90.0,20)
      YDADD = YD + 0.50
      CALL SYMBOL (-0.5,-YDADD ,0.15,'DISTANCE BETWEEN TRACES IS .29 KM.
     1',90.0,34)
      GO TO 39
   30 DO 10 J=1 NTP
      DO 5 JA = NPSTAR,NPEND
    5 XFILT(J,JA) = XFILT(J,JA)/SCALE
   10 CONTINUE
      IF (MNTR.NE.0) GO TO 36
   33 CALL PLOT (-XLEN,0.0,-3)
      IP = IP + 1
   36 IF (KF.NE.1) GO TO 39
      CALL PLOT (0.0,-2.0,-3)
      IP = IP + 1
      CALL AXIS (0.0,0.0,'TIME IN SECONDS',+15,XLEN,0.0,TSTART,ABSINT,
     110.0)
```

```
      CALL SYMBOL (-1.0,-0.7,.20,'VELOCITY',90.0,8)
      CALL SYMBOL (-0.7,-0.7,0.20,'FILTERED',90.0,8)
      CALL SYMBOL (-0.3,-0.4,0.20,'DATA',90.0,4)
39    IF (KF.EQ.0) GO TO 44
      YD = 2.1 + FLOAT(NOUT-1)*SEPT
      FNUM1 = FLOAT (CENTER - NTAU)/COPS
      IF (FNUM1.NE.0.) GO TO 40
      VEL1 = 1.0
      GO TO 41
40    VEL1 = 0.293/FNUM1
41    FNUM2 = FLOAT (CENTER+NTAU)/COPS
      IF (FNUM2.NE.0.) GO TO 42
      VEL2 = 1.0
      GO TO 43
42    VEL2 = 0.293/FNUM2
43    CALL SYMBOL(-1.0,-YD,.15,'V1',90.0,2)
      CALL SYMBOL(-0.9,-YD+.25,.10,'APP',90.0,3)
      CALL WHERE (XP,YP,FCTR)
      YP = YP + 0.2
      CALL SYMBOL (-1.0,YP,.15,' IS ',90.0,4)
      CALL WHERE (XP,YP,FCTR)
      YP = YP + 0.2
      CALL NUMBER (-1.0,YP,.15,VEL1,90.0,1)
      CALL WHERE (XP,YP,FCTR)
      YP = YP + 0.2
      CALL SYMBOL (-1.0,YP,.15,'K/S',90.0,3)
      CALL SYMBOL(-0.5,-YD,.15,'V2',90.0,2)
      CALL SYMBOL(-0.4,-YD+.25,.10,'APP',90.0,3)
      CALL WHERE (XP,YP,FCTR)
      YP = YP + 0.2
      CALL SYMBOL (-0.5,YP,.15,' IS ',90.0,4)
      CALL WHERE (XP,YP,FCTR)
      YP = YP + 0.2
      CALL NUMBER (-0.5,YP,.15,VEL2,90.0,1)
      CALL WHERE (XP,YP,FCTR)
      YP = YP + 0.2
      CALL SYMBOL (-0.5,YP,.15,'K/S',90.0,3)
44    DO 80 J=1,NTP
      MJ = MOD J,2)
      IF (J.NE.1) GO TO 45
      CALL PLOT (0.0,-2.0,-3)
      IP = IP + 1
      GO TO 46
45    IF (MJ.EQ.0) GO TO 60
      CALL PLOT (-XLEN,-SEPT,-3)
      IP = IP+1
46    CALL SYMBOL (0.0,0.0,.15,04,0.0,-1)
      GO TO (47,49), INDEX
47    CALL PLOT (0.0,XDATA(J,NPSTAR),3)
      DO 48 JA = NPSTAR,NPEND
```

```
      TSCALE = T * FLOAT(JA-NPSTAR+1)
48    CALL PLOT (TSCALE,XDATA(J,JA),2)
      GO TO 75
49    CALL PLOT (0.0,XFILT(J,NPSTAR),3)
      DO 50 JA = NPSTAR,NPEND
      TSCALE = T * FLOAT(JA-NPSTAR+1)
50    CALL PLOT (TSCALE,XFILT(J,JA),2)
      GO TO 75
60    CALL PLOT (XLEN,-SEPT,-3)
      IP = IP+1
      CALL SYMBOL (0.0,0.0,.15,04,0.0,-4)
      GO TO (61,64), INDEX
61    CALL PLOT (0.0,XDATA(J,NPEND),3)
      DO 62 JA = NPSTAR,NPEND
      TSCALE = - T * FLOAT(JA-NPSTAR+1)
      JCC = NPEND - JA + NPSTAR - 1
      IF (JCC.LT.NPSTAR) JCC = NPSTAR
62    CALL PLOT (TSCALE, XDATA(J,JCC),2)
      GO TO 75
64    CALL PLOT (0.0,XFILT(J,NPEND),3)
      DO 65 JA = NPSTAR,NPEND
      TSCALE = - T * FLOAT(JA-NPSTAR+1)
      JCC = NPEND - JA + NPSTAR - 1
      IF (JCC.LT.NPSTAR) JCC = NPSTAR
65    CALL PLOT (TSCALE, XFILT(J,JCC),2)
75    CALL PLOT (TSCALE,0.0,3)
      CALL SYMBOL (TSCALE,0.0,.15,04,0.0,-4)
80    CONTINUE
      GO TO (81,84), INDEX
81    DO 83 J=1,NTP
      DO 82 JA = NPSTAR,NPEND
82    XDATA(J,JA) = XDATA(J,JA)*SCALE
83    CONTINUE
      GO TO 92
84    DO 90 J=1,NTP
      DO 85 JA = NPSTAR,NPEND
85    XFILT(J,JA) = XFILT(J,JA)*SCALE
90    CONTINUE
92    WRITE (6,1000) IP
1000  FORMAT (1HO,'NUMBER OF TIMES ORIGIN IS SET TO ZERO IS ',I5
      IF (KF.NE.3) GO TO 100
      IF (MNTR.EQ.0) GO TO 95
      XPOS = XLEN + 5.0
      GO TO 97
95    XPOS = 5.0
97    YPOS =11.0 + FLOAT(3*NTP + 8) * SEPT
100   NTR PT = NTP
      RETURN
      END
```

The synthetic seismogram program

The principal basis of the synthetic seismogram program is an iterative formula for calculation of the transfer function of a layered medium in which the velocity may vary linearly with depth in any layer. The formula is from a development by Berryman et al. (1958) which has been rederived in order that the effects of attenuation may be included. The computed transfer function is plotted.

A choice of two different input waveforms is provided in the program. One of these is the form of Gram-Charlier wavelet used by Berryman et al. (loc. cit.). By proper specification of the input parameters, the principal frequency component of the wavelet can be controlled. The second form of input pulse is specified by its amplitude versus frequency characteristics, assuming a constant phase of zero. An inverse Fourier transform of this is taken to produce an approximation to a delta function centered at zero time. The pulse is then delayed and a Fourier transform of the delayed pulse is computed to obtain both real and imaginary parts of the pulse spectrum.

An inverse Fourier transform of the product of the complex pulse spectrum and the transfer function yields the amplitude values of the synthetic seismogram. These are plotted on a specified time scale.

A facility is included to allow computation of the autopower spectra from up to four different time intervals on the synthetic seismogram. The autopower spectral density of the first interval is plotted over the entire range from zero to the Nyquist frequency. Any other spectra computed are plotted on one additional graph and for the frequency range from 5 to 25 Hz.

The execution time of the program is controlled by the calculation of the transfer function of the layered medium. A large number of layers coupled with the necessity of having small frequency increments causes the transfer function to be computationally expensive. The generation of the synthetic seismograms used in this thesis required considerable computing time. Because a velocity log, averaged over 20 foot intervals, was used to model the sedimentary layers, about 242 layers were introduced for this part only. Depending on the complexity of the remaining part of the specified layered medium, approximately 250 layers would have to be considered. In order to generate a seismogram at least 18 seconds long required a small frequency increment since the inverse of this increment is the maximum time interval which can be calculated without aliasing problems. The frequency increment is constrained by the specified Nyquist frequency and the requirements of the fast Fourier subroutines which use a number of points that must be a power of two. For most calculations, the writer used a Nyquist frequency of 80 and N/2 = 11 resulting in frequency increments of $80/2^{11}$. On the basis of the quantities mentioned, the total execution time of the synthetic seismogram program on the IBM 360/67 computing system was about 16 minutes. On the other hand, for a ten-layer case, a Nyquist frequency of 80 and N/2 = 10, the execution time was less than 1 minute.

```
C  THIS PROGRAM IS DESIGNED TO PRODUCE A SYNTHETIC SEISMOGRAM AT
C    VERTICAL INCIDENCE ALLOWING FOR ATTENUATION WITH DEPTH.  IN
C    THE PROCESS, IT PLOTS THE INPUT PULSE, ITS FOURIER TRANSFORM,
C    THE REFLECTION COEFFICIENT OF THE HORIZONTALLY LAYERED MEDIA,
C    THE FINAL SYNTHETIC SEISMOGRAM AND AUTOPOWER SPECTRA OF SPECIFIED
C    TIME INTERVALS OF THE SEISMOGRAM.
C
  999 FORMAT (16F5.0)
 1000 FORMAT (4I5,12F5.0)
 1001 FORMAT ('1 THE SYNTHETIC SEISMOGRAM AMPLITUDE VALUES'//)
 1002 FORMAT (10(1X,E11.3))
 1003 FORMAT ('1 THE NUMBER OF POINTS IN THE TIME SERIES IS ',I5//
     1'  THE NUMBER OF POINTS BETWEEN FREQUENCIES OF 0 AND NYQUIST IS ',
     2I5//'  THE NYQUIST FREQUENCY FOR THIS RUN OF THE PROGRAM IS ',F7.1
     3//'  THE CORRESPONDING DIGITIZING INTERVAL IS ',F7.3//
     4'  THE APPROXIMATE PERIOD OF THE INPUT PULSE IS ',F7.3//
     5'  FOR PLOTTING TIME SERIES, THE NO. OF INCHES/SECOND IS ',F7.3//
     6'  THE AMOUNT OF TIME TO BE PLOTTED FOR THE S. S. IS ',F7.3)
 1004 FORMAT (2(5X,F10.3,5X,E15.5))
 1005 FORMAT ('1 FREQUENCY AND AMPLITUDE VALUES FOR THE A.P. SPECTRA OF
     1THE S. S. FROM ',F5.2,' SEC. TO ',F5.2,' SEC.')
 1006 FORMAT ('1 THE GAIN CONTROL FACTOR AS A FUNCTION OF TIME FOLLOWS.'
     1//'  TIME STARTS AT 0, WITH AN INCREMENT BETWEEN VALUES OF TWICE '
     2,F6.3,' SEC.'//)
 1007  FORMAT ('0 INCIDENT PULSE SPECTRUM IS ZERO FROM 0 HZ. TO ',F5.1,
     1' REACHES UNITY AT ',F5.1,' AND SYMMETRICALLY RETURNS TO ZERO AT '
     2,F5.1//'  THE GAIN IS ',F8.1,' RAISED TO THE POWER OF TIME WITH A
     3MAXIMUM VALUE OF ',F8.1)
      COMPLEX RZ(2049), FW(2049)
      COMMON /STORE1/ RZ, FW
      COMMON /STORE2/ FREQ(2051), AMPL(2051), SS(4098), SI(4098)
      COMMON/STORE3/IP, YPOS, YTOT, TAU, TINCH, TPLOT,NAP,TST(4),TEND(4)
      DIMENSION SPARE (4098)
      EQUIVALENCE (RZ(1),SPARE(1))
      READ (5,1000) LOG2N, NAP, IPULS, LOGEST, ZEROLO, FLOCUT, HICUT,
     1 DELAY, FNYQ, PERIOD
      READ (5,999) TINCH, TPLOT, BETA, GMAX, ((TST(I),TEND(I)),I=1,4)
C
C  LOG2N    2**LOG2N GIVES THE NO. OF POINTS IN THE INPUT AND OUTPUT
C           TIME SERIES.  (LOG2N.LE.12)
C  NAP      NO. OF TIME RANGES FOR COMPUTING AUTOPOWER SPECTRA.
C           IF NAP=0, NO SPECTRA ARE COMPUTED.
C  IPULS    = 1 AND THE GRAM-CHARLIER WAVELET IS COMPUTED
C           = 2 AND THE PULSE FREQUENCY RESPONSE IS UNITY FROM FLOCUT TO
C           HICUT DECREASING TO ZERO FROM FLOCUT TO ZEROLO
C  LOGEST   2**LOGEST GIVES THE NO. OF FREQUENCY ESTIMATES FOR THE
C           AUTOPOWER SPECTRA OF THE SYNTHETIC SEISMOGRAM
C  ZEROLO   AMPLITUDE IS ZERO FROM 0 TO ZEROLO FREQUENCY
C  FLOCUT   LOW CUT-OFF FREQUENCY FOR SPECIFYING SPECTRUM OF INC. PULSE
C  HICUT    HIGH CUT-OFF FREQUENCY FOR SPECIFYING SPECTRUM OF INC. PULSE
```

```
C  DELAY   TIME DELAY TO POSITION MAX. AMPLITUDE OF INPUT PULSE
C  FNYQ    THE NYQUIST FREQUENCY FOR THE SPECTRA OF THE DATA TO BE CALC.
C  PERIOD  THE APPROXIMATE PERIOD OF THE INPUT PULSE FOR THE S.S.
C    ACTUALLY CENTRAL FREQ. IS ABOUT 20% LESS THAN (1/PERIOD).
C  BETA    GAIN CONTROL FACTOR IS BETA RAISED TO THE POWER OF
C          TIME WITH A MAXIMUM VALUE OF GMAX.
C  GMAX    MAXIMUM GAIN VALUE BY WHICH S.S. IS MULTIPLIED.
C  TINCH   NO. OF INCHES OF PAPER PER SECOND FOR PLOTTING TIME SERIES
C  TPLOT   TIME LENGTH OF PLOT (STARTS AT 0) FOR SYNTHETIC SEISMOGRAM
C  TST     START TIMES FOR CALCULATING AUTOPOWER SPECTRA OF S. S.
C  TEND    END TIMES FOR CALCULATING AUTOPOWER SPECTRA OF S. S.
C
      N = 2**LOG2N
      M = N/2
      MPLUS1 = M + 1
      NEST = 2**LOGEST
      TAU = 1./(2.*FNYQ)
      WRITE (6,1003) N, M, FNYQ, TAU, PERIOD, TINCH, TPLOT
      WRITE (6,1007) ZEROLO, FLOCUT, HICUT, BETA, GMAX
C
C  GENERATE THE INPUT PULSE AND TAKE ITS FOURIER TRANSFORM
C
      CALL PULSE (LOG2N,PERIOD,IPULS,HICUT,FLOCUT,DELAY,ZEROLO)
C
C  GENERATE THE REFLECTION COEFFICIENTS AS FUNCTIONS OF FREQUENCY.
C  THIS REQUIRES READING AS INPUT VELOCITY AND DEPTH VALUES PLUS
C  Q AND Q-DEPTH VALUES.
C
      CALL COEFF (LOG2N,FNYQ)
C
C  MULTIPLY THE PULSE TRANSFORM AND COEFFICIENT VALUES IN THE F DOMAIN.
C
      DO 20 I=1,MPLUS1
   20 FW(I) = FW(I)*RZ(I)
C
C  PUT FW IN SS IN A FORM TO USE FAST F.T.
C
      DO 30 I=1,MPLUS1
   30 SS(I) = REAL (FW(I))
      DO 40 I=2,M
      IA = N + 2 - I
   40 SS(IA) = - AIMAG (FW(I))
C
C  PERFORM THE INVERSE FOURIER TRANSFORM
C
      CALL ONE C FT (LOG2N,SS)
      FLN = FLOAT(N)
      DO 43 I=1,N
   43 SPARE(I) = SS(I)/FLN
      SI(1) = 1.0
```

```
      SS(1) = SS(1)/FLN
      DO 50 I=2,N
      IF (SI(I-1).GE.GMAX) GO TO 45
      SI(I) = BETA**((I-1)*TAU)
      GO TO 50
   45 SI(I) = GMAX
   50 SS(I) = SS(I)*SI(I)/FLN
      WRITE (6,1006) TAU
      WRITE (6,1002) (SI(I),I=1,N,2)
      WRITE (6,1001)
      WRITE (6,1002) (SS(I),I=1,N)
C
C  PLOT THE SYNTHETIC SEISMOGRAM
      CALL PLOT SS (4,LOG2N,NSAMP)
C
C  CALCULATE AUTOPOWER SPECTRA OF SPECIFIED TIME INTERVALS
      IF (NAP.EQ.0) GO TO 100
      DO 53 I=1,N
   53 SS(I) = SPARE(I)
      LOGP1 = LOGEST + 1
      NES = NEST + 1
      DO 55 I=1,NES
   55 FREQ(I) = FNYQ*(I-1)/NEST
      FREQ(NEST+2) = 0.0
      FREQ(NEST+3) = FLOAT(5*IFIX(1./(82.0*TAU)+1))
      DO 80 I=1,NAP
      NST = IFIX(TST(I)/TAU) + 1
      NEND = IFIX(TEND(I)/TAU) + 1
      NSAMP = NEND - NST + 1
      DO 60 IA = NST,NEND
      IB = IA - NST + 1
   60 SI(IB) = SS(IA)
      CALL TAPER (NSAMP,N)
      CALL ONE R FT (LOG2N,SI)
      DO 70 IA=1,N
   70 SPARE(IA) = SI(IA)
      CALL TWO C A C (LOG2N,SI,SPARE)
      CALL PARZEN (NEST,SI)
      DO 75 IA=2,NEST
      SI(IA) = 2.0*SI(IA)
      IB = IA + NEST
   75 SI(IB) = 0.0
      SI(NES) = 0.0
      CALL ONE R FT (LOGP1,SI)
      WRITE (6,1005) TST(I), TEND(I)
      WRITE (6,1004) ((FREQ(IA),SI(IA)),IA=1,NES)
C
C  PLOT THE AUTOPOWER SPECTRUM
      CALL PLOT SS (5,LOGP1,I)
   80 CONTINUE
```

```
  100  CONTINUE
       STOP
       END


       SUBROUTINE PULSE (LOG2N,PERIOD,IPULS,HICUT,FLOCUT,DELAY,ZEROLO)
C
C   THIS SUBROUTINE CALCULATES AN INPUT PULSE FOR THE SYNTHETIC SEISMO-
C   GRAM AND TAKES ITS FOURIER TRANSFORM UTILIZING THE FAST F.T.  THE
C   PULSE IS A GRAM-CHARLIER WAVELET CALCULATED FROM THE 5TH AND 6TH
C   DERIVATIVES OF THE GAUSSIAN ERROR FUNCTION.  ALTERNATIVELY, THE
C   PULSE IS AN APPROXIMATION TO A DELTA FUNCTION AND IS SPECIFIED
C   BY ITS AMPLITUDE SPECTRUM.
C
       COMPLEX RZ(2049), FW(2049)
       COMMON /STORE1/ RZ, FW
       COMMON /STORE2/ FREQ(2051), AMPL(2051), SS(4098), SI(4098)
       COMMON/STORE3/IP, YPOS, YTOT, TAU, TINCH, TPLOT,NAP,TST(4),TEND(4)
  1000 FORMAT (6(2X,E14.7))
  1001 FORMAT (1H1,4X,9HREAL S(W),8X,9HIMAG S(W),8X,9HAMPLITUDE,10X,5HPHA
      1SE,11X,9HFREQUENCY)
  1002 FORMAT ('0 THE AMPLITUDE SPECTRUM OF THE INCIDENT PULSE HAS BEEN S
      1PECIFIED')
  1003 FORMAT ('1 THE FIRST 500 AMPLITUDE VALUES FOR THE PULSE RESULTING
      1FROM A UNITY SPECTRUM FOLLOW'//)
  1004 FORMAT (10(2X,E10.3))
  1010 FORMAT (1H0,53X,'X',15X,'PULSE(I)',5X,'I')
  1011 FORMAT (40X,2(5X,E15.7),I10)
       N = 2**LOG2N
       M = N/2
       MPLUS1 = M + 1
       FINTL = 1./(2.*TAU*M)
       GO TO (5,50), IPULS
C
C   A GRAM CHARLIER WAVELET IS TO BE CALCULATED
    5  TWO PI = 6.2831854
       A = 1./SQRT(TWO PI)
       NSAMP = IFIX( 6*PERIOD/TAU) + 1
       DO 10 I=1,4098
   10  SS(I) = 0.0
       WRITE (6,1010)
       DO 30 I=1,NSAMP
       X = 2.0*(FLOAT(I-1)*TAU - 3*PERIOD)/PERIOD
       FX = (EXP(-X*X/2))*((((((-X+1)*X+15)*X-10)*X-45)*X+15)*X+15)*A
       SS(I) = FX
   30  WRITE (6,1011) X, FX, I
       NSAMP = 2*NSAMP
C
C   PLOT THE GRAM CHARLIER WAVELET
```

```
      CALL PLOT SS (1,LOG2N,NSAMP)
      CALL ONE R FT (LOG2N,SS)
C
C   SS NOW CONTAINS THE COMPACT STORED FOURIER TRANSFORM OF THE
C   INPUT PULSE
C
      CALL RECOVR (LOG2N,SS,SI)
C
C   THE REAL PART OF THE F.T. IS NOW IN SS, THE IMAG. PART IN SI
C
      WRITE (6,1001)
      DO 40 I=1,MPLUS1
      FREQ(I) = (I-1)*FINTL
      FW(I) = CMPLX(SS(I),SI(I))
      AMPL(I) = CABS(FW(I))
      IF ((SI(I).EQ.0.0).AND.(SS(I).EQ.0.0)) SS(I) = 1.0
      PHASE = ATAN2(SI(I),SS(I))
      IF (I.GT.200) GO TO 40
      WRITE (6,1000) FW(I), AMPL(I), PHASE, FREQ(I)
   40 CONTINUE
C
C   PLOT THE AMPLITUDE SPECTRUM OF THE GRAM CHARLIER WAVELET
      CALL PLOT SS (2,LOG2N,NSAMP)
      RETURN
C
C   A DELTA FUNCTION INPUT PULSE IS TO BE CALCULATED.  THE AMPLITUDE
C   CHARACTERISTICS ARE FIRST COMPUTED.
   50 LZ = IFIX(ZEROLO/FINTL)
      LY = LZ + 1
      IF (LZ.EQ.0) GO TO 52
      DO 51 I=1,LZ
      FW(I) = (0.0,0.0)
      AMPL(I) = 0.0
   51 SS(I) = 0.0
   52 LA = IFIX(FLOCUT/FINTL) + 1
      LB = LA + 1
      LC = IFIX(HICUT/FINTL) + LA - LY + 1
      LD = LC - LA + LY - 1
      LE = LC + 1
      PI = 3.14159265
      ARG = 0.5*PI/(LA-LY)
      DO 55 I=LY,LA
      IB = I - LY
      IA = LC - IB
      SINE = SIN(ARG*IB)
      FW(IA) = CMPLX(SINE,0.0)
      AMPL(I) = SINE
      SS(I) = SINE
      FW(I) = CMPLX(SINE,0.0)
      AMPL(IA) = SINE
```

```
   55   SS(IA) = SINE
        DO 60 I=LB,LD
        FW(I) = (1.0,0.0)
        AMPL(I) = 1.0
   60   SS(I) = 1.0
        DO 65 I=LE,MPLUS1
        FW(I) = (0.0,0.0)
        AMPL(I) = 0.0
   65   SS(I) = 0.0
        DO 68 I=MPLUS1,N
   68   SS(I) = 0.0
C
C   AN INVERSE F.T. PRODUCES A PULSE IN THE TIME DOMAIN
        CALL ONE C FT (LOG2N,SS)
        FLN = FLOAT(N)
        DO 70 I=1,N
   70   SS(I) = SS(I)/FLN
C
C   A DELAY IN TIME OF THE PEAK AMPLITUDE OF THE PULSE IS MADE
        IF (DELAY.EQ.0.0) GO TO 85
        LDEL = IFIX(DELAY/TAU) + 1
        LDEL1 = LDEL + 1
        DO 75 I=1,LDEL
        IA = LDEL - I + 1
   75   SI(I) = SS(IA)
        DO 80 I=LDEL1,N
        IA = I - LDEL1 + 2
   80   SI(I) = SS(IA)
        DO 83 I=1,N
   83   SS(I) = SI(I)
   85   WRITE (6,1003)
        WRITE (6,1004) (SS(I),I=1,500)
        NSAMP = 4.0/(TINCH*TAU)
C
C   PLOT THE INPUT PULSE
        CALL PLOT SS (1,LOG2N,NSAMP)
C
C   THE COMPLEX SPECTRUM OF THE PULSE IS COMPUTED.
        DO 100 I=1,MPLUS1
  100   FREQ(I) = (I-1)*FINTL
        WRITE (6,1002)
        IF (DELAY.EQ.0.0) GO TO 120
        CALL ONE R FT (LOG2N,SS)
        CALL RECIVR (LOG2N,SS,SI)
        WRITE (6,1001)
        DO 110 I=1,MPLUS1
        FW(I) = CMPLX(SS(I),SI(I))
        AMPL(I) = CABS(FW(I))
        IF ((SI(I).EQ.0.0).AND.(SS(I).EQ.0.0)) SS(I) = 1.0
        PHASE = ATAN2(SI(I),SS(I))
```

```
      IF (I.GT.200) GO TO 110
      WRITE (6,1000) FW(I), AMPL(I), PHASE, FREQ(I)
  110 CONTINUE
C
C  PLOT THE AMPLITUDE SPECTRUM OF THE INPUT PULSE
  120 CALL PLOT SS (2,LOG2N,NSAMP)
      RETURN
      END



      SUBROUTINE COEFF (LOG2N,FNYQ)
C
C  THIS SUBROUTINE GENERATES THE REFLECTION COEFFICIENTS OF THE
C  LAYERED MEDIA, WITH ATTENUATION, AS A FUNCTION OF FREQUENCY.
C
      COMPLEX RZ(2049), FW(2049)
      COMMON /STORE1/ RZ, FW
      COMMON /STORE2/ FREQ(2051), AMPL(2051), SS(4098), SI(4098)
      COMMON/STORE3/IP, YPOS, YTOT, TAU, TINCH, TPLOT,NAP,TST(4),TEND(4)
      REAL VR(600), Z(600), Q(20), ZQ(20)
      COMPLEX B(600), VEL(600), S(600), R, D, F, E, RZERO
 1000 FORMAT (2I5)
 1001 FORMAT (1X,E14.7,1X,E14.7,11X,E14.7,1X,E14.7)
 1002 FORMAT (8F10.0)
 1008 FORMAT ('0 THE COMPLEX SLOPE VALUES FOLLOW (4 VALUES/LINE)')
 1009 FORMAT (4(4X,E12.4,2X,E12.4))
 1010 FORMAT ('1 DEPTH VALUES AND COMPLEX VELOCITIES (2 SETS/LINE)')
 1011 FORMAT (2(4X,E12.4,6X,E12.4,2X,E12.4))
 1012 FORMAT (1H1,24X,'FREQUENCY',8X,'REFLECTION COEFFICIENT',8X,
     1'PHASE OF R',4X,'AMPLITUDE OF R')
 1013 FORMAT (21X,5E16.6)
 1014 FORMAT ('0 Q-DEPTH VALUES AND Q VALUES (4 SETS/LINE)')
      N = 2**LOG2N
      M = N/2
      MPLUS1 = M + 1
      READ (5,1000) NZ, NZQ
      NZ1 = NZ + 1
      READ (5,1001) (VR(J),Z(J), J=2,NZ1)
      READ (5,1002) (Q(J),ZQ(J), J=1,NZQ)
C
C  NZ       THE NO. OF VELOCITY AND DEPTH VALUES TO BE READ IN
C  NZQ      THE NO. OF Q AND Q-DEPTH VALUES TO BE READ IN
C  VR(J)    THE VELOCITY VALUES
C  Z(J)     AND THE CORRESPONDING DEPTH VALUES
C  Q(J)     THE Q (INVERSE ATTENUATION) VALUES
C  ZQ(J)    AND THE CORRESPONDING Q-DEPTH VALUES
C
      VR(1) = VR(2)
      Z(1) = 0
```

```
      IA = 1
      DO 10 I=1,NZ1
      IF (Z(I).LE.ZQ(IA)) GO TO 5
      IA = IA + 1
    5 VI = 0.5*VR(I) / Q(IA)
   10 VEL(I) = CMPLX(VR(I),VI)
      S(1) = CMPLX(0.001,0.0)
      S(NZ1) = S(1)
      WRITE (6,1010)
      WRITE (6,1011) ((Z(I),VEL(I)),I=1,NZ1)
      WRITE (6,1014)
      WRITE (6,1009) ((ZQ(I),Q(I)),I=1,NZQ)
      DO 20 I=2,NZ
      S(I) = (VEL(I+1) - VEL(I)) / (Z(I+1) - Z(I))
      SR = REAL(S(I))
      IF (ABS(SR).GE.0.001) GO TO 20
      SII = AIMAG(S(I))
      S(I) = CMPLX(.001,SII)
   20 CONTINUE
      WRITE (6,1008)
      WRITE (6,1009) (S(I),I=1,NZ1)
      WRITE (6,1012)
      DO 100 I=1,MPLUS1
      W = 6.2831854*FREQ(I)
      IF (I.EQ.1) GO TO 60
      DO 30 IA=1,NZ1
   30 B(IA) = CSQRT(1. - 4.*(W/S(IA))**2)
      R = (0.0,0.0)
      DO 50 IA=1,NZ
      IB = NZ - IA + 1
      IC = IB + 1
      D = S(IB)*B(IB)
      E = S(IC) - S(IB)
      F = S(IC)*B(IC)*(1.-R)/(1.+R)
      IF ((REAL(VEL(IC)).EQ.REAL(VEL(IB))).AND.(AIMAG(VEL(IC)).EQ.
     1 AIMAG(VEL(IB)))) GO TO 40
      R = ((D+E-F) / (D-E+F)) * CEXP(-B(IB)*CLOG(VEL(IC)/VEL(IB)))
      GO TO 50
   40 R = (D+E-F) / (D-E+F)
   50 CONTINUE
      RZERO = -R
      GO TO 70
   60 RZERO = (VEL(1) - VEL(NZ1)) / (VEL(1) + VEL(NZ1))
   70 RZ(I) = RZERO
      AMPL(I) = CABS(RZERO)
      PHASE = ATAN2 (AIMAG(RZERO),REAL(RZERO))
      FR = W/6.2831854
      WRITE (6,1013) FR, RZERO, PHASE, AMPL(I)
  100 CONTINUE
C
```

```
C   PLOT THE TRANSFER FUNCTION OF THE LAYERED MEDIUM
       CALL PLOT SS (3,LOG2N,NSAMP)
       RETURN
       END



       SUBROUTINE PLOT SS (ITYPE,LOG2N,NSAMP)
C
C   THIS SUBROUTINE PLOTS THE VARIOUS QUANTITIES CALCULATED ELSEWHERE,
C   INCLUDING THE FINAL SYNTHETIC SEISMOGRAM.
C
 1000 FORMAT ('0 THE TOTAL NUMBER OF CALCOMP PLOTS FOR THE PLOTTER REQUE
     1ST SLIP IS ',I5)
       DIMENSION BUFF(2048)
       COMPLEX RZ(2049), FW(2049)
       COMMON /STORE1/ RZ, FW
       COMMON /STORE2/ FREQ(2051), AMPL(2051), SS(4098), SI(4098)
       COMMON/STORE3/IP, YPOS, YTOT, TAU, TINCH, TPLOT,NAP,TST(4),TEND(4)
       N = 2**LOG2N
       M = N/2
       MPLUS1 = M + 1
       MPLUS2 = M + 2
       MPLUS3 = M + 3
       GO TO (20, 40, 60, 80, 120), ITYPE
 20    CALL PLOTS (BUFF(1),8192)
       IP = 1
       YTOT = 0.0
       CALL PLOT (2.0,1.0,-3)
       IP = IP + 1
       NS1 = NSAMP + 1
       NS2 = NSAMP + 2
       DO 25 I=1,NSAMP
       AMPL(I) = SS(I)
 25    FREQ(I) = FLOAT(I-1)*TAU
       FREQ(NS1) = 0.0
       FREQ(NS2) = 1./TINCH
       CALL SCALE (AMPL,4.0,NSAMP,1,10.)
       CALL AXIS (0.0,0.0,'TIME (SECONDS)',-14,4.0,0.0,FREQ(NS1),
      1FREQ(NS2),10.)
       CALL AXIS (0.0,0.0,'PULSE AMPLITUDE',15,4.0,90.0,AMPL(NS1),
      1AMPL(NS2),10.)
       CALL LINE (FREQ,AMPL,NSAMP,1,0,3)
       CALL SYMBOL (0.0,4.5,0.25,'INPUT PULSE',0.0,11)
       YPOS = 8.0
       YTOT = YTOT + YPOS
       RETURN
 40    CALL PLOT (0.0,YPOS,-3)
       IP = IP + 1
       FREQ (MPLUS2) = 0.0
```

```
      FREQ (MPLUS3) = FLOAT(5 *IFIX(1./(82.0*TAU)+1))
      CALL SCALE (AMPL,6.0,MPLUS1,1,10.)
      CALL AXIS (0.0,0.0,'FREQUENCY(HZ.)',-15,8.0,0.0,FREQ(MPLUS2),
     1 FREQ(MPLUS3),10.)
      CALL AXIS (0.0,0.0,'PULSE TRANSFORM AMPLITUDE',25,6.0,90.0,
     1 AMPL(MPLUS2),AMPL(MPLUS3),10.)
      CALL LINE (FREQ, AMPL, MPLUS1, 1, 0, 3)
      CALL SYMBOL (0.0,6.5,0.25,'AMPLITUDE SPECTRUM OF INPUT PULSE',
     1 0.0,33)
      YPOS = 10.0
      YTOT = YTOT + YPOS
      RETURN
   60 CALL PLOT (0.0,YPOS,-3)
      IP = IP + 1
      CALL SCALE (AMPL,6.0,MPLUS1,1,10.)
      CALL AXIS (0.0,0.0,'FREQUENCY(HZ.)',-15,8.0,0.0,FREQ(MPLUS2),
     1 FREQ(MPLUS3),10.)
      CALL AXIS (0.0,0.0,'AMPLITUDE',9,6.0,90.0,AMPL(MPLUS2),
     1 AMPL(MPLUS3),10.)
      CALL LINE (FREQ, AMPL, MPLUS1, 1, 0, 3)
      CALL SYMBOL (0.0,6.5,0.25,'TRANSFER FUNCTION OF LAYERED MEDIA',
     1 0.0,34)
      YPOS = - YTOT
      YTOT = 0.
      RETURN
   80 CALL PLOT (11.0,YPOS,-3)
      IP = IP + 1
      N = IFIX(TPLOT/TAU) + 10
      IF (N.GT.2**LOG2N) N = 2**LOG2N
      DO 83 I=1,N
   83 SI(I) = SS(I)
      CALL SCALE (SS,4.0,N,1,10.)
      SS(N+1) = - SS(N+1)
      NPLUS2 = N + 2
      SS(NPLUS2) = - SS(NPLUS2)
      DO 85 I=1,N
   85 SS(I) = SS(I)/SS(NPLUS2)
      TINCR = 1.0/TINCH
      YDIST = TPLOT*TINCH
      NLINES = IFIX(YDIST/25.05) + 1
      XP = 0.0
      T2 = 0.0
      T1 = 0.0
      N2 = 1
      T = TINCH * TAU
      DO 110 I=1,NLINES
      IF (YDIST.LE.25.0) GO TO 90
      YD = 25.0
      YDIST = YDIST - 25.0
      GO TO 95
```

```
 90   YD = YDIST
 95   T1 = T1 + T2
      T2 = T2 + YD/TINCH
      CALL AXIS (XP,0.,'TIME (SECONDS)',14,YD,90.0,T1,TINCR,10.)
      CALL AXIS(XP+.5,0.0,'OUTPUT AMPLITUDE',-16,4.0,0.0,SS(N+1),
     1 SS(NPLUS2),10.)
      CALL PLOT (XP+2.5, 0., -3)
      IP = IP + 1
      XP = 3.0
      N1 = N2
      N2 = N1 + IFIX((T2-T1)/TAU)
      DO 100 IA=N1,N2
      TPOS = T*FLOAT(IA-N1)
100   CALL PLOT (SS(IA), TPOS, 2)
110   CONTINUE
      CALL PLOT (XP,0.0,-3)
      IP = IP + 1
      CALL SYMBOL (0.0,0.0,0.30,'SYNTHETIC SEISMOGRAM',90.0,20)
      CALL PLOT (4.0,0.0,-3)
      IP = IP + 1
      DO 115 I=1,N
115   SS(I) = SI(I)
      IF (NAP.NE.0) RETURN
      CALL PLOT (0.0,0.0,999)
      WRITE (6,1000) IP
      RETURN
120   IF (NSAMP.NE.1) GO TO 130
      CALL AXIS (0.0,0.0,'FREQUENCY (HZ.)',-15,8.0,0.0,FREQ(MPLUS2),
     1 FREQ(MPLUS3),10.)
      SMIN = SI(1)
      DO 122 I=2,MPLUS1
      IF (SMIN.GT.SI(I)) SMIN=SI(I)
122   CONTINUE
      DO 125 I=1,MPLUS1
      IF (SI(I .EQ.0.0) SI(I) = SMIN
125   SI(I) = ALOG10(SI(I))
      YPO = 0.0
      XPO = 0.0
      GO TO 140
130   IF(NSAMP.NE.2) GO TO 133
      YPO = 10.0
      XPO = 0.0
      YPOS = 0.5/(TAU*MPLUS1)
      N1 = IFIX(5.0/YPOS) + 1
      N2 = IFIX(25.0/YPOS)
      DO 131 I=N1,N2
      IA = I-N1+1
131   FREQ(IA) = FREQ(I)
      MPLUS1 = N2 - N1 + 1
      MPLUS2 = MPLUS1 + 1
```

```
      MPLUS3 = MPLUS1 + 2
      FREQ(MPLUS2) = 5.0
      FREQ(MPLUS3) = 2.5
      GO TO 135
  133 YPO = 2.0
      XPO = -0.7*(NSAMP-2)
      N1 = IFIX(5.0/YPOS) + 1
      N2 = IFIX(25.0/YPOS)
      MPLUS1 = N2 - N1 + 1
      MPLUS2 = MPLUS1 + 1
      MPLUS3 = MPLUS1 + 2
  135 N11 = N1 + 1
      SMIN = SI(N1)
      DO 134 I=N11,N2
      IF (SMIN.GT.SI(I)) SMIN = SI(I)
  134 CONTINUE
      DO 137 I=N1,N2
      IF (SI(I).EQ.0.0) SI(I) = SMIN
      IA = I-N1+1
  137 SI(IA) = ALOG10(SI(I))
  140 CALL PLOT (0.0,YPO,-3)
      IP = IP + 1
      IF (NSAMP.EQ.2) CALL AXIS (0.0,0.0,'FREQUENCY (HZ.)',-15,8.0,0.0,
     1 FREQ(MPLUS2),FREQ(MPLUS3),10.)
      CALL SCALE (SI,8.0,MPLUS1,1,10.)
      CALL AXIS (XPO,0.0,'AUTOPOWER SPECTRAL DENSITY (LOG 10 SCALE)',41,
     18.0,90.0,SI(MPLUS2),SI(MPLUS3),10.0)
      CALL LINE (FREQ,SI,MPLUS1,1,10,NSAMP)
      YY = (SI(MPLUS1) - SI(MPLUS2)) / SI(MPLUS3)
      ST = TST(NSAMP)
      SE = TEND(NSAMP)
      CALL NUMBER (8.5,YY,.15,ST,0.0,2)
      CALL WHERE (XX,YZ,FCTR)
      CALL SYMBOL (XX,YY,.15,' TO ',0.0,4)
      CALL WHERE (XX,YZ,FCTR)
      XX = XX + 0.1
      CALL NUMBER (XX,YY,.15,SE,0.0,2)
      CALL WHERE (XX,YZ,FCTR)
      CALL SYMBOL (XX,YY,.15,' SEC.',0.0,5)
      IF (NSAMP.NE.NAP) RETURN
      IF (NAP.NE.1) GO TO 150
      YPO = 0.)
      GO TO 160
  150 YPO = -2.0*(NAP-2) - 10.0
  160 CALL PLOT (11.0,YPO,-3)
      IP = IP + 1
      CALL PLOT (0.0,0.0,999)
      WRITE (6,1000) IP
      RETURN
      END
```

```
      SUBROUTINE TAPER (NSAMP,N)
C
C  THIS SUBROUTINE TAPERS THE FIRST AND LAST 10% OF THE DATA FOR WHICH
C    THE AUTOPOWER SPECTRA IS TO BE COMPUTED.
C
      COMMON /STORE2/ FREQ(2051), AMPL(2051), SS(4098), SI(4098)
      COMMON/STORE3/IP, YPOS, YTOT, TAU, TINCH, TPLOT,NAP,TST(4),TEND(4)
      NS1 = NSAMP + 1
      NS10 = NSAMP/10
      PI = 3.141592654
      ARG = 5.0*PI/NSAMP
      DO 10 JA=1,NS10
      JAA = NSAMP - JA + 1
      S = SIN(ARG*(JA-1))
      SI(JA) = S*SI(JA)
   10 SI(JAA) = S*SI(JAA)
      DO 20 JA=NS1,N
   20 SI(JA) = 0.0
      RETURN
      END
```

```
      SUBROUTINE PARZEN ( M, C )
C.....
C
C      MODIFIES THE COVARIANCE FUNCTION C(T) BY THE PARZEN LAG WINDOW.
C         THE RESULTS ARE STORED IN C(T), T=1,2,3,...,M+1.
C
      REAL  C (10), D
      INTEGER M, M UPON 2, TWO M
C
      M UPON 2 = M/2
      DO 10 J=1,M UPON 2
         D = 1.0 - 6.0*( FLOAT(J)/FLOAT M) )**2
     .           + 6.0*( FLOAT(J)/FLOAT M) )**3
         C(J+1) = D * C(J+1)
   10    C O N T I N U E
      M UPON 2 = M UPON 2 + 1
      DO 20 J=1 UPON 2,M
         D = 2.0*(1.0 - FLOAT(J)/FLOAT(M) )**3
         C(J+1) = D * C(J+1)
   20    C O N T I N U E
      R E T U I N
      E N D
```

```
      SUBROUTINE TWO C A C (LOG2N,X,Y)
C.....................................................................
C     TWO CYCLIC AUTO COVARIANCES
C
      INTEGER LOG2N
      REAL X (10), Y (10)
C
      INTEGER J,K,N,N UPON 2
      REAL P1,P2
C
      N=2**LOG2N
      X(1)=X(1)**2
      Y(1)=Y(1)**2
      N UPON 2=N/2
      DO 100 J=2,N UPON 2
      K=N+2-J
      P1=X(J)**2+X(K)**2
      P2=Y(J)**2+Y(K)**2
      X(J)=P1
      X(K)=P1
      Y(J)=P2
      Y(K)=P2
  100 CONTINUE
      K=N/2+1
      X(K)=X(K)**2
      Y(K)=Y(K)**2
      CALL MR 1D FT (LOG2N,X,Y)
      RETURN
      END


      SUBROUTINE ONE R FT (LOG2N,X)
C.....................................................................
C     ONE REAL FOURIER TRANSFORM
C
      INTEGER LOG2N
      REAL X (10)
C
      INTEGER ,,JN,K,KN,N,N OVER 2
      REAL ARG,C,PI,S,T,XI,XR,YI,YR
C
      PI=3.141!92654
      N=2**(LOG2N-1)
      CALL R SUB B O (LOG2N,X)
      CALL R SUB B O (LOG2N-1,X(1))
      CALL R SUB B O (LOG2N-1,X(N+1))
      CALL MR 1D FT (LOG2N-1,X(1),X(N+1))
      N OVER 2=N/2+1
```

```
      DO 100 J=2,N OVER 2
      K=N+2-J
      JN=J+N
      KN=K+N
      XR=(X(J)+X(K))*.5
      XI=(X(JN)-X(KN))*.5
      YR=(X(JN)+X(KN))*.5
      YI=(X(K)-X(J))*.5
      ARG=PI*FLOAT(J-1)/FLOAT(N)
      C=COS(ARG)
      S=SIN(ARG)
      T=YR*C+YI*S
      YI=YI*C-YR*S
      YR=T
      X(J)=XR+YR
      X(K)=XR-YR
      X(KN)=XI+YI
      X(JN)=YI-XI
  100 CONTINUE
      XR=X(1)+X(N+1)
      YR=X(1)-X(N+1)
      X(1)=XR
      X(N+1)=YR
      RETURN
      END


      SUBROUTINE R SUB B O (LOG2N,X)
C.....................................................................
C     REVERSE SUBSCRIPT BIT ORDER
C
      INTEGER LOG2N
      REAL X.(10)
C
      INTEGER J
      REAL T
C
      INTEGER A,B,C,D,E,F,G,H,I,J,K,L,M,N,BS,CS,DS,ES,FS,GS,HS,IS,JS,KS,
     .LS,MS,NS,AL,BL,CL,DL,EL,FL,GL,HL,IL,JL,KL,LL,ML,NL, S (14), U (14)
      EQUIVALENCE (BS,S(2)),(CS,S(3)),(DS,S(4)),(ES,S(5)),(FS,S(6)),
     .(GS,S(7)),(HS,S(8)),(IS,S(9)),(JS,S(10)),(KS,S(11)),(LS,S(12)),
     .(MS,S(13)),(NS,S(14)),(AL,U(1)),(BL,U(2)),(CL,U(3)),(DL,U(4)),
     .(EL,U(5)),(FL,U(6)),(GL,U(7)),(HL,U(8)),(IL,U(9)),(JL,U(10 ),
     .(KL,U(11)),(LL,U(12)),(ML,U(13)),(NL,U(14))
C
      NS=2**(LOG2N-1)
      NL=2*NS
      DO 100 K=2,13
      J=15-K
```

```
      U(J)=S(J+1)
      S(J)=1
      IF(S(J+1).GT.1) S(J)=S(J+1)/2
  100 CONTINUE
      AL=BS
      JJ=0
      DO 200 A=1,AL
      DO 200 B=A,BL,BS
      DO 200 C=B,CL,CS
      DO 200 D=C,DL,DS
      DO 200 E=D,EL,ES
      DO 200 F=E,FL,FS
      DO 200 G=F,GL,GS
      DO 200 H=G,HL,HS
      DO 200 I=H,IL,IS
      DO 200 J=I,JL,JS
      DO 200 K=J,KL,KS
      DO 200 L=K,LL,LS
      DO 200 M=L,ML,MS
      DO 200 N=M,NL,NS
      JJ=JJ+1
      IF (JJ.LE.N) GO TO 200
      T=X(JJ)
      X(JJ)=X(N)
      X(N)=T
  200 CONTINUE
      RETURN
      END


      SUBROUTINE MR 1D FT (LOG2N,X,Y)
C.....................................................................
C     MIXED RADIX ONE DIMENSIONAL FOURIER TRANSFORM
C
      INTEGER LOG2N
      REAL X (10), Y (10)
C
      INTEGER JJ,J0,J1,J2,J3,N,M4
      REAL ARG,C1,C2,C3,I0,I1,I2,I3,R0,R1,R2,R3,S1,S2,S3,T
C
      INTEGER A,B,C,D,E,F,G,H,I,J,K,L,M,BS,CS,DS,ES,FS,GS,HS,IS,JS,KS,
     .LS,MS,AL,BL,CL,DL,EL,FL,GL,HL,IL,JL,KL,LL,ML, S (13), U (13)
      EQUIVALENCE (BS,S(2)),(CS,S(3)),(DS,S(4)),(ES,S(5)),(FS,S(6)),
     .(GS,S(7)),(HS,S(8)),(IS,S(9)),(JS,S(10)),(KS,S(11)),(LS,S(12)),
     .(MS,S(13)),(AL,U(1)),(BL,U(2)),(CL,U(3)),(DL,U(4)),(EL,U(5)),
     .(FL,U(6)),(GL,U(7)),(HL,U(8)),(IL,U(9)),(JL,U(10)),(KL,U(11)),
     .(LL,U(12)),(ML,U(13))
C
      N=2**LOG2N
```

```
      IF (LOG2N.LE.1) GO TO 500
      DO 400 K=2,LOG2N,2
      M=2**(LOG2N-K)
      M4=4*M
      DO 300 J=1,M
      ARG=6.283185307*FLOAT(J-1)/FLOAT(M4)
      C1=COS(ARG)
      S1=SIN(ARG)
      C2=C1*C1-S1*S1
      S2=C1*S1+C1*S1
      C3=C2*C1-S2*S1
      S3=C2*S1+S2*C1
      DO 200 I=M4,N,M4
      J0=I+J-M4
      J1=J0+M
      J2=J1+M
      J3=J2+M
      R0=X(J0)+X(J2)
      R1=X(J0)-X(J2)
      I0=Y(J0)+Y(J2)
      I1=Y(J0)-Y(J2)
      R2=X(J1)+X(J3)
      R3=X(J1)-X(J3)
      I2=Y(J1)+Y(J3)
      I3=Y(J1)-Y(J3)
      X(J0)=R0+R2
      Y(J0)=I0+I2
      IF (ARG.EQ.0.0) GO TO 100
      X(J2)=(R1+I3)*C1+(I1-R3)*S1
      Y(J2)=(I1-R3)*C1-(R1+I3)*S1
      X(J1)=(R0-R2)*C2+(I0-I2)*S2
      Y(J1)=(I0-I2)*C2-(R0-R2)*S2
      X(J3)=(R1-I3)*C3+(I1+R3)*S3
      Y(J3)=(I1+R3)*C3-(R1-I3)*S3
      GO TO 200
  100 CONTINUE
      X(J2)=R1-I3
      Y(J2)=I1-R3
      X(J1)=R0-R2
      Y(J1)=I0-I2
      X(J3)=R1-I3
      Y(J3)=I1-R3
  200 CONTINUE
  300 CONTINUE
  400 CONTINUE
  500 CONTINUE
      IF (LOG2N.EQ.LOG2N/2*2) GO TO 700
      DO 600 I=1,N,2
      R0=X(I)+X(I+1)
      R1=X(I)-X(I+1)
```

```
      I0=Y(I)+Y(I+1)
      I1=Y(I)-Y(I+1)
      X(I)=R0
      Y(I)=I0
      X(I+1)=R1
      Y(I+1)=I1
  600 CONTINUE
  700 CONTINUE
      MS=N/2
      ML=N
      DO 800 K=2,12
      J=14-K
      S(J)=1
      U(J)=S(J+1)
      IF (S(J+1).GT.1) S(J)=S(J+1)/2
  800 CONTINUE
      AL=BS
      JJ=0
      DO 900 A=1,AL
      DO 900 B=A,BL,BS
      DO 900 C=B,CL,CS
      DO 900 D=C,DL,DS
      DO 900 E=D,EL,ES
      DO 900 F=E,FL,FS
      DO 900 G=F,GL,GS
      DO 900 H=G,HL,HS
      DO 900 I=H,IL,IS
      DO 900 J=I,JL,JS
      DO 900 K=J,KL,KS
      DO 900 L=K,LL,LS
      DO 900 M=L,ML,MS
      JJ=JJ+1
      IF (JJ.LE.M) GO TO 900
      T=X(JJ)
      X(JJ)=X(M)
      X(M)=T
      T=Y(JJ)
      Y(JJ)=Y(M)
      Y(M)=T
  900 CONTINUE
      RETURN
      END


      SUBROUTINE RECOVR (LOG2N, RE, IM)
C.....
C
C       RECOVERS THE REAL AND THE IMAGINARY PARTS OF THE FOURIER
C       TRANSFORM WHICH HAS BEEN STORED IN COMPACT HERMETIAN FORM
```

```
C
C       THE COMPACT STORED FOIRIER TRANSFORM IS ORIGINALLY IN RE( )
C          SEE  TWO R FT  FOR DETAILS.
C
C       IN EFFECT THIS SUBROUTINE DOUBLES THE STORAGE AREA REQUIRED
C       BUT GIVES EASE IN THE MANIPULATION OF THE COEFFICIENTS WHERE
C          FTX(J) = RE(J) + IM(J)
C
      REAL  RE (10), IM (10)
      INTEGER LOG2N, N, N UPON2, MORE
C
      N = 2**LOG2N
      N UPON 2 = N/2
      MORE = N UPON 2 + 2
      IM(1) = 0.0
      DO 10 J=2,N UPON 2
         I = N-J+2
         IM(J) = RE(I)
   10    CONTINUE
      J = N UPON 2 +1
      IM(J) = 0.0
      DO 20 J=MORE,N
         I = N-J+2
         IM(J) = -RE(J)
         RE(J) = RE(I)
   20    CONTINUE
      RETURN
      E  N  D



      SUBROUTINE ONE C FT (LOG2N,X)
C.....................................................................
C       ONE COMPLEX FOURIER TRANSFORM
C
      INTEGER LOG2N
      REAL X (10)
C
      INTEGER J,JN,K,KN,N,N OVER 2
      REAL AI,AR,ARG,BI,BR,C,PI,S,T
C
      N=2**(LOG2N-1)
      PI=3.141592654
      N OVER 2=N/2+1
      DO 100 J=2,N OVER 2
      K=N+2-J
      JN=J+N
      KN=K+N
      AR=X(J)+X(K)
      AI=X(KN)-X(JN)
```

```
      BR=X(J)-X(K)
      BI=X(JN)+X(KN)
      ARG=PI*FLOAT(J-1)/FLOAT(N)
      C=COS(ARG)
      S=SIN(ARG)
      T=BR*C+BI*S
      BI=BI*C-BR*S
      BR=T
      X(J)=AR-BI
      X(K)=AR+BI
      X(JN)=BR+AI
      X(KN)=BR-AI
  100 CONTINUE
      AR=X(1)+X(N+1)
      BR=X(1)-X(N+1)
      X(1)=AR
      X(N+1)=BR
      CALL MR 1D FT (LOG2N-1,X(1),X(N+1))
      CALL R SUB B O (LOG2N-1,X(1))
      CALL R SUB B O (LOG2N-1,X(N+1))
      CALL R SUB B O (LOG2N,X)
      RETURN
      END
```

B29931